IOSR Journal of Electronics and Communication Engineering (IOSR-JECE)
e-ISSN: 2278-2834,p- ISSN: 2278-8735. Volume 5, Issue 6 (Mar. - Apr. 2013), PP 01-07
www.iosrjournals.org

Optimal fuzzy system design for additive noise removal in color images

Snekha[1], Bandaru Vasu Mani Kumar[2]
[1](ECE Department, Delhi Technological University , India)
[2](ECE Department, Delhi Technological University , India)

Abstract: *This paper presents a new approach to remove the additive noise using fuzzy logic and modified bacterial foraging in color images. In the first step the bacterial foraging technique is used to find the edges using a set of bacteria's that are randomly initialized to image pixel then they will try to search their nutrients which are edges in this case. The second step is to remove the gaussian and salt & pepper noise denoising we will leave edge pixel detected in step 1 as it is and rest of pixels in image will be candidate pixels for Denoising.We will use pixel similarity based concept.The Gaussian noise will be removed by using weighted mean filtering of peer group members. We tested the proposed method on color images that are corrupted with mixed noise both Gaussian and Salt & Pepper noise.*

Keywords: *BFOA ,Noise Removal, Fuzzy Way*

I. Introduction

Noise Filtering is a fundamental pre-processing step before further image processing techniques like image segmentation, image compression, and texture analysis can be performed. Noise often occurs in Images during Image acquisition, transmission/ reception and image storage or retrieval processes which affects the visual quality of image and results in poor and unpleasant visual image. So it is essential to remove noise. Linear filtering techniques like averaging filter, weighted mean filter available for image de-noising tend to blur the edges.[1] In Images, Edges contains essential information. Edges are the sharp features. Generally noises like Gaussian and salt &pepper are very common. Gaussian noise affects every pixel of the image. On the other hand, salt & pepper noise does not affect every pixel. Only the affected pixels intensity gets 0(pepper) or 255(salt).

Van De Ville et al. [6], the effective fuzzy derivatives are used for differentiating the noise and edge pixels in images corrupted with Gaussian noise. In Russo [7], FIRE (Fuzzy inference ruled by else sections) operators are used. Tuan-Anh Nguyen et al. [8] proposed spatially adaptive De-noising algorithm. This algorithm is consists of two stages; first noise detection and then noise removal filtering. Local weighted mean, local maximum and local weighted activity is defined to use local statistics of the image into De-noising process. Depending on local statistics, constraint for noise detection is specified. K. Rank et al. [9] proposed an adaptive 2-D recursive low-pass filter with some coefficients for restoring images corrupted with Gaussian Noise.

O.P Verma et al. [10], proposed an efficient fuzzy filter for edge preservation for color images. The algorithm is able to reduce salt & pepper noise with satisfactory results. Kenny Kal Vin Toh et al. [11] proposed a"Cluster-Based Adaptive Fuzzy Switching Median Filter for Universal Impulse Noise Reduction". In this filter, an easy to implement impulse detector and a detail preserving noise filter are cascaded.

In this proposed approach in the first step we are detecting the edges using bacteria foraging and in the second stage using the results from the first stage we are removing the noise using fuzzy rules by ignoring the edges.The paper is organized as follows. In Section 2, First bacterium foraging algorithm is discussed. Then an algorithm to calculate edge map using modified bacterium foraging algorithm is discussed after that a 2- stage filter to de-noise a colour image corrupted with Gaussian and Salt & pepper noise.In Section 3, we explain our proposed method for determining the components of interest. Section 4 describes the details of the simulations. Finally,in Section 5, we present the results of applying the proposed method.

II. Bacterial Foraging Algorithm

BFA is an optimization method developed by the (Passino, 2000; Passino, 2002)[2] based on the Foraging strategy of E. coli bacteria, which live in the human Intestine. Foraging means- The way of searching for food and provisions or we can generalize it foraging is an activity of looking thoroughly in order to find something. Foraging strategy is a method of animals for locating, handling and ingesting their food. It can be modeled as an optimization process, where bacteria search for and obtain nutrients in a way that maximize their energy E obtained per unit time spent T during foraging. In this process, the nutrient function is defined and each bacterium tries to maximize the amount of nutrient while minimizing time

spent T and energy cost E by following four stages: 1) Chemo taxis, 2) Swarming, 3) Reproduction, and 4) Elimination & Dispersal. In the beginning, there are as many solutions as the number of bacteria. So, each bacterium produces a solution for set of optimal values of parameters iteratively, and gradually all the bacteria converge on the global optimum.

II a. Presented method for edge detection

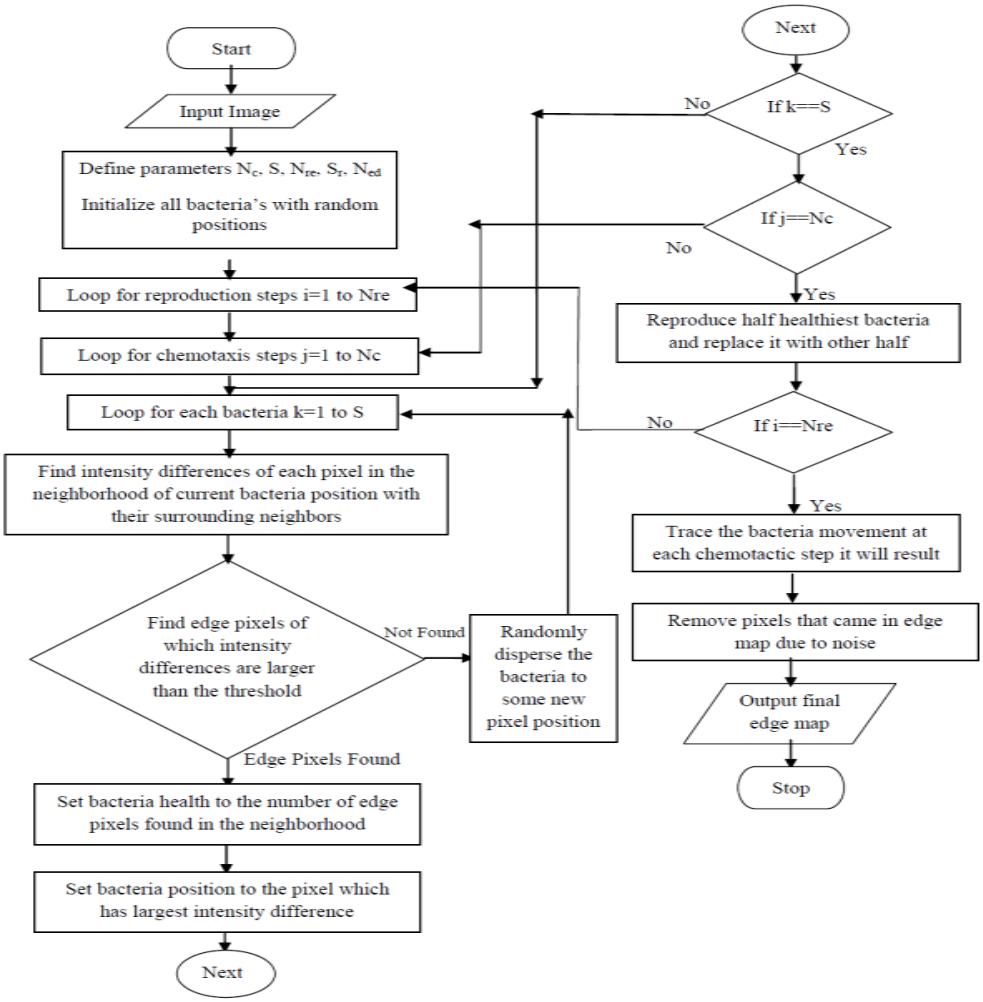

Fig.1 Flow chart of proposed edge detection method

Edge detection is the process of identifying and then locating sharp discontinuities or sharp changes in brightness in an image. The discontinuities are random changes in pixel intensity which characterize objects boundaries in a scene.

Bacterial Foraging Algorithm [Passino 2002], briefly described above is modified here to extract edges from noisy image. In this modified bacterial foraging algorithm, a set of bacteria's are randomly initialized to image pixel then they will try to search their nutrients which are edges in this case. This whole process will be carried out in 3 steps: Chemotaxis, Reproduction and elimination & dispersal step. Swarming step is avoided to make the algorithm simpler and to reduce the complexity of the algorithm. Following are the steps to be followed to extract edges using modified bacterial foraging algorithm.

Search Space

First we need to define the search space where the bacteria will forage. In this case, since we are searching for edges in image so whole image is the search space. Image is 2-dimensional search space consisting of x-y coordinates of pixels. Image size is limited by its x y dimension so the search space is finite in our case.

Defining the nutrient function

Now we need to define, what will be the nutrients for the bacteria. So by definition, edges are sharp changes in image brightness. So the nutrient function is based on the difference in intensities of a bacteria placed at a pixel position with respect to pixels in the surroundings. Here we have considered neighbourhood pixels which
are coming in window size of 3*3. Each bacterium will try to find out edges in these neighbourhood pixels depending on the difference of those with their surrounding pixels.

Criteria for choosing the edge pixel

For a pixel to be considered as edge pixel, it should have average intensity difference greater than a threshold value with its surrounding pixels that are 8- neighborhoods in our case. Intensity difference will be taken as component wise difference in color images. This is explained with the following example:

P1	P2	P3
P4	P	P5
P6	P7	P8

A pixel with its neighborhood pixel in window size 3*3. Suppose we want to find whether pixel P with coordinates (x, is edge pixel or not, we will calculate component wiseintensity difference with its neighborhood pixels in following way.These component wise differences will be added say in total variable. Now if this total is greater than a threshold value, then the pixel in interest that is P will be called as edge pixel otherwise not.

Choosing the threshold value

The threshold value is being used to differentiate edge pixels from non-edge pixels. It decides number of edge pixels to be detected. In case of high deviation of Gaussian Noise, a high threshold value is used. Following table is the optimal suggested setting to choose proper threshold value:

Standard Deviation	Threshold Value
Low in [0,10]	20
Medium[10,20]	35
High[20,30]	45

Table 1 for Threshold Value according to amount of Standard Deviation

III. Image noise removal using fuzzy way

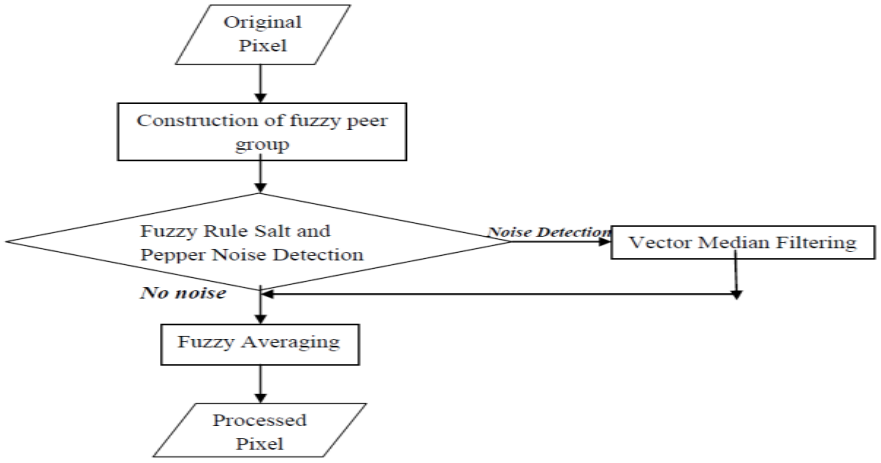

Fig.2 Flow chart of the proposed Filter

Now we will denoise the color image which is corrupted with additive noise i.e. Gaussian noise and salt & pepper noise. In Denoising we will leave edge pixel detected in step 1 as it is and rest of pixels in image will be candidate pixels for Denoising. We will be used to decide that the current pixel is corrupted

with salt and pepper noise or not. If it corrupted then using peer group members filtering will be applied. Then the Gaussian noise will be removed by using weighted mean filtering of peer group members. This algorithm is able to remove mixed noise with satisfactory results.

III a.Peer Group

The peer group of a given pixel is a set constituted by this pixel and those of its neighbors which are similar to it. The cardinality of peer group set will be used to decide the pixel in interest is free of noise or not. There are basically two ways to determine this peer group set i.e. Crisp way and Fuzzy way.
Here we used fuzzy way. If some fuzzy metrics are used to define Peer Group set then it is called Fuzzy Peer Group. We will define membership of each pixel $P_i \varepsilon W$ in fuzzy way.

Construction of Fuzzy Peer Group

- We use a **fuzzy similarity function M** defined as:
  $$\mathbf{M(P_0, P_i) = e^{-\| P_0 - P \|/Fq}} \quad (1)$$
  where $\| . \|$ denotes Euclidean norm and Fq>0 is a parameter. M will take values in [0, 1]. $M(P_0, P_i) = 1$ if and only if $P_i=P_0$. After calculating M, the color vectors or pixels $P_i \varepsilon W$ are sorted in descending order with respect to its similarity to P_0 which results in ordered set W'.
- Now we will define a **fuzzy set C^P_0** considering the proposition that P_i is similar to P_0 on the pixels P_i present in the window W' where membership function is given by:
  $$\mu(C^P_0(P_i)) = M(P_0, P_i) \text{ for } i=0,1,2,\ldots n^2-1 \quad (2)$$
- Now we will define **accumulated similarity AS** for each pixel P_i.
  $$AS^P_0(P_i) = \sum_{k=0:i} M(P_0, P_k), i=0,1,2\ldots n^2 \quad (3)$$
  Clearly $AS^P_0(P_0)=1$ and $AS^P_0(P_i)$ takes i+1 if $P_0=P_1=\ldots\ldots P_i$. Largest value AS^P_O can take is n^2
- Now we will create a **fuzzy set $L^P_0(P_i)$** by considering the vague proposition that $AS^P_0(P_i)$ is large. Clearly the memberships value of minimum value that ASP0(P0)=0 will be zero.Since it is the minimum value that AS^P_0 can take and memberships value of maximum value that is $AS^P_0(P_8)$=9 will be 1.So the membership function for the fuzzy set $L^P_0(P_i)$ is $\mu(AS^P(P))$ is defined as follows:
  $$LP0(Pi) = \mu(ASP0(Pi)) = -(ASP0(Pi) - 1)(ASP0(Pi) - 2n2 + 1) \text{ where } i=0, 1, 2.....n2-1 \quad (4)$$
- Now we will select **best number m** of members among window pixels W'. We aim to determine m number of members such that fuzzy peer group is the largest set that contain only similar pixels. The best number m where m can be 0, 1, 2…..n^2-1 is chosen such that it maximizes the certainty of following fuzzy rule.

Fuzzy Rule 1: If "Pm is similar to P_0" and "$AS^P_0(P_m)$ is large" then " the certainty of m to be the best number of members is high".
"P_m is similar to P_0" is given by fuzzy set $C^P_0(P_m)$, "$AS^P_0(P_m)$ is large" is given by $L^P_0(P_m)$.
The certainty of Fuzzy rule 1 is computed for each value of m and the value which maximizes this certainty is selected as the best number m of members for peer group on window W'
We use the product t-norm as the conjunction operator , so no de-fuzzification is needed.

$$C_{FR1}(m) = C^P_0(P_m)\, L^P_0(P_m) \quad (5)$$

So m is chosen such that $C_{FR1}(m)$ is maximum.Now we will define fuzzy peer group $FP^P_0(m)$ with first m members from W' and their membership function will be defined by $M(P_0,P_i)$.

Filtering with help of fuzzy peer group:
This filter works in 2-steps.
1.Salt and pepper noise detection and correction
2.Gaussian noise smoothing
To reduce Salt and Pepper Noise, a fuzzy rule based procedure is used. First with the help of fuzzy rule based procedure, it is decided that the pixel in interest is corrupted with Salt & pepper noise or not. A threshold value is used to detect corrupted pixel. If a pixel is found to be corrupted, then Vector median filtering is applied to correct those noisy pixels. For Gaussian noise smoothing, fuzzy averaging is done among the members of fuzzy

peer group of the pixel under processing. In Fuzzy averaging, weights are given by the membership function which defines the similarity or how strong they are similar to the peer group of the pixel in interest.

III b.Salt and pepper noise detection and correction

A salt and pepper noise pixel can be defined as a pixel which is significantly different in intensity from its neighborhood pixels. Conversely, a salt and pepper noise-free pixel should have some neighbors quite similar to it. According to the above, we can model this condition in terms of fuzzy peer groups as follows:

A pixel P_0 is free of salt and pepper noise if for the fuzzy peer group $FP^P{}_0(m)$ it is satisfied that $AS^P{}_0(P_m)$ is large and P_m is similar to P_0.Determining the certainty of the pixel P_0 to be free of salt and pepper noise.

The following fuzzy rule 2 represents this condition:

Fuzzy Rule 2: If "$AS^P{}_0(P_m)$ is large" and "Pm is similar to P0" then P0 is free of salt and pepper noise. "P_m is similar to P_0 is given by fuzzy set $C^P{}_0(P_m)$, "$AS^P{}_0(P_m)$ is large" is given by fuzzy set $L^P{}_0(P_m)$. We use the product t-norm as the conjunction operator.

$$\mathbf{C_{FR2}(P_0)= L^P{}_0(P_m)\, C^P{}_0(P_m)} \qquad \mathbf{(6)}$$

It is already calculated in C_{FR1}. So no more computations are required. We will use C_{FR2} to detect and replace salt and pepper noisy pixel according to threshold-based rule. If $C_{FR2}(P_0)>=F_t$ then P_0 is free of salt and pepper noise. Else P_0 is a noisy pixel and replace P_0 with VMF_{out}(Vector median Filtering) where F_t is a parameter.

Gaussian Noise smoothing procedure:

To remove Gaussian noise, a weighted averaging operation is performed among color vectors. So, to smooth the pixel P_0, we use the members of fuzzy peer group $FP^P{}_0(m)$, where the weighting coefficient for each color vector is its membership degree to the fuzzy peer group $FP^P{}_0(m)$. Every pixel is smoothed by weighted averaging operation in following manner:

$$\mathbf{P_{out}} = \frac{\sum_{i=0}^{m} FP\,m^{P0}(Pi)*(Pi)}{\sum_{i=0}^{m} FP\,m^{P0}(Pi)} \qquad \mathbf{(7)}$$

Suggested setting for parameters used

Following are the suggestion for proper setting of parameters that are being used in the filter that is Fq and Ft.

Table 2 :Suggested setting for Ft parameter

Percentage of Salt and Pepper Noise	Ft
Low [in (0,10)]	0.05
Medium [in (10,20)]	0.15
High [in (20,30)]	0.25

Table 3: Suggested setting for Fq parameter

Standard Deviation of Gaussian Noise	Fq
Low [in (0,10)]	50
Medium [in (10,20)]	100
High [in (20,30)]	175

IV. Results

Table 4 represents the values of entropy measure for Majority image and for the results of various approaches: Sobel, Prewitt, Canny and proposed approach. The entropy for results of Sobel and Prewitt is comes out to be smaller than the proposed approach for all the four test images, because they provide less edge information. The canny method gives very thin edges and it does not work on the color images thus there will be information loss in the result, therefore the entropy value obtained using this methods is less than the proposed method.

Table 4: Entropy of different methods

	Canny	Sobel	Prewitt	Proposed method
Lena	2.8616	2.2515	1.6566	2.9818
Penguins	2.6962	1.6316	1.6502	2.7085
Peppers	2.9926	1.8438	1.7062	2.6610
House	2.0682	1.4315	1.4999	2.1286

a)Original images b) Noisy images c) proposed approach

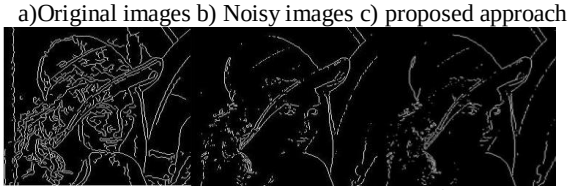

d) Canny e) Sobel f) prewitt

The colour images of Lena Peppers of size 256 * 256 corrupted with the Gaussian and Impulse noise is considered as test images. The performance of the proposed approach is evaluated on test images with density of salt & pepper noise 10% , 15%, 20% and with standard deviation 10, 20, 30. The results of the proposed approach are compared in terms of PSNR with methods "Restoration of images corrupted by mixed Gaussian-impulse noise via l1–l0minimization" (RICMG)[12],"Spatially Adaptive Denoising Algorithm for a Single Image Corrupted by Gaussian Noise" (SADA) [12]. Comparison of PSNR values resulting from applying the proposed filter and the other methods is shown in table 5. Looking at the table we can see the proposed filter is superior in case of PSNR with other method shown in the table. Now we will show denoised image of Lena and Peppers with the outputs of other filters.

a)Original Lena Image

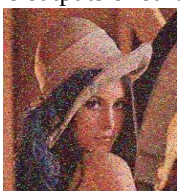

b) Lena Image Corrupted with σ =10 and 10% salt and pepper noise

c) Output of RICMG

d)Output of SADA

e)Output of Proposed Filter

f)Original image

g) Lena Image Corrupted with σ =20 and 20% salt and pepper noise

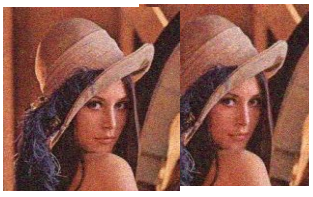

h) Output of RICMG

i)Output of SADA

j) Output of Proposed Filter

Table 5: Comparison of PSNR of Proposed filter with other filter

Standard Deviation	Density of Salt and Pepper Noise	Noisy	RICMG	SADA	Proposed Method
Lena Image					
σ = 10	10%	19.1908	31.0342	30.2316	31.5431
σ = 20	15%	17.2428	29.1864	28.9976	29.7025
σ = 30	20%	16.2325	27.4152	27.6519	28.6229

V. Conclusions

For de-noising an image, first edge detection using modified bacterial foraging algorithm is done on noisy image. Edge map is calculated to keep image edges and sharp features intact. Experimental results showed that our calculated edge map is better in terms of quality as well as visual aspects comparing with any other technique. The entropy value of the presented method is better than any other method. In second step, we have presented a fuzzy peer group technique to denoise the image. To remove Gaussian noise fuzzy weighted averaging is done where weights are given by the membership function used to calculate pixel membership to the peer group. Experimental results showed that our method to denoise the image is better both in qualitative and quantitative measures. We are able to get a better PSNR with other techniques with good visual quality output images. The proposed filter is also able to work on high density of Gaussian and Salt & pepper noise.

References

[1]. A.K.Jain, Fundamentals of digital image processing (Prentice Hall, Englewood Cliffs, 1989)

[2]. Kevin M. Passino, "Biomimicry of Bacterial Foraging", IEEE Control Systems Magazine IEEE, 2002.

[3]. K. N. Plataniotis and A. N. Venetsanopoulos, "Color Image Processing and Applications", Berlin, Germany: Springer, 2000.

[4]. Om Prakash Verma, Madasu Hanmandlu, Anil Singh Parihar and Vamsi Krishna Madasu, "Fuzzy Filters for Noise Reduction in Color Images",ICGST-GVIPJournal, Volume 9, Issue 5, September 2009, ISSN: 1687-398X.

[5]. Om Prakash Verma, Madasu Hanmandlu, Puneet Kumar, Sidharth Chhabra, Akhil Jindal, "A novel bacterial foraging techniquefor edge detection",ScienceDirect Pattern Recognition Letters 32 (2011) 1187–1196.

[6]. D. Van de Ville, M. Nachtegael, D. Van der Weken, W. Philips, I.Lemahieu, and E. E. Kerre, "Noise reduction by fuzzy image filtering," IEEE Transactions on Image Processing, vol. 11, no. 4, pp. 429–436, Apr. 2001.

[7]. F. Russo and G. Ramponi, "A noise smoother using cascaded FIRE filters", Proc. of 4th Intl. Conf. on Fuzzy Systems, Vol.1, pp. 351- 358, 1995.

[8]. Tuan-Anh Nguyen, Won-Seon Song, Min-Cheol Hong, "Spatially adaptive Denoising algorithm for a single image corrupted by Gaussian noise", Consumer Electronics, IEEE Transactions on Volume:56, Issue: 3, 2010 , Page(s): 1610 – 1615.

[9]. Rank, K., Unbehauen, R., "An adaptive recursive 2-D filter for removal of Gaussian noise in images", Image Processing, IEEE Transactions on Volume: 1, Issue: 3, 1992, Page 431 – 436.

[10]. O.P. Verma, A.S. Parihar, M. Hanmandlu, "An Edge Preserving Fuzzy Filter for Color Images", Computational Intelligence and Communication Networks (CICN), 2010 International Conference, on page(s): 122, Print ISBN: 978-1-4244-8653-3, INSPEC Accession Number: 11776685.

[11]. Kenny Kal Vin Toh, Student Member, IEEE, and Nor Ashidi Mat Isa, Member, IEEE, "Cluster- Based Adaptive Fuzzy Switching Median Filter for Universal Impulse Noise Reduction", IEEE Transactions on Consumer Electronics, Vol. 56, No. 4, November 2010.

[12]. Yu Xiao, Tieyong Zeng, JianYu, Michael K.Ng, "Restoration of images corrupted by mixed Gaussian-impulse noise via l1–l0 minimization", Pattern Recognition 4

IOSR Journal of Electronics and Communication Engineering (IOSR-JECE)
e-ISSN: 2278-2834,p- ISSN: 2278-8735. Volume 5, Issue 6 (Mar. - Apr. 2013), PP 08-13
www.iosrjournals.org

Performance Evaluation of Basic Segmented Algorithms for Brain Tumor Detection

[1]Suchita Yadav , [2]Sachin Meshram
[1](Department of ETC / Chouksey Engineering College, Bilaspur India)
[2](Department of ETC / Chouksey Engineering College, Bilaspur India)

***Abstract**: In the field of computers segmentation of image plays a very important role. By this method the required portion of object is traced from the image. In medical image segmentation, clustering is very famous method . By clustering, an image is divided into a number of various groups or can also be called as clusters. There are various methods of clustering and thresholding which have been proposed in this paper such as otsu , region growing , K Means , fuzzy c means and Hierarchical self organizing mapping algorithm. Fuzzy c-means (FCM) is a method of clustering which allows one piece of data to belong to two or more clusters. This method (developed by Dunn in 1973 and improved by Bezdek in 1981) is frequently used in pattern recognition. As process of fuzzy c mean is too slow, this drawback is then removed. In this paper by experimental analysis and performance parameters the segmentation of hierarchical self organizing mapping method is done in a better way as compared to other algorithms. The various parameters used for the evaluation of the performance are as follows: segmentation accuracy (Sa) , area (A), rand index (Ri),and global consistency error (Gce) .*

***Keywords** - area (A), Fuzzy C means, global consistency error (Gce) , HSOM, K means , Otsu , rand index (Ri), Region Growing , segmentation accuracy (Sa) , and variation of information (Vi).*

I. Introduction

The brain is a very important part of the body and is one of the special organ . The brain consists of large number of cells which grow on increasing from third month upto the seven years of age. Each cell has its own special function. When some of the cells in the body grow in an orderly way to generate new cells then the body is healthier. But if cells grow irregularly then various cells which are in excess form a cluster or mass of tissue known as tumor. Brain tumor is one of the most common and deadly diseases in the world. Detection of the brain tumor in its early stage is the key of its cure [1]. Brain tumors may be benign or malignant[2].

The term gray level is often used to refer to the intensity of the monochrome images. In the field of medical, segmentation has wide application . Color images are formed by a combination of individual 2-D images. An image may be continuous with respect to the x and y coordinates and also in amplitude. A continuous image is converted to digital image which requires that the coordinates as well as the amplitude be digitized. By using image segmentation, the image can be divided into various parts such as mutually exclusive and exhausted regions. Image segmentation is an important and challenging factor in the medical image segmentation [3]. The ultimate aim in a large number of image processing applications is to extract important features from the image data, from which a description, interpretation, or understanding of the scene can be provided by the machine .Image segmentation is too complex to be used in image processing and is very sensitive and important component when image is being analyzed. In this paper various methods of image segmentation are used, mentioned as follows : Thresholding such as Region growing, Otsu,Clustering such as k means, Fuzzy cmeans and Hierarchical Self Organizing mapping [4].It utilized the HSOM, thresholding and clustering methods to identify which type of brain tumor suffered by patient regarding to the image of brain tumor from the Magnetic Resonance Imaging (MRI) and scan as inputs for the network and other methods.

II. Problem Description

The required area of an image is exploited by using the undesired component, atmospheric interference. So rather than analyzing the original image, the image segmentation technique is used.Various experiments with published benchmarks are required for this research field to progress [4] .The drawback which occurs in this paper is that image is divided into number of segmentation [5] .This drawback is overcome by selecting an appropriate model for segmentation and then modified with reduced computational time and output is of high quality.

III. Segmentation Of Image By Thresholding And Clustering Methods

Clustering can be taken as a process of partitioning or grouping a given portion which is an unlabeled pattern into a large number of clusters such that a group is assigned to similar patterns. Clustering is used for pattern recognition in image processing, and usually requires a high volume of computation. Thresholding is

the simplest method of image segmentation. From a grayscale image, thresholding can be used to create binary images. During the thresholding process, individual pixels in an image are marked as "object" pixels if their value is greater than some threshold value (assuming an object to be brighter than the background) and as "background" pixels otherwise. This convention is known as threshold above. Variants include threshold below, which is opposite of threshold above; threshold inside, where a pixel is labeled "object" if its value is between two thresholds; and threshold outside, which is the opposite of threshold inside. Typically, an object pixel is given a value of "1" while a background pixel is given a value of "0." Finally, a binary image is created by coloring each pixel white or black, depending on a pixel's labels. The major drawback to threshold-based approaches is that they often lack the sensitivity and specificity needed for accurate classification.

1 Fuzzy C Means Algorithm

The goal of a clustering analysis is to divide a given set of data or objects into a cluster, which represents subsets or a group. The partition should have two properties: 1. Homogeneity inside clusters: the data, which belongs to one cluster, should be as similar as possible. 2. Heterogeneity between the clusters: the data, which belongs to different clusters, should be as different as possible. Clustering is a process to obtain a partition P of a set E of N objects Xi (i=1, 2,…, N), using the resemblance or dissemblance measure, such as a distance measure d. A partition P is a set of disjoint subsets of E and the element Ps of P is called cluster and the centers of the clusters are called centroid or prototypes. Many techniques have been developed for clustering data. In this report c-means clustering is used. It's a simple unsupervised learning method which can be used for data grouping or classification when the number of the clusters is known[4]. It consists of the following steps:
Step 1: Choose the number of clusters - K
Step 2: Set initial centers of clusters c1, c2… ck
Step 3: Classify each vector x [x , x ,....x] T into the closest centre ci by Euclidean distance measure ||xi - ci || = min || xi -ci||
Step 4: Recomputed the estimates for the cluster centers ci. Let ci = [ci1 ,ci2 ,....cin] T
cim be computed by, cim = Σxli ∈ Clter(Ixlim) Ni .Where, Ni is the number of vectors in the ith cluster. Step 5:If none of the cluster centers changes in step 4 stop; otherwise go to step 3.

2 K Means

It is also one of the clustering method and is very famous because it is simpler and easier in computation. It is the simplest unsupervised learning algorithms that solve the well known clustering problem. It classifies the input data points into multiple classes based on their intrinsic distance from each other. The algorithm assumes that the data features form a vector space and tries to find natural clustering in them[4]. The algorithm which follows for the k-means clustering is given below: The cluster centers are obtained by minimizing the objective function :

xi ∈ si ..... (1)

*1.*Initialize the centroids with k random values. 2. Repeat the following steps until the cluster labels of the image do not change anymore. 3. For each data point, we calculate the Euclidean distance from the data point to the mean of each cluster :

C (i) = arg min || x (i) - μ_j ||^2 ……..(2)

If the data point is not closest to its own cluster, it will have to be shifted into the closest cluster. If the data point is already closest to its own cluster, we will not shift it. 4. Compute the new centroid for each of the clusters. Where *k* is a parameter of the algorithm (the number of clusters to be found), i iterates over the all the intensities, *j* iterates over all the centroids and μ_i are the centroid intensities.

3 Region Growing

Region growing comes under region-based segmentation method [5]. In this an image is partition into regions. There is predefined criteria where there are k clusters Si , i= 1,2,….,k and μ_i is the centroid or mean point of all the points, according to which groups of pixels are formed or groups of sub-regions are formed into larger regions as a result region growing takes place If suppose there is no priori information, then the procedure is to compute at every pixel the same set of properties that ultimately will be used to compute at every pixel the same set of properties that ultimately will be used to assign pixels to regions during the growing process.

4 Otsu Method

In image processing, Otsu's method is used for thresholding [6] of image by histogram method which is done automatically. The gray level image is converted to a binary image. In this method, the image on which this thresholding process has to be done is done in such a way that there are two models of histogram, known as bimodal histogram of the image. In other words, there are two classes of pixels one is background and other is

foreground. In image segmentation, the sub-division of image is done by using intensity of background and object. So both the different regions are then distinguished by a suitable value of threshold value. It consists of two classes within class variance and between class variance. In Otsu's method the value the threshold is chosen such that it minimizes the intra-class variance, defined a weighted sum of variances of the two classes :

$\sigma^2_{\omega}(t) = \omega_1(t)\,\sigma_1^2(t) + \omega_2(t)\,\sigma_2^2(t)$ ……..(3)

$\omega 1$ & $\omega 2$ are weights, probabilities of the two classes separated by a threshold and variances of these classes.In this, threshold operation is done in such a way that an image is sub-divided into two classes R0 and R1 at gray level t. Let partitioning of the pixels is done between objects and background. Therefore, R_0 = {0, 1, 2, ….t} and R_1 = {t+1, t+2 … L-1}. The within-class variance, between class variance, and the total variance are denoted by σ_{2w}, σ_{2b}, and σ_{2T} respectively. So an optimal value of threshold is obtained by minimizing one of the following (equivalent) criterion functions with respect to :

t = Arg Min η ……..(4)

The value of η lies between 0 & 1. There are two limits in the value of η. Where when η= upper limit = 1, then only two-valued images are given and when η= lower limit = 0, then only single constant gray-level is given.

5 Hierarchical Self Organizing Mapping (HSOM)

A self organizing map (SOM) comes under unsupervised learning of feedback networks. SOM is another type of neural networks also known as SOFM (Self Organizing Feature Maps).As in the brain, SOM also has self organization property. There is direct connection between input and output devices, and output nodes are also interconnected (different from general feed forward NN).The weights of the output nodes will be adjusted based on the input connected to them, and also the weights of the neighborhood output nodes. Therefore, output nodes will be ordered in a natural manner. Similar nodes will be close to each other. There are two modes in which SOMs operate, such as : training and mapping. Training is a competitive process, also called vector quantization. Mapping automatically classifies a new input vector. The HSOM is the extension of the conventional self organizing map used to classify the image row by row. In this lowest level of weight vector, a higher value of tumor pixels, computation speed is achieved by the HSOM with vector quantization. In the field of medical, segmentation has wide application. The hierarchical self organizing map has been used for multi scale image segmentation. The combination of self organization and graphic mapping technique is known as HSOM. Here hybrid technique is used which has the advantages of HSOM, so as to implement for the MRI image segmentation. MR brain image is loaded into MATLAB 7.0. in the form of matrix. Next initialize the variables sigma, weight vector and winning neuron .In that Calculate the neighborhood function, weight vector and winning neuron .Here neuron is the input and winning neuron is the output [3].

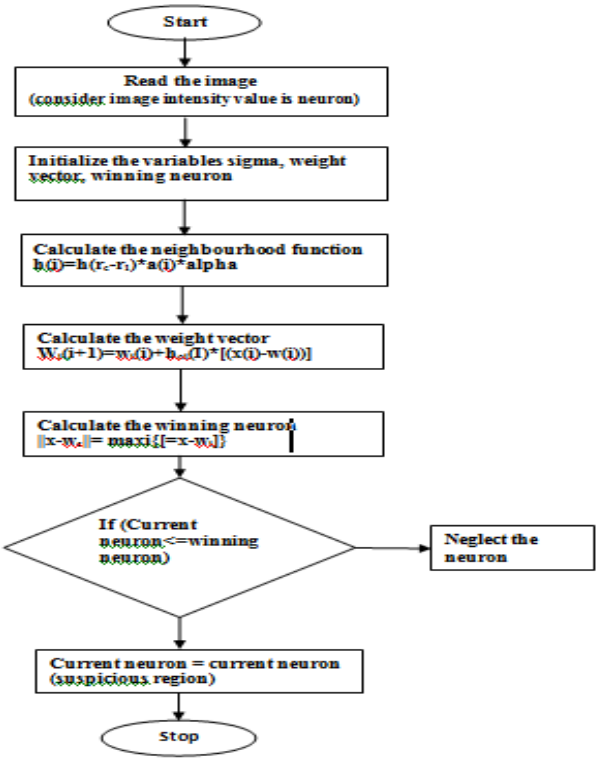

Fig 3.1 : Flow chart of HSOM Method

IV. Results And Discussion

The proposed algorithms have been implemented using MATLAB. Here various methods of image segmentation are analyzed and discussed. In this system, based on the power of Artificial Neural Network (ANN), a computer-aided brain tumor diagnosis based on hierarchical Self Organizing Mapping is done. It is too much complex to measure the segmentation of image because of no common algorithm. So in order to measure the quality of segmentation of image the statistical measurements are used. The experiment is conducted over the five MRI images using the algorithms Hierarchical Self Organizing mapping, Region Growing, Otsu,K Means and FCM. To evaluate the performance various parameter values are found such as rand index (Ri), global consistency error (Gce), segmentation accuracy (Sa), variations of information (Vi), and area (a).

Rand Index : The Rand index (RI) counts the fraction of pairs of pixels and pixels are those whose labeling are consistent between the segmentation which was computed and the ground truth averaging across multiple ground truth segmentations.

Global Consistency Error : The Global consistency error (Gce) measures the extent by which one segmentation can be viewed as a refinement of the other.

Variation of Information : The variation of information (Vi) represents the distance between two segmentations as the average conditional entropy of one segmentation given the other, and as a result measures the amount of randomness in one segmentation which cannot be explained by the other.

In this paper the comparison of methods i.e. cluster based algorithms, thresholding algorithms and hierarchal self organizing mapping algorithms was done and HSOM was found as the best method for image segmentation .Fig 4.1(a) shows the original MRI image, Fig 4.1(b) shows the ground truth image, Fig 4.1(c) shows the segmented image of HSOM method, Fig4.1(d), (e),(f) and (g) shows the segmented images of Region Growing, Otsu,K Means and FCM respectivly.Table4.1 shows the Segmentation Accuracy of different MRI Images which is best for HSOM method as compared to other methods. Table 4.2 shows Areas of Ground Truth Images and Segmented Images.Table 4.3 shows Performance Parameters for different methods.Table 4.4 shows Average values of Ri, Gce and Vi for various methods. The Graph 4.1 shows the comparison of performance parameters for various methods. The Graph shows the comparison of average values of rand index, average values of global consistency error,and average values of variation of information for various methods. For better performance Ri should be higher comparatively, Gce and Vi should be lower which is clear from the Graph 4.1. The performance parameters chart reveals that the rand index of hierarchical self organizing mapping is higher than others while the global consistency error and variation of information error of hierarchical self organizing mapping is lower than others.

Fig 4.1: Results of Different MRI Images by applying various methods shown in the fig (a) Original Image, fig (b) Ground Truth image fig (c) to fig (g) Segmented Images of HSOM, Region Growing , Otsu , K Means , FCM

For image-1

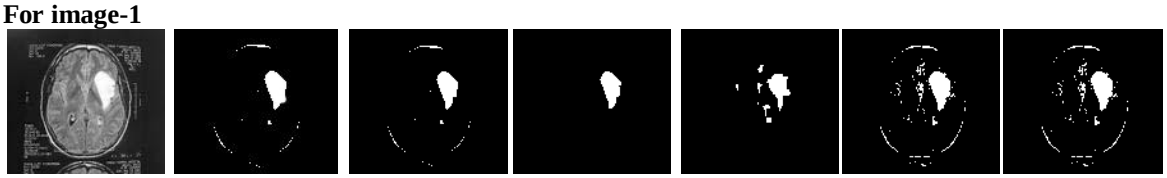

Fig (a) (b) (c) (d) (e) (f) (g)

For image-2

For image-3

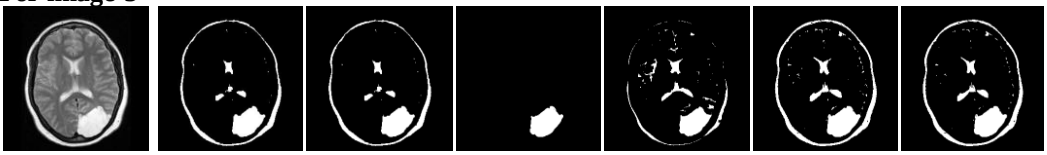

For image-4

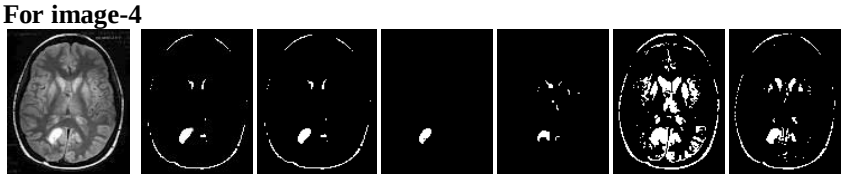

For image-5

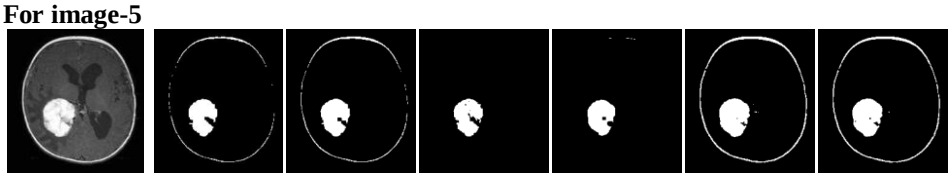

Table-4.1 : Segmentation Accuracy of different MRI Images

Images	Methods	Hierarchical Self Organizing Mapping	Region Growing	Otsu	K means	Fuzzy C means
1	Segmentation Accuracy	94.6622	91.7153	89.8599	167.5377	107.9257
2		96.2918	96.0347	91.2184	93.5783	97.9332
3		99.0744	93.5562	89.6722	70.1631	103.721
4		93.6552	89.3195	67.9729	169.8229	135.7683
5		99.4895	100.0756	96.8309	70.7531	116.6366

Table-4.2 : Areas of Ground Truth and Segmented Images

Images	Methods	Hierarchical Self Organizing Mapping	Region Growing	Otsu	K means	Fuzzy C means
1	Area 1 (Ground Truth Image)	8.9322	8.9415	8.9608	8.948	8.944
	Area 2	8.4554	8.2007	8.0522	14.9913	9.6529
2	Area 1 (Ground Truth Image)	34.2238	34.1763	34.1872	34.2281	34.2142
	Area 2	32.9548	32.8242	31.185	32.0301	33.5071
3	Area 1 (Ground Truth Image)	82.8334	83.0213	83.3506	83.3506	83.3621
	Area 2	82.0667	77.6715	74.7423	58.4813	86.464
4	Area 1 (Ground Truth Image)	2.9107	2.9229	2.913	2.9107	2.9129
	Area 2	2.726	2.6107	1.98	4.93	3.9548
5	Area 1 (Ground Truth Image)	54.7087	54.7087	54.6859	54.6933	54.6814
	Area 2	54.4274	54.75	52.93	38.6972	63.7785

Table 4.3 : Performance Parameters for different methods

Images	Methods/ Parameters	Hierarchical Self Organizing Mapping	Region Growing	Otsu	K means	Fuzzy C means
1	Rand Index	0.9037	0.7866	0.7118	0.7438	0.7499
	Global Consistency Error	0.2713	0.4426	0.5639	0.5305	0.5458
	Variation of Information	1.7587	3.3427	4.4336	4.3895	4.5025
2	Rand Index	0.956	0.8808	0.7845	0.7767	0.834
	Global Consistency Error	0.1365	0.2957	0.3957	0.4105	0.3457
	Variation of Information	0.9222	2.2362	3.2923	3.7277	2.8733
3	Rand Index	0.9764	0.8009	0.7687	0.818	0.8347
	Global Consistency Error	0.1134	0.3446	0.453	0.3919	0.3738
	Variation of Information	0.7604	3.1271	3.8279	3.3293	3.0942
4	Rand Index	0.9228	0.7184	0.6667	0.6793	0.7108
	Global Consistency Error	0.1543	0.3534	0.4765	0.6056	0.5579
	Variation of Information	1.1188	3.0827	3.9671	4.9737	4.1204
5	Rand Index	0.9794	0.823	0.7865	0.7735	0.776
	Global Consistency Error	0.1102	0.3734	0.3951	0.3691	0.3576
	Variation of Information	0.6893	3.1773	3.4585	3.3129	3.2637

Table 4.4: Average values of Parameters for different methods

Methods	Rand Index	Global Consistency Error	Variation of Information
Hierarchical Self Organizing Mapping	0.94766	0.15714	1.0498
Region Growing	0.80194	0.36194	2.9932
OTSU	0.74364	0.45684	3.79714
K MEANS	0.75826	0.46152	3.94662
FUZZY CMEANS	0.78108	0.43616	4.5025

Graph 4.1 : Comparison of Average Values of Ri, Gce & Vi from Various methods

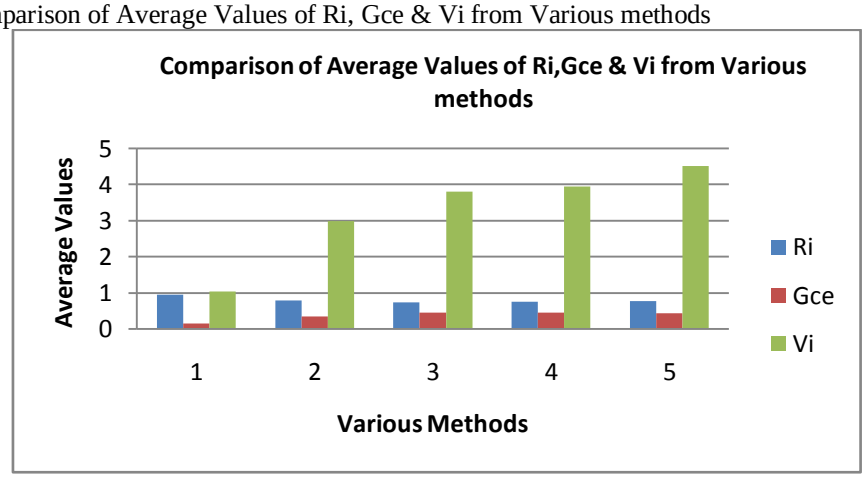

In this graph 4.1 axis of various methods showing 1, 2 ,3 ,4 and 5 which represents HSOM, Region Growing , Otsu, K Means and Fuzzy CMeans methods respectively.

References

[1] Arjan Simonetti , "Investigation of brain tumor classification and its reliability using chemometrics on MR spectroscopy and MR imaging data",2004.

[2] Noworolski , S.M.; Nelson, S.J.; Henry, R.G.; Day, M.R.; Wald, L.L.; Star-Lack, J.; Vigneron, D.B. Magnetic resonance in medicine 1999, 41, 21-29.

[3] T.Logeswari1 and M.Karnan2,"An improved implementation of brain tumor detection using segmentation based on soft computing",Journal of Cancer Research and Experimental Oncology Vol. 2 pp. 06-014, March, 2010.

[4] B.Sathya and R. Manavalan ,"Image Segmentation by Clustering Methods: Performance Analysis", IJCA vol 29-No.11,September 2011.

[5] Rafael C.Gonzalez and Richard E. Woods,"Digital Image Processing",Second Edition,Prentice Hall of India Private Limited ,New Delhi – 2007.

[6] OtSu NA. "Threshold selection method from aray level histogram". IEEE Trans. On system, man, and cybernetics. Vol. 9. No. 1. Pp. 62-66, 1979.

[7] Krishna Kant Singh and Akansha Singh, "A study of Image Segmentation Algorithms for Different Types Of Images", IJCSI International Journal of Computer Science Issues 2010.

[8] Mrs. Bharati R. JipKate et al., A comparative Analysis of Fuzzy C-Means Clustering and K-Means Clustering Algorithm", IJCER / May-June, 2012 / Vol. 21 / Issue No. 3 / 737-739.

[9] M. Sezgin and B. Sankur (2004). "Survey over image thresholding techniques and quantitative performance evaluation". Journal of Electronic Imaging 13(1) : 146-165.

IOSR Journal of Electronics and Communication Engineering (IOSR-JECE)
e-ISSN: 2278-2834,p- ISSN: 2278-8735. Volume 5, Issue 6 (Mar. - Apr. 2013), PP 14-18
www.iosrjournals.org

Effects of EM Radiation on Living System

P.gauthamipriyadarshini[1], C.H.R.Phani kumar[2]
[1](*Second M.tech RF and MICROWAVE ENGINEERING, GITAM university, Visakhapatnam, India)*
[2](*Assistant Professor/ Dept of ECE, GITAM University, Visakhapatnam,, India)*

Abstract : *Electrical excitability and signaling frequently associated with rapid responses to environmental stimuli, as well as in some algae and some higher plants. The presence of electrical signal, such as action potentials (AP) in plant cells suggested that plant cells, too, make use of ion channels to transmit information over long distances. In the light of rapid progress in plant biology during the past decade, the assumption the electrical signals donot only trigger rapid leaf movements in sensitive plant such as mimosa pudica, the electromagnetic radiations may also cause effect on mechanical and electrical stimulis. Summarizing recent progress in the field of electromagnetic radiation on plants, the present review will focus on the mechanical and electrical stimuli of plants.*

Keywords *– Electromagnetic radiation, Electrical signal, Mimosa pudica, Mechanical and electrical stimulis.*

I. INTRODUCTION

Mobile phone companies often sell more batteries than phones to consumers. The phones sold to user include a rechargeable battery so that the device is immediately useful, but a certain number of consumers are expected to own more than one battery during the life of their phone. The same can probably be said for laptops and camcorders. Yet, there is little incentive for consumers to buy new batteries except for when they fail or when the consumer feels the need for a larger battery. Unlike other areas of mobile computing that benefit from exponential improvements in performance, battery energy density changes slow that there is little pressure for consumers to upgrade. Wireless connectivity is also a conundrum for mobile designers. While the designer can control the CPU, RAM, disk, and battery in his device, wireless connectivity is often provided by another party. In the extreme case, a wireless provider may go out of business and significantly impact the quality of service that can be expected. Even on a minute – by – minute basis a, wireless connection may or may not be available at any given moment. The device designer must either cache information for the user or refuse service when the network is not available. Many RF transmitters of various sorts distributed throughout today's urban environments, one might consider background RF as a potential power reservoir for mobile devices. Electronic systems that harvest energy from ambient radiation sources, however, tend to be extremely power-limited and generally require a large collection area or need to be located very close to the radiated sources. A classic example can be found in old –fashioned crystal radio kits that draw their power directly from Am radio stations, which play audibly through high - impedance headphones without needing a local source of energy. The size of the require antenna, however can be prohibitive for wearable applications unless the bearer is very close to the transmitter, and access to a good ground is usually required. Capturing enough energy from vibrations to power sensors and telemetry has a long history in vehicles, where considerable mechanical excitation is usually available. In the patent literature, one can find techniques ranging from linear motor generators with bouncing spring- mounted magnet arrays for use in trucks and trains to piezoelectric generators embedded in tires and wheels for monitoring air pressure and tire conditions. In this project we want to analyze the effects of electromagnetic radiation on living system. We want to perform the experiment on Mimosa pudica seeds. The reason for selecting Mimosa pudica seeds for the experiment is that they assure the fast growth. The objective of the project is to carry the effects of electromagnetic radiation based on various parameters. The methods followed by analyzing the radiation effects are discussed.

II. Methodology

2.1 Radiating The Seeds:

The seeds which are collected are using a microwave bench setup and horn antenna. The setup works in microwave x-band range and the frequency of the microwaves is found to be 10MHz.
The seeds are divided into six categories:

1. Seeds that are not radiated.
2. Seeds that are radiated for 10 min.
3. Seeds that are radiated for 20 min
4. Seeds that are radiated for 30 min
5. Seeds that are radiated for 45 min

6. Seeds that are radiated for 60 min

2.2 Planting The Seeds:

Plants grown in pots mixture of sandy, gravel and peat, were used. Plants were grown in a greenhouse at 15-22°c, in normal humidity and without artificial light.

Fig: 1 Mimosa pudica plants

2.3 Analysis Of Electromagnetic Radiation Effects On Plants Based On Physical Growth :

In this type of analysis we want to analyze the effects of electromagnetic radiations based on physical growth. The growth of the plant is analyzed based on the size of the leaf, leaflet size and closing of leaves. Averaging concept is used for more accurate results.

2.4 Comparision Of Closing Of Leaves:

The leaf is attached to its stalk exhibited the opening-closing movements in response to light stimulis. Closing leaves in response to physical stimuli present several energetic challenges for mimosa pudica. The leaf folding behavior of mimosa pudica has benefits for the plant. The leaf folding was a mechanism for reducing nutrient loss in response to rainfall.

2.5 Comparision Of Leaf Let Size:

The leaf let are measured for every week. In order to achieve better accuracy have used averaging concept. We have measured the leaflet of five leaves one from each plant of every sample and averaged them, which gives average leaflet of leaf. The access of the leaf movement quantitatively, we devised. This tool can be folded small in order to adjust to the opening angle between the main vein of a leaflet and stalk of the excised leaf, and makes the measurement of the leaflet opening angle and quick and accurate.

III. Circuit Design For Action Potential

The values of action potentials of living organisms are very small. Hence we are using a transducer unit for visualizing the signal in a better way. The design of transducer unit is discussed in this chapter.

The design of development transducer unit includes three subunits:

1 .A high sense amplifier
2. A Butterworth filter
3. A voltage to current converter

3.1 High Sense Amplifier:

An amplifier is a device for increasing the power of a signal by use of an external energy source. Here we are using voltage amplifier. Generally the action potentials of the plants are very small. Hence we need a high sense amplifier for amplifying this voltage. The simulation of the high sense amplifier is carried using top spice simulation software. The schematic drawn in the top spice simulation is as shown.

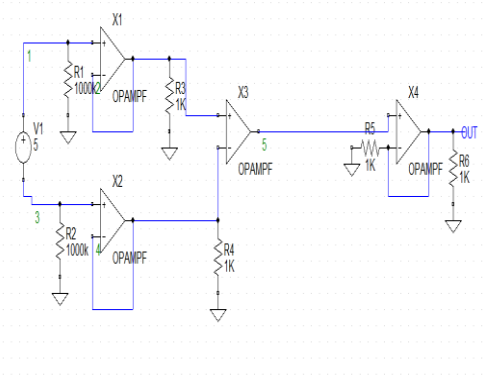

Fig 2: high sense amplifier –schematic diagram

The high sense amplifier is very much essential for the amplification of the small voltages. The graph of the amplifier output versus amplifier input is as shown.

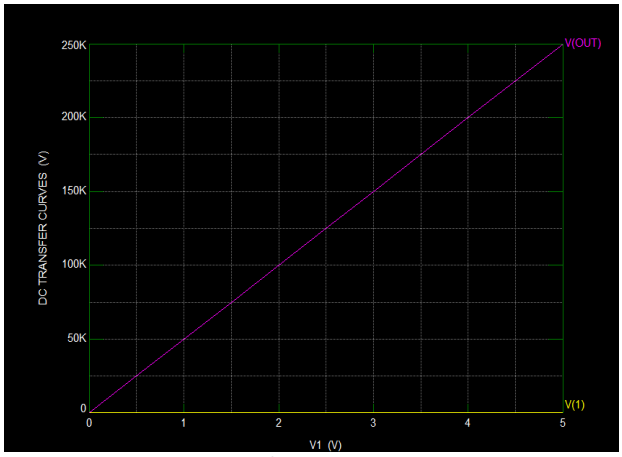

Fig 3 : High Sense Amplifier- Input Signal Vs Output Signal

3.2 8TH ORDER BUTTERWORTH FILTER:

Amplifier input is given to butterworth filter. The butterworth filter is very essential in transducer unit. . Due to high amplification the noise levels also may raise. To filter the unwanted noise components we need a butterworth filter. For good filtering we are using 8th order Butterworth filter.

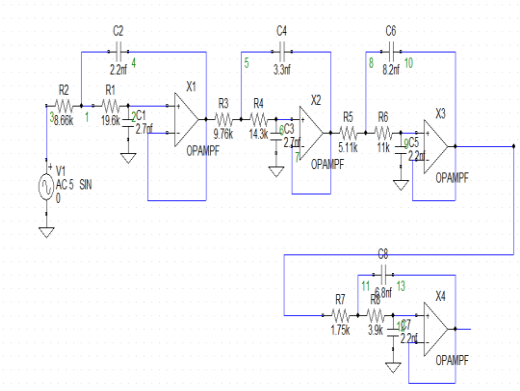

Fig 4 : 8th order buttrworth filter- schematic diagram

The butter worth filter designed with a cutoff frequency 2KHz.The frequency response of the Butterworth filter obtained from the simulation as shown.

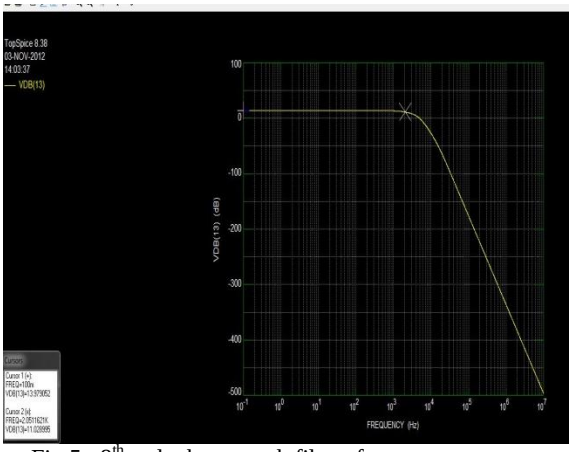

Fig 5 : 8th order buttrworth filter- frequency response

3.3 Voltage To Current Converter:

A voltage to current converter is also used in the transducer. . For transmission, was designed a high sense Voltage to Current converter. The circuit is shown in Fig. 7 is used so that the signal could be transmitted reliably.

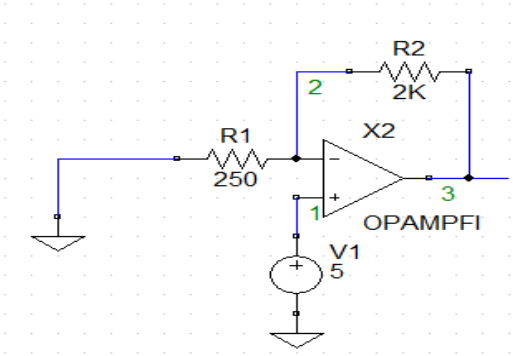

Fig 6:Voltage to current converter-schematic diagram

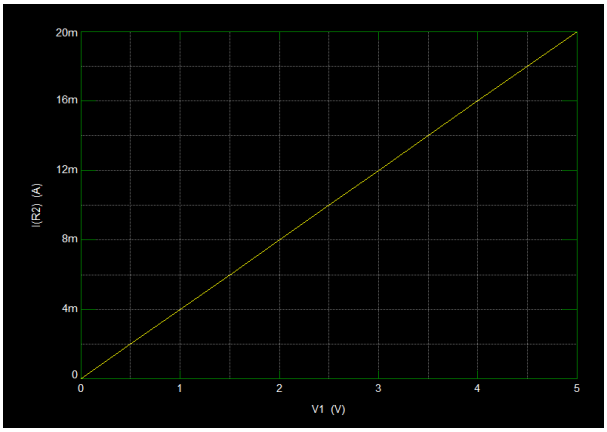

Fig 7 : Voltage to current converter-input voltage vs output current

IV. Conclusion

The communication plays a major role in our day to day life. Microwaves play a key role in various communication technologies now days. But these microwaves are harmful to living organisms. From the above analysis we know that microwave radiation shows a negative impact on plants growth. From the image histograms we can observe that the intensity of green component is more in no radiated leaf than the others. The green component intensity of leaf decreases as time of radiation increases. We can conclude based on image thresholding results that the spots are increasing as the radiation time is more. The analysis based on action potentials will be done and the results will be compared with biological analysis.

REFERENCES

Journal Papers:

[1]. Jensen, Evelyn L., Lawrence M. Dill, and James F. Cahill Jr. "Applying behavioral-ecological theory to plant defense: Light-dependent movement in Mimosa pudica suggests a trade-off between predation risk and energetic reward." *The American Naturalist* 177.3 (2011): 377-381.

[2]. Jackson, Douglas J., et al. "Portable high-voltage power supply and electrochemical detection circuits for microchip capillary electrophoresis."*Analytical chemistry* 75.14 (2003): 3643-3649.

[3]. Neshatvar, Nazanin. *DESIGNING LOW FREQUENCY IC FILTER USING PSEUDO RESISTOR FOR BIOPOTENTIAL MEASURMENTS*. Diss. American University, 2010.

[4]. Kocher, Mark J., and Robert L. Steigerwald. "An AC-to-DC converter with high quality input waveforms." *Industry Applications, IEEE Transactions on* 4 (1983): 586-599.

IOSR Journal of Electronics and Communication Engineering (IOSR-JECE)
e-ISSN: 2278-2834,p- ISSN: 2278-8735. Volume 5, Issue 6 (Mar. - Apr. 2013), PP 19-23
www.iosrjournals.org

Design, Electrostatic and Eigen Frequency Analysis of Fixed–Fixed Beam MEMS Resonator

Deepak Kumar[1], A. Vimala Juliet[2]
[1, 2](Department of Instrumentation & Control Engineering / SRM University, India)

Abstract : *The objective of this paper is to design of fixed–fixed MEMS Resonator. The beam of resonator is made up of poly-silicon. This paper also presents the electrostatic and Eigen frequency analysis of MEMS resonator. The resonator used in oscillator which can be fabricated on chip. It can also be used as Switch. The size of crystal oscillator is in order of centimeter but the size of MEMS Resonator is in order of microns, so by replace a crystal oscillator by MEMS Resonator, we can reduce the size of the system. The dc voltage is given to the beam of resonator for electrostatic analysis & Eigen frequency analysis in different modes.*

Keywords - *MEMS Resonator, fixed-fixed beam, mechanical restoring force;*

I. INTRODUCTION

Micro-Electro-Mechanical Systems (MEMS) are a latest technology in area of mechanical, electrical, electronics and chemical engineering. Micro-Electro-Mechanical Systems, or MEMS, consists of mechanical, electrical systems whose order of size in microns. It is a technology used to miniaturize systems. Electrical components such as inductors and tunable capacitors can be improved significantly compared to their integrated counterparts if they are made using MEMS and Nanotechnology [7]. Resonator is a system that having resonant behavior, it oscillates at some frequencies, called its resonant frequencies. MEMS Resonator is normally used in analog systems, communication systems, switches etc. MEMS resonators are basically time based generators or references whose operating principle is similar to the mechanical tuning fork which is used to tune musical instruments [7]. The oscillations in a resonator can be either electromechanically or electromagnetic. MEMS Resonator have high quality factor as compared to crystal oscillator. Crystal oscillator is bulky and cannot be integrated in IC technology [6]. This paper presents a fixed-fixed beam MEMS Resonator. The resonating beam is fixed at both end, called Anchor that is why called fixed-fixed Resonator. In this paper, fixed–fixed beam resonator is modeled by COMSOL Multiphysics software. The MEMS resonator is designed on silicon-on insulator (SOI). A lot of modes of vibration can be found in a rectangular plate resonator either by changing the thickness of electrodes or by changing the mode number.

II. PRINCIPLE

The principle of operation of MEMS Resonator based upon a two electrodes of a capacitor. One electrode is fixed and other is moving called Resonator beam. When an voltage is applied between a fixed–fixed beam and the pull-down electrode, an electrostatic force is induced on the beam. Due to the Electrostatic force the beam will bend and beam will oscillates by applying ac signal at fixed electrode. The resonance frequency is given by [2], [1], [3]

$$f_0 = 1.03\sqrt{\frac{E}{\rho}}\frac{h}{L^2} \tag{1}$$

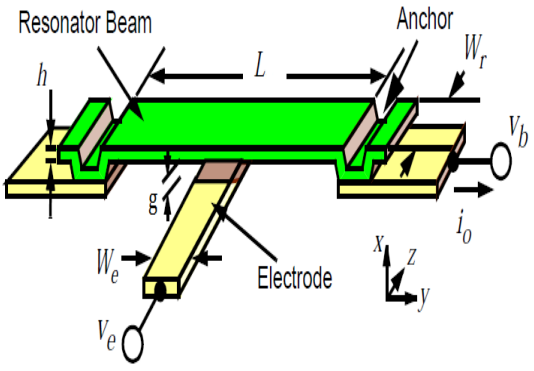

Fig. 1. Fixed-Fixed beam resonator

Suppose V_e is the voltage applied to the electrode and V_b is the voltage applied to the beam, then the effective voltage (V_e - V_b) is applied across the electrode to resonator capacitor gap, due to this a force will induced on a beam and amount of force is [4]

$$F_b = \frac{\partial E}{\partial X} = \frac{1}{2}(V_e - V_b)^2 \frac{\partial C}{\partial X} \quad (2)$$

Where x is the displacement and ∂C is the change in capacitance between electrodes.
The electrostatic force which is on the plates of a capacitor under an applied voltage is modelled as a parallel-plate capacitor. Given that A is the effective area of the beam, which is overlapped by pull-down electrode, the parallel plate Capacitance is [5]

$$C = \frac{\varepsilon_0}{g} A \quad (3)$$

Where, g is the height of the beam above the electrode. Energy stored in electrode which act as parallel plate capacitor is

$$E = \frac{1}{2} CV^2 \quad (4)$$

The electrostatic force act on a resonator beam is given by [5]

$$\mathrm{F_e} = \frac{1}{2} \mathrm{V}^2 \frac{dC(g)}{dg} = -\frac{1}{2} \frac{\varepsilon_0 A V^2}{g^2} \quad (5)$$

Where, V is the Voltage applied between the beam and the electrode.
Equating the applied electrostatic force with the mechanical restoring force due to the stiffness of the beam (F = k x), we find [5]

$$\frac{1}{2} \frac{\varepsilon_0 A V^2}{g^2} = k(g_0 - g) \quad (6)$$

where, g_0 is the zero-bias bridge's height. Solving this equation for the voltage results in

$$V = \sqrt{\frac{2k\, g^2 (g_0 - g)}{\varepsilon_0 A}} \quad (7)$$

The spring constant K of a fixed-fixed beam is [5]

$$K = 32\, Ew \left(\frac{h}{L}\right)^3 \quad (8)$$

Where, E is Young's modulus
h is the thickness of a beam
L is the length of a beam
w is the width of a beam .
The condition for which the resonator beam will be stable under electrostatic force is given by

$$\frac{dV}{dg} = 0 \quad (9)$$

By solving the equation we get

$$g = \frac{2}{3} g_0 \quad (10)$$

This is a result of the beam position becoming unstable at (2/3)g_0, which is due to positive feedback in the electrostatic actuation. At (2/3) g_0 the increase in the electrostatic force is greater than the increase in the restoring force, resulting in a beam position becoming unstable and collapse of the beam to the down-state position. The pull-down voltage is found to be

$$V_p = \sqrt{\frac{8k{g_0}^3}{27\varepsilon_0 A}} \quad (11)$$

III. ANALYSIS

The analysis of MEMS Resonator is done by using software COMSOL Multiphysics. The Resonator has some dimensions which are given in table I.
The Materials used in MEMS resonator:

- Poly Silicon (Electrode)
- Silicon Nitride (Insulator)
- Air (Dielectric)

The poly-silicon material has a varied number of properties which are given in table II.
Fig. 2 shows the design of a MEMS Resonator. The model was introduced in air as a dielectric.

TABLE 1. Dimension of model

Dimension	**Value**
Length of beam (L)	50μm
Width of beam (W)	10μm
Thickness of beam (h)	2μm
Gap spacing (g)	8μm

3.1 Electrostatic Analysis

In electrostatic analysis of MEMS Resonator, dc voltage is given to the beam and fixed electrode is kept as a ground. As a voltage is applied the electric field is generated which puts a force on a beam. The pull-down voltage is given by equation (9)

$$V_p = \sqrt{\frac{8kg_0{}^3}{27\varepsilon_0 A}}$$

3.2 Eigen Frequency Analysis

In Eigen frequency analysis there are 6 modes of frequencies. The lowest frequency for which these stationary waves are formed is called fundamental harmonic. The modes of oscillation have different shapes for different frequencies. The Fundamental frequencies is given by

$$f_0 = 1.03\sqrt{\frac{E}{\rho}}\frac{h}{L^2}$$

(Length) L = 50 µm
(Thickness) h = 2 µm
E=160x10^9 Pa
ρ=2320 Kg/m^3
f_0 = 1.03 [160x10^9/2320]$^{-2}$ x 2 x 10^{-6} / (50x10^{-6})^2
= 6.84 MHz
But the simulated frequency is 7.09 MHz.

TABLE 2. Properties of Material

Property	**Value**
Relative Permittivity	4.5
Density (ρ)	2320 kg/m^3
Young's modulus (E)	160× 10^9 P_a
Poisson's Ratio	0.22

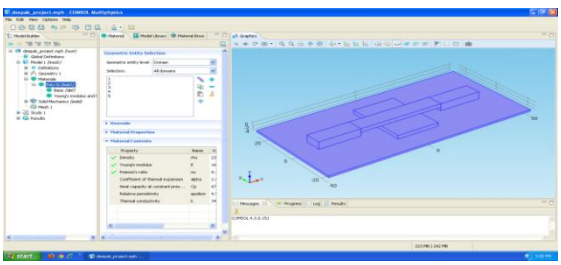

Fig. 2. Design of Resonator

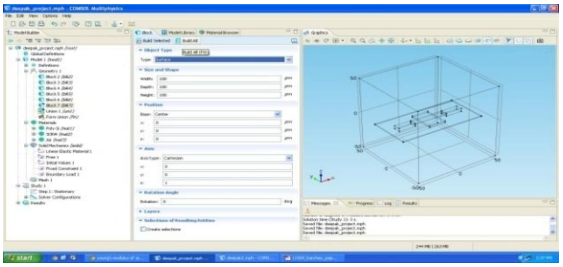

Fig. 3. Model Introduce in Air Dielectric

3.3 Analysis using COMSOL Multiphysics

For Eigen frequency analysis, the physics included for the analysis were Electrostatic (es), Solid Mechanics (solid) and study included for the analysis were Eigen Frequency Analysis. The figure shows a simulation results for all modes.

Fig. 4. shows Resonator Beam oscillates Sinusoidal having maximum displacement in middle.
Fig. 5. shows 1st half of the resonator beam oscillates sinusoidal and 2nd half oscillates opposite to the 1st.
Fig. 6. Shows 1st Front half of the resonator beam oscillates sinusoidal and 2nd Back half oscillates opposite to the 1st.
Fig. 7. Shows only half part of the Resonator Beam oscillates Sinusoidal.
Fig. 8. Shows Resonator Beam oscillates sinusoidal in 3 parts .1st and 2nd oscillates opposite to the 2nd part.
Fig. 9. Shows 1st half of the resonator beam oscillates same as mode 2 and 2nd half oscillates opposite to the 1st.

TABLE 3. Frequencies of different mode

Modes	**Frequency**
Mode 1	7.09 MHz
Mode 2	30.08 MHz
Mode 3	34.37 MHz
Mode 4	35.63 MHz
Mode 5	59.16 MHz
Mode 6	71.55 MHz

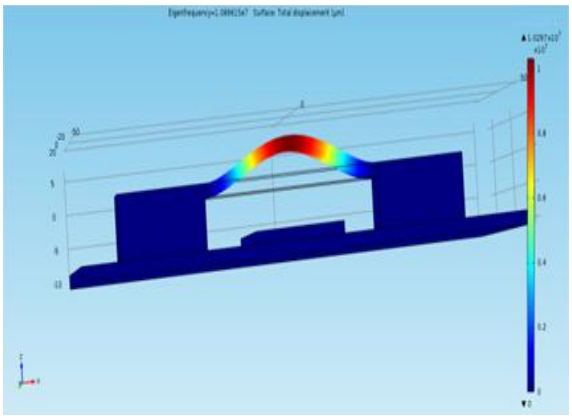

Fig. 4. Mode 1, f_0=7.09 MHz

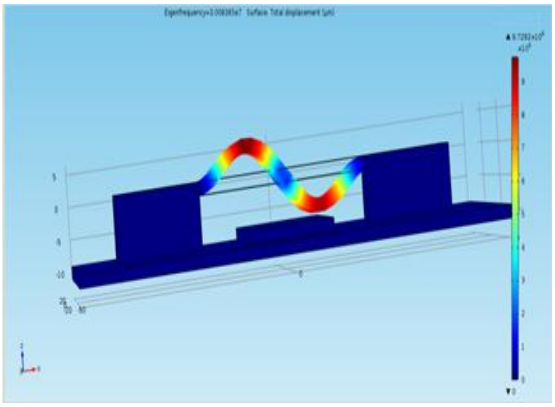

Fig. 5. Mode 2, f_0=30.08 MHz

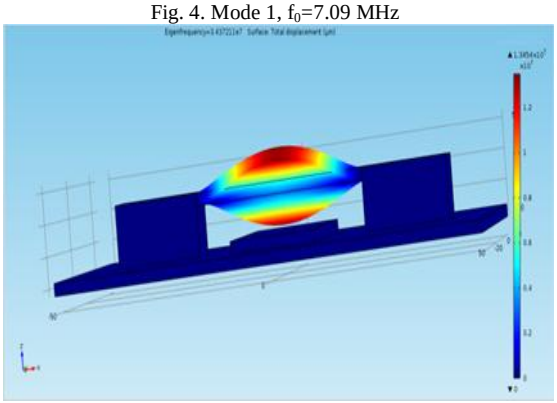

Fig. 6. Mode 3, f_0=34.37 MHz

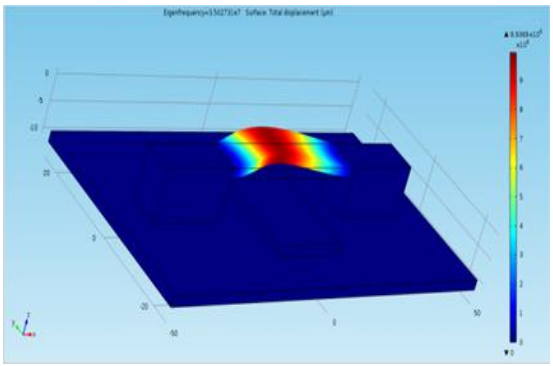

Fig. 7. Mode 4, f_0=35.03 MHz

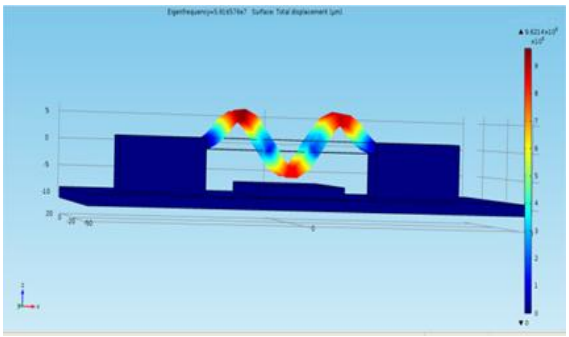

Fig. 8. Mode 5, f_0=59.16 MHz

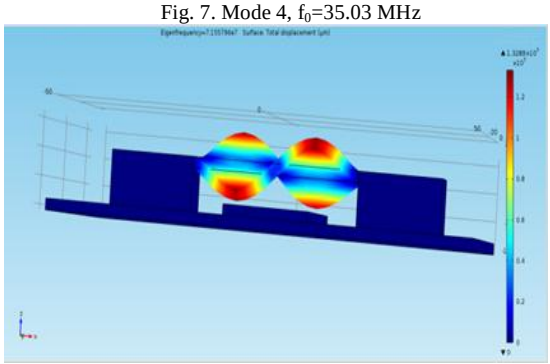

Fig. 9. Mode 6, f_0=71.55 MHz

IV. CONCLUSION

In simulation, we analyzed the Eigen frequencies of fixed-fixed resonator beam. There are six possible modes of frequencies. 1st mode has fundamental frequency 7.09 MHz, also we get different modes with higher frequencies. This method is not limited to fixed-fixed MEMS resonator, this analysis can also be done in other models of MEMS Resonator. Poly-silicon MEMS resonators have been demonstrated up to 71.55 MHz frequencies

REFERENCES

[1] Frederic Nabki, Karim Allidina, Faisal Ahmad, Paul-Vahe Cicek, Mourad N. El Gamal, "Highly Integrated 1.8 GHz Frequency Synthesizer Based on a MEMS Resonator" *IEEE Journal of solid-state circuits, Vol. 44, No. 8, August 2009*, 2154-2168.

[2] G.Meenakshi sundaram, Mahesh Angira, Kamaljit Rangra "Design and Simulation of two port RF MEMS Resonator" *International Conference on Computer Communication and Informatics (ICCCI -2012), Jan. 10 – 12, 2012, Coimbatore, INDIA.*

[3] Vivek Harshey, Amol Morankar, Dr. R.M. Patrikar "MEMS Resonator for RF Applications" *Proceeding of the 2011 COMSOL Conference in Banglore, INDIA.*

[4] C. T.-C. Nguyen, "Vibrating RF MEMS for low power communications (invited)," *Proceedings, 2002 MRS Fall Meeting, Boston,Massachusetts, Dec. 2-6, 2002*, pp. J12.1.1-J2.1.12.

[5] Gabriel M.Rebeiz " RF MEMS Theory , Design and Technology" *John Wiley and Sons Ltd*.

[6] Joep Jacques Marie Bontemps "Design of a MEMS-based 52 MHz Oscillator" *Universiteitsdrukkerij Technische Universiteit Eindhoven, The Netherlands-2009*

[7] Ravi Patni, Mohit Joshi, Sameer Mehra, and Akhilesh Mohan "Design of Piezoelectric Aluminum Nitride MEMS Resonator"*Proceedings of the World Congress on Engineering and Computer Science 2011 Vol I WCECS 2011, October 19-21, 2011, San Francisco, USA.*

IOSR Journal of Electronics and Communication Engineering (IOSR-JECE)
e-ISSN: 2278-2834,p- ISSN: 2278-8735. Volume 5, Issue 6 (Mar. - Apr. 2013), PP 24-28
www.iosrjournals.org

Speed and Position Control of Train Sytem Using GPS

Arshiya [1], Kehkeshan Jalall S[2], Sufia banu [3]
[1](*Department Electronics & Communication, HKBK College of Engineering, India)*
[2](*Department Electronics & Communication, HKBK College of Engineering, India)*
[3] *(Department Electronics & Communication, HKBK College of Engineering, India)*

Abstract : *The passengers face some problems regarding the arrival time of the train and they go on asking the ticket checkers about the arrival. This creates trouble to the ticket checker to keep answering thousands of passengers who are boarding the train. The GPS (Global Positioning System) gives the position of any object on which it as placed with respect to the latitude and longitude of the earth. This technique would be helpful in tracking the exact location of the train and as well the speed of the moving* object. *Some of the human activities causing accidents include railway level crossing during the approach of train, misplaced fish plates and high speed at places where speed should actually be less. So the system designed here which is called as ATCS (Advanced train control system) helps in reducing the accidents to an extent.*

Keywords – *NMEA format, GPS, RBC track switch, Tarang (Zigbee transceiver*), *Microcontroller, Level crossing.*

I. INTRODUCTION

In most of the countries' railway systems, there are many accidents occurring due to human activities and natural calamities. In hilly regions, the railways are built by breaking the hills. In such places, huge boulders fall naturally on the track and hence block the way suddenly. Due to such sudden actions, there might be some chances of accidents. Also the signals at track are not seen due to foggy weather conditions due to which train accidents occur as the driver will not be able to see the signals clearly. Not only due to natural activities, but due to human activities, there are many accidents occurring too. Some of the human activities causing accidents include railway level crossing during the approach of train, misplaced fish plates and high speed at places where speed should actually be less. So the system designed here which is called as ATCS (Advanced train control system) helps in reducing the accidents to an extent.

The passengers also face some problems regarding the arrival time of the train [1] and they go on asking the ticket checkers about the arrival. This creates trouble to the ticket checker to keep answering thousands of passengers who are boarding the train. The GPS (Global Positioning System) gives the position of any object on which it as placed with respect to the latitude and longitude of the earth. This technique would be helpful in tracking the exact location of the train and as well the speed of the moving object. So this method can be used in the railway system also to get the exact position of the train and it can be displayed in the train as well as the railway station which is called as RBC section in this module.

The train monitoring system using GPS addresses issues like detecting the real time position and current speed of the train. The current system only gives the position of the train in between the two stations but can't detect the real time position of the train where it is right now. Our system receives the train's position and velocity information from the GPS. The same information is sent to the RBC[2] (Control Section) via ZigBee(Tarang) and speed of the train is made to increase or decrease based on algorithm provided.

What was needed in the current Indian Railways was a system that would detect the current position and the speed of the train and command the driver what speed should be maintained till the next instruction comes. The current command system uses the radio signals, which had limitations. There will be some signal distortions and irrelevant messages are heard using the walkie-talkie system which is used in the current railways systems. The TMS was a major improvement for the simple fact that it would utilize a railway map database via Global Positioning Systems to provide the driver with the exact data.

II. MODULE FEATURES

The system is divided into the following module and is developed in the given order:

- NMEADL: the GPS sends the data in NMEA format. The microcontroller will be programmed with decoder logic which extracts the information and converts it into a format readable by the speed calculation algorithm.
- Speed Calculating Algorithm: the RBC calculates the position and speed of the train using dead reckoning algorithm.

- The module has an algorithm to calculate the distance at which brakes must be applied when there is a normal condition, emergency conditions and unavoidable conditions.
- Database: The position and speed of the train are found using the GPS. These coordinates are stored in the database.
- Obstacle Detection: This module contains all the necessary hardware interfaces.
- Collision avoidance: This module contains all the necessary hardware interfaces.
- Level crossing: it has a stepper motor which makes the gate closure automatic and an APR to alert the automobiles regarding the arrival of the train.

III. BASIC BLOCK DIAGRAM

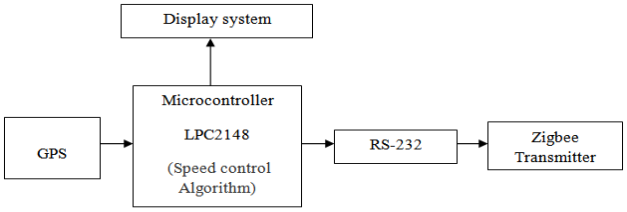

Fig.1 Train Section

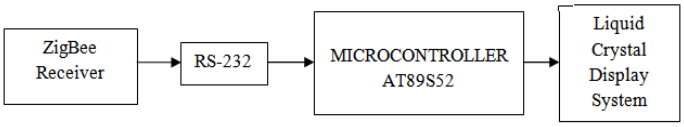

Fig.2 RBC Section

The data inputs to the controller from the GPS (Latitude, Longitude and Speed) are the major inputs and the display alerts are the outputs. This alert gives the exact location and speed at which the train is moving to the train-driver which is displayed on the on-train LCD display and will also be sent to the RBC section. All the components of the system are integrated on a single board. The hardware platform used in the system is LPC2418 and the Embedded C will be used as the working platform to program the microcontroller. The data from the GPS will be given as input to the LPC2148 which will be programmed to extract the required NMEA data format and will be converted into a form which directly displays the Latitude, Longitude, Speed and other information. This information about the location and speed of the train will also be sent to RBC section by using Zigbee which is used for the wireless transmission of the information from the train to RBC. The maximum distance between the transmitter and the receiver can go up to 300feet.At RBC the Zigbee receiver is used to receive this information which will be given to an 8051 microcontroller serially by making use RS232. This information will also be displayed on the LCD which is present at the RBC.

The GPS is used here to calculate the position and the speed of the train by getting the signals through the antenna. The GPS is connected to the satellite through the antenna and obtain the data in a format that is acceptable by the microcontroller. This is given to the microcontroller through the RS-232 which converts the incoming signal in a form of logic level data. The microcontroller used here is of 8051 architecture. Microcontroller is provided with a speed control[3-4] algorithm whose sole purpose is to provide the control the speed by informing the driver to increase or decrease the speed through a visual unit.

With the help of database and a calculation algorithm, the speed and position is calculated and a message is passed about the same on to the zigbee transmitter. At the control station we have a zigbee receiver which receives the incoming signal and is displayed on the display system through Microcontroller.

IV. OPERATING PRINCIPLE

1.1 On Train

1.1.1 Mode 1

a. T Switch ON the Respective Track Switch whose information is needed.
b. Get the data from RBC which is in the format S-5-3-L-3-1-R-2-1-S-6-3
(Direction-Distance to be travelled- Speed to be maintained) Store the data
c. Get the GPS data, decode the data and store the Start_Latitude, Start_Longitude, Departure_Time data of the starting point and then Start the Train.
d. Initialize Position to 2, Speed to 3.
e. Get the GPS data, decode the data and store the Previous_Latitude, Previous_Longitude, Previous_Time data.
f. Distance_to be_travelled = (Position+3)*10
Speed_to_be_maintained = (Speed+3)*10

g. Get the GPS data, decode the data and store the New_Latitude, New_Longitude, New_Time data
h. Calculate the Current_Distance i.e. using the formula given below

$$a = \sin^2(\Delta lat/2) + \cos(lat_1).\cos(lat_2).\sin^2(\Delta long/2)$$
$$c = 2.atan2(\sqrt{a}, \sqrt{(1-a)})$$

Haversine formula: $d = R.c$

Where R is earth's radius (mean radius = 6,371km); note that angles need to be in radians to pass to trig functions!

Current_Time = (Previous_Time – New_time)
Current_Speed = (Current_Distance / Current_time)
Difference_In_Speed=(Current_Speed ~ Speed_to_be_maintained)

i. If Difference in Speed is not equal to zero Go to step j else Go to step k
j. Display the Difference_In_Speed and Advice the Driver and Send the Information about Position and Difference_In_Speed to RBC in the Format : 02-23-00
(Position - Difference_In_Speed - Braking Zone)
k. If the Current_Distance is equal to Distance_to be_travelled Go to Step d else Go to Step g.

1.1.2 Mode 2

a. Receive the Track Signal which will be in the Format Z-1,2……3-R/Y/G .Store the Data
b. Get the data from RBC which is in the format S-5-3-L-3-1-R-2-1-S-6-3 (Direction-Distance to be travelled- Speed to be maintained) Store the data
c. Initialize Position to 2, Speed to 3, Current_Zone to 0, Braking_Zone to 0.
d. Store the Status of the First 4 Consecutive Zones in LED[ ]. Ex: LED [4] = {GGRG}
e. Get the GPS data, decode the data and store the Previous_Latitude, Previous_Longitude, Previous_Time data.
f. Distance_to be_travelled = (Position+3)*10
Speed_to_be_maintained = (Speed+3)*10
g. Get the GPS data, decode the data and store the New_Latitude, New_Longitude, New_Time data
h. Display and Store the Status of the FOUR Consecutive Zones from Current_Zone in LED[ ].
Ex: LED[4]={GGRG}
i. If LED [i]=R then make LED [i – 1]= Y
j. Ex: LED[4]={GYRG}
k. If any of the LED variable status is Y or R store the position of the Zone in Braking_Zone.
l. If Current_Zone = Braking_Zone then go step 0
m. Calculate the Current_Distance i.e using the formula given below

$$a = \sin^2(\Delta lat/2) + \cos(lat_1).\cos(lat_2).\sin^2(\Delta long/2)$$
$$c = 2.atan2(\sqrt{a}, \sqrt{(1-a)})$$

Haversine formula: $d = R.c$

where R is earth's radius (mean radius = 6,371km); note that angles need to be in radians to pass to trig functions!

Current_Time = (Previous_Time – New_time)
Current_Speed = (Current_Distance / Current_time)

n. If the Current_Distance is equal to Distance_to be_travelled
o. Increment Current_Zone then Go to Step e else Go to Step g.

p. Apply brakes at the respective Zone and send the information about the BRAKES APPLIED and Stop.

1.13 Mode 3

Switch ON the Respective Track Switch whose information is needed.

a. Get the data from RBC which is in the format S-5-3-L-3-1-R-2-1-S-6-3 (Direction-Distance to be travelled- Speed to be maintained)Store the data
b. Initialize Position to 2.
c. Get the GPS data, decode the data and store the Previous_Latitude, Previous_Longitude, Previous_Time data
d. Distance_to be_travelled = (Position+3)*10
e. Get the GPS data, decode the data and store the New_Latitude, New_Longitude, New_Time data
f. Calculate the Current_Distance i.e using the formula given below

$$a = \sin^2(\Delta lat/2) + \cos(lat_1).\cos(lat_2).\sin^2(\Delta long/2)$$

Haversine formula:

$$c = 2.\text{atan2}(\sqrt{a}, \sqrt{(1-a)})$$

$$d = R.c$$

where R is earth's radius (mean radius = 6,371km); note that angles need to be in radians to pass to trig functions!

Current_Time = (Previous_Time – New_time)
Current_Speed = (Current_Distance / Current_time)

g. Send position

1.2 At RBC

a. Initialize Gate to 0
b. Receive and decode the data
c. If the request is to send the Track information send the same from the database
d. Else if the data is in the Format 02-23-0 (Position - Difference_In_Speed - Braking Zone) Decode the Data to get the Position, Difference_In_Speed, Braking Zone
e. Display the Position of the Train.
f. If Position = Gate_Position and Gate = 0 send Close to Level Crossing and make Gate =1
g. If Position = Gate_Position and Gate= 1 send Open to Level Crossing and make Gate =0
h. If Braking Zone is != 0 Display the Braking Postion
i. If Difference_In_Speed is != 0 Display the Difference_In_Speed else Go to Step b

V. CONCLUSION

It is used to avoid accidents in railways and saves the lives of a large number of passengers in the train. The GPS receives signals from a group of three satellites for getting the latitude and longitude of the object which is the train in our case. The data is precise and is always compatible with real time systems as the satellites are continuously monitoring. If we carefully set up the GPS system with précised parameters, the person in the control station will be able to track the position and speed of the train. This module gives the information related to the train and will alert the train driver whether to continue with the same speed or make any changes in the speed. Accordingly the control station will receive the information about the speed [5] and position of the train.

The module can have an additional feature of having the database that stores the information about the speed at various stages which can be used for investigation purposes in case of accidents. Changing the speed can be made automatic rather than manually. In case of emergency send the information about the position of train to Helping Authorities. Controlling of the speed can be made automatic. Information can be updated in communication media such as Internet. A lay man or a common man can access the information about the train through the devices like mobiles.

Acknowledgements

The authors thank the reviewers for their valuable comments and suggestions that helped us to make the paper in its present form

REFERENCES

Journal Papers:

[1] Dai, Ling-Long ; Wang, Zhaocheng ; Yang, Zhi-Xing , Time-Frequency Training OFDM with High Spectral Efficiency and Reliable Performance in High Speed Environments, *IEEE Journal on Selected Areas in Communications, Volume: 30 , Issue: 4,* 695 - 707

Proceedings Papers:

[2] BuBing, Wang, XiShi, Wu, XinYao, Wireless data transmission for high-speed train control, Vehicular Technology Conference, 2000. IEEE-VTS Fall VTC 2000. 52nd , Vol : **6,** Pg : 2998 -3001

[3] Mei, T. X. ; Li, H., , Monitoring train speed using bogie mounted sensors — Accuracy and robustness, IET International Conference on Railway Condition Monitoring, 2008 , Pg:1 – 6

[4] Wei, ShangGuan ; Cai Bai-gen ; Gou Chen-xi ; Chen Jian-qiu ; Wang Jian, ,Research on key techniques of high-speed train control system simulation & testing, International Conference on Mechatronics and Automation (ICMA) 2010 , Page(s): 1695 – 1700

[5] Bing, Bu ; Xishi, Wang, The effect of speed on error rate in wireless train control Proceedings of the 3rd World Congress on Intelligent Control and Automation, 2000, vol.4, Pg : 2484 - 2487

IOSR Journal of Electronics and Communication Engineering (IOSR-JECE)
e-ISSN: 2278-2834,p- ISSN: 2278-8735. Volume 5, Issue 6 (Mar. - Apr. 2013), PP 29-33
www.iosrjournals.org

Embedded Web Server based Interactive data acquisition and Control System

Miss.Pulate S.V.[1],Mrs.Diggikar A.B.[2]
[1]*Electronics ,SPWEC,Sharanpur, Aurangabad,India,*
[2]*Electronics,SPWEC,Sharanpur, Aurangabad,India*

ABSTRACT: *Design of on-line embedded web server is a one of the difficult task of many real time data acquisition and control system applications. The global system of interconnected computer networks is called as World Wide Web which uses the standard Internet Protocol Suite (TCP/IP) to aid billion of users worldwide and enables the user to interface many real time embedded applications like data acquisition,Industrial automations and safety measures etc,. This paper tells the design and development of on-line Interactive Data Acquisition and Control System (IDACS) using ARM9 based embedded web server. It is permitted to a network, intelligent and digital distributed control system. Single chip IDACS method increses the processing speed of a system and also avoids the problem of poor real time and reliability.This system uses ARM9 Processor and RTLinux. Web server application is ported into an ARM processor using embedded 'C' language. Web pages are designed in Hyper text markup language (HTML).*

Keywords *- Embedded ARM9 Processor, RTLinux RTOS, Embedded web server, IDACS.*

I. INTRODUCTION

Online Interactive Data Acquisition and Control system plays the major role in the rapid development of the fast popularization and control in the field of measurement and control systems. It has been designed with the help of many electrical, electronic and high voltage equipments; it makes the system more complicated and not reliable. This paper approaches a new system that contains inbuilt Data Acquisition and Control system (DACS) with on-line interaction. It makes the system more reliable and avoids more complication. It is the great demand in consumer applications and many industries.

This system replaces various complex cables which are used for acquisition and it uses Ethernet and ARM processor for data acquisition and digital diagnosis.There are various digital DAC systems are available for the substitution of multisite job operation. A single worker can interact with the machine and collect various data from ongoing work in a single work station. The simplest design of data acquisition system is detailed in [1], which is based on Linux Operating system [2]; it is the popular choice for many embedded real time applications and PC systems. This system process the client based on dynamic manner by server response and it maintains separate data base with DAC controller. A web server can be embedded into any appliance and connected to the Internet so the appliance can be monitored and controlled from remote places through the browser in a desktop. This brings in a need for web services being deployed on various embedded processors such as Advanced RISC Machine (ARM) in real time context.In [3] advanced traffic survey mechanism uses data collection process for post processing of vehicle's position. Signal conditioning is the major part of any data acquisition unit. High level integration architecture was discussed in [4]; it allows signals to be conditioned, simultaneously acquired according to the external clock and triggers processed and transferred data to real time servers.Signal measurement from astrophysical sources is described in [5]; where the shared memory and internet protocols are used for data handling and process from remote users. It was developed with Global Positioning System (GPS) and Environmental monitoring system. Similarly depends on industry and its location General Packet Radio Service (GPRS) also used for data transmission through on-line. But this paper doesn't use GPRS and GPS systems for data uploading into internet. It reduces the system complexity and effective for all kind of real time applications. Every real time embedded system should be run by real time operating systems. In this paper Real time Linux Operating system is ported in ARM9 processor. Generally all ARM9 processors have the portability with any kind of higher end RTOSes. Here the embedded web server application is developed and ported into ARM9 with this setup. This single ARM board has been act as data acquisition unit, control unit, embedded web server and self diagnosis. All processes are allocated with essential resources and associated with reliable scheduling algorithms and internet protocols followed by ARM processor. This miniaturized setup reduces the complexity & size of system.

It contains an operating system, web pages to run the application and a large memory space for server functionality. When the configured IP address is entered in the web browser, the predesigned HTML web pages gets displayed through which we can remotely monitor and control the sensor and device status respectively. The heart of communication is TCP/IP protocol. Network communication is performed by the IEEE 802.3

Ethernet standard. ARM processor is chosen because ARM has high data processing capability. It also has multi parameter acquisition and multi level monitoring and networking. It can reduce operation pressure on data reduction and ensures real-time monitoring of system performance. On the other hand, our proposed web server requires only a very low d.c. supply of 3.3V for its operation. This system ensures portability and high reliability. When RTOS is incorporated into this system, more devices could be controlled and monitored. The multi tasking capability and fast response time along with added advantage of easy deployment makes this system capable for a wide variety of applications. The system designed here is an example of embedded technology integrated with network technology where communication and processing technology also meets.

II. SYSTEM ARCHITECTURE

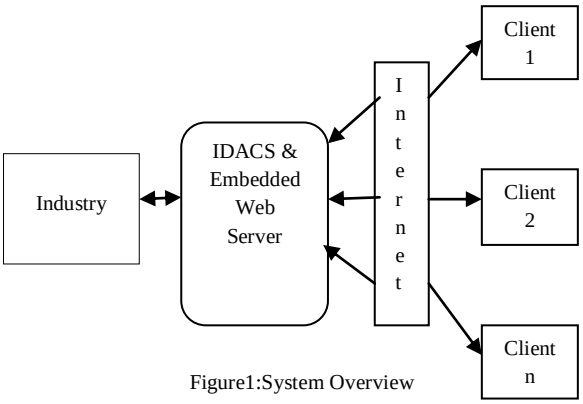

Figure1:System Overview

Fig.1 shows the overview of IDAC system. Here the system consists of three different parts. First is the Embedded Web Server. Second is the user part or client and third one is the industry or sensors and appliances to be monitored. The client thus monitors various parameter status through sensors and also controls many industrial appliances with the help of the web server.Every client can access the industry directly without any interaction with additional server and modules. The client PC is connected to the Internet through a browser and then gets access to the embedded Web server. Through this way, remote login and operation are realized.IDACS shows Intelligent Data Acquisition and Control System. This system contains single ARM9 processor which is portable with Real Time Linux RTOS. ARM processor is the heart of this work. It handles two modes at same time, DAC and Web server.During DAC mode Processor can measure signals which are coming from various external sources and applications. And it can control the industry machineries by the control instruction sent by client via embedded web server. During signal measurements Analog to digital converter is very important, because almost every external source is giving analog signal only. While converting these analog to digital processor has to handle asynchronous interrupts.

This system uses RTLinux so it can handle many interrupts in an efficient manner because RTLinux has preemptive kernel with required privilege levels. Similarly during web server mode processor will handle client request and response to the particular client by sending web pages, client can interact the industry by giving instruction in web page on its own web browser. This setup can be suitable for inter communication with other nodes via Ethernet and higher end ports. Ethernet programming and execution is very easy and adaptable with various applications. Embedded web pages are designed by HTML language. Fig 1. Shows the proposed concept of Data Acquisition and Control Systems (DACS) with embedded web server. It contains RTOS portable ARM processor. The real time operating system manages all the tasks such as measuring signals, conversion of signals, data base up-dation, sending HTML pages and connecting/communicating with new users etc.The RTOS manages all the required tasks in parallel and in small amounts of time. Web based management user interfaces using embedded web server have many advantages: ubiquity, user-friendly, low-development cost and high maintainability.

III. SYSTEM DESIGN

Hardware design, Software design and Porting are the entire important steps in whole system design.

A Hardware design of the system

1) IDACS Design:

IDACS design is the major part in hardware. ARM9 processor is a centre core of this system. The general hardware structure of the IDACS is shown in Fig 2. The online intelligent data acquisition and control system based on embedded ARM platform has high universality, each acquisition and control device equipped with 24-way acquisition/control channels and isolated from each other.Each I/O channel can select a variety of

electrical and nonelectrical signals like current, voltage, resistance etc.,Digital acquisition are done by special ADC. The measured data are stored in external memory in which the memory is act as a data base during web server mode. The ARM9 Processor directly supports the Ethernet service and RS485 communication. Hence the data has been stored and controlled by some other PCs or network via RS485 & Ethernet. ARM processor has internal I2C module. So it has the ability to communicate with any other peripherals.

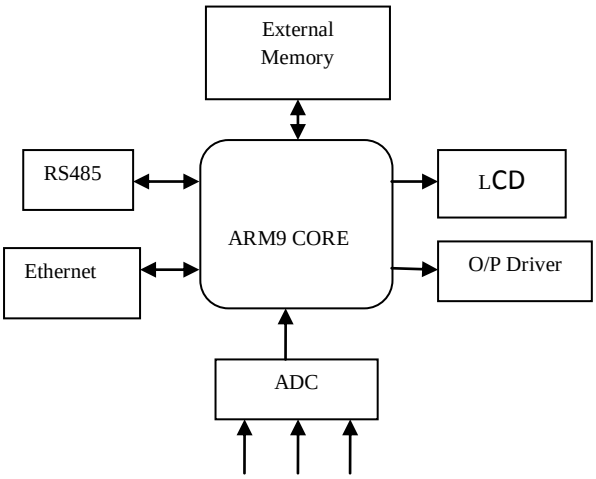

Figure 2. General Structure of the IDACS

I2C is the wired communication protocol to communicate with other processor or peripherals through two wired link. This system has 128*64 LCD to display the information and measured parameters which makes the debugging and modification of the parameter easy. The Analog to digital interfacing module is independent with the embedded system, which is beneficial to the system maintenance and upgrade. As the embedded Ethernet interface makes the remote data exchange between the applications become very easy.The Linux sockets are used to communicate between ARM server and webpage's form clients. The communication between ARM platform and client board is by RS232 protocol. A PIC microcontroller act as the CPU of the client board.

2) Analog to Digital Converter:

Fig 2. uses 16bit ADC chip AD7715. This is digital chip having I2C module internally. It has the ability to transfer the converted digital data to ARM processor. It needs only five lines, which are DOUT – Data output, DRDY – Data ready, DIN – Data Input, CS – Chip select and SCLK –system Clock. Converted digital data will be sending out by DOUT pin of the chip. This ADC chip is driven by 2.4576MHz crystal. It contains separate Reference signals Ref+ and Ref- and separate Analog input channels AIN+ and AIN- . During communication with ARM processor this ADC chip should be synchronized with the processor's clock.

3) RS485 Communication:

RS-485 is a telecommunications standard for binary serial communications between devices. It is the protocol or specifications that need to be followed to allow devices that implement this standard to communicate with each other.This protocol is an updated version of the original serial protocol known as RS-232. While the original RS-232 standard allowed for the connection of two devices through a serial link, RS-485 allows for serial connections between more than 2 devices on a networked system.

B. Software design of the system

1) Real Time Linux:

RTCore is a POSIX 1003.13 PE51 type real-time kernel,something that looks like a multithreaded POSIX process with its own internal scheduler. RTCore can run a secondary operating system as a thread, using a small virtual machine to keep the secondary system from disabling interrupts. This is a peculiar model: a UNIX process with a UNIX operating system as a thread, but it provides a useful avenue to modularity. RTLinux is RTCore with Linux as the secondary kernel. RTCore with BSD UNIX as the secondary kernel. Real-time applications run as real-time threads and signal handlers either within the address space of RTCore or within the address spaces of processes belonging to the secondary kernel. Real-time threads are scheduled by the RTCore scheduler without reference to the process scheduler in the secondary operating system. The secondary operating system is the idle thread for the realtime system. The virtual machine virtualizes the interrupt controller so the secondary kernel can preserve internal synchronization without interfering with real-time

processing. Performance is adequate to allow standard PC and single board computers to replace DSPs in many applications.

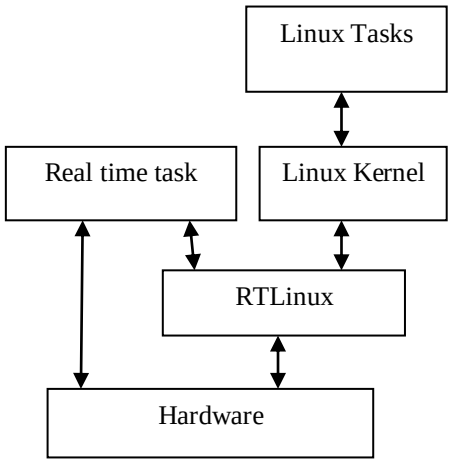

Figure 3.RTLinux Run time Model

Unlike Linux, RTLinux provides hard real-time capability. It has a hybrid kernel architecture with a small real-time kernel coexists with the Linux kernel running as the lowest priority task. This combination allows RTLinux to Provide highly optimized, time-shared services in parallel with the real-time, predictable, and low-latency execution.Besides this unique feature, RTLinux is freely available to the public. As more development tools are geared towards RTLinux, it will become a dominant player in the embedded market. RTLinux is a typical dual-kernel, one is Linux kernel, which provides various features of general purpose OS, other one is RTLinux kernel, which support hard real time capability.

IV. PROPOSED SYSTEM

General web server requires more resources and huge amount of memories. This system can only measure the remote signals and it cannot be used to control the process.

Limited processing capacity and the problem of poor real time and reliability of DAS system has been overcome by the substitution of embedded ARM processor for single chip method to realize interactive data acquisition and control (IDACS). This IDACS system can able to measure the remote signals and can control the remote devices through reliable protocols and communication network. This system uses RTLinux Multi-tasking operating system to measure and control the whole process. And the embedded web server mode requires less resource usage, high reliability, security, controllability and portability.

V. CONCLUSIONS

With the rapid development of the field of industrial process control and the wide range of applications of network, intelligence, digital distributed control System, it is necessary to make a higher demand of the data accuracy and reliability of the control system. This embedded ARM system can adapt to the strict requirements of the data acquisition and control system such as the function, reliability, cost, size, power consumption, and remote access and so on. This system operated by DACS mode to acquire the signals and control the devices remotely. Embedded web server mode is used to share the data with clients in online.Both modes are efficiently carried out by real time multi tasking operating system (RTLinux). This system can be widely applied to electric power, petroleum, chemical, metallurgy, steel, transportation, Electronic & Electrical industries, Automobiles and so on.

REFERENCES

[1] K.JackerandJ.Mckinney,"TkDAS- A data acquisition system using RTLinux, COMEDI, and Tcl/Tk," inProc. Third Real Time Linux Workshop, 2001. [Online].Available: The Real TimeLinuxFoundation:http://www.realtimelinuxfoundation.org/events/rtlws-2001/papers.html

[2] E.Siever, A.Weber, S.Figgins, and R.Love, CA:O'Reilly, "Linux in a Nutshell,",2005.

[3] J. E. Marca, C. R. Rindt, M. Mcnally, and S. T. Doherty, "A GPS enhanced in-vehicle extensible data collection unit," Inst. Transp.Studies, Univ. California, Irvine, CA, Uci-Its-As-Wp-00-9, 2000.

[4] Y. C.Wu, J. R. Luo, and J. Z. Shan, "Development of the central timing system on the EAST Tokamak," *IEEE Trans. Nuclear science*, Vol. 30, No. 9, pp. 789–792, 2007.

[5] F. Acernese, P. Amico, M. Alshourbagy, F. Antonucci, S. Aoudia, P.Astone, S. Avino, D. Babusci, G. Ballardin,"Data Acquisition System of the Virgo Gravitational Waves Interferometric Detector,"*IEEE Trans. Nuclear science* , Vol. 55, No. 1, pp.225-232, February 2008

[6] D. Vijendra Babu, P. Subramanian and N. Ravi Kanan, "*Microblaze and Uclinux Based Data Acquisition on Spartan 3E* " Proc. Of International Conference on VLSI Design and Embedded Systems,pp1-4, 2008.

[7] S. B. Silverstein, J. Rosenqvist, and C. Bohm, "A simple Linux-based platform for rapid prototyping of experimental control systems,"*IEEE Trans. Nucl. Sci.*, vol. 53, no. 3, pp. 927–929, Jun. 2006.
[8] Peng D.G, Zhang H., Yang L., etc, "Design and Realization of Modbus Protocol Based on Embedded Linux System". The 2008 International Conference on Embedded Software and Systems Symposia. July 29-31, 2008, Chengdu, Sichuan, China, pp:275-280.
[9] Soumya Sunny P1, Roopa .M2; "Data Acquisition and Control System Using Embedded Web Server" International Journal of Engineering Trends and Technology- Volume3Issue3- 2012.
[10] Alen Rajan, Aby K. Thomas; "ARM Based Embedded Web Server for Industrial Applications" International Conference on Computing and Control Engineering (ICCCE 2012), 12 & 13 April, 2012
[11] Linux Kernel API ,http:www.kernel . org/doc/htmldocs/kernelapi/index.html
[12] RTLinux – http://www.rtlinux.org
[13] www.opensource.org
[14] www.embeddedarm.com

IOSR Journal of Electronics and Communication Engineering (IOSR-JECE)
e-ISSN: 2278-2834,p- ISSN: 2278-8735. Volume 5, Issue 6 (Mar. - Apr. 2013), PP 34-40
www.iosrjournals.org

Characteristics analysis of silicon carbide based 1-D Photonic crystal with 2 layered unit cell using MATLAB

Avik Chakraborty
Assistant Professor, Electronics & Communication Engg. Dept., Bengal Institute of Technology & Management, Bolpur, Birbhum. Contact Address: Senpara, Kalitala Road, PO+Dist- Jalpaiguri, Pin-735101, West Bengal,

Abstract: *Silicon carbide based 1-D Photonic crystals with 2 layered unit cell are analyzed in this paper. The transmission characteristics of photonic crystals are computed by transfer matrix method and performance of such photonic crystals of different material combinations are also compared, and after comparison some one able to know the characteristics such as pass band width, stop band width, centre band gap of a light wave of a particular wave length traveling through this 2 layered unit cell photonic crystal in nano meter range where one layer of this unit cell must be made of semiconductor material named silicon carbide (SiC).*
Key word*: 1-D photonic crystal, transmission coefficient, light wave.*

I. Introduction

In this paper first to know about photonic crystal [1] the statement is like that periodic optical nanostructures that are designed to affect the motion of photons in a similar way that periodicity of a semiconductor crystal affects the motion of electrons. such photonic crystals with photonic band gap (for some frequency range, a photonic crystal prohibits the propagation of electromagnetic waves of any polarization travelling in any direction from any source, then we say that the crystal has a complete photonic band gap) preventing light from propagating in certain directions with specified frequencies In order to construct these crystals in the optical regime, suitable nanofabrication techniques have to be developed and demonstrated, including high resolution electron beam lithography and anisotropic chemically assisted ion beam etching. These periodic dielectric structures are expected to exhibit interesting properties in both fields of physics and engineering. Silicon Carbide (SiC) being an important semiconductor in the situation. The basic characteristics of Silicon Carbide (SiC) – based photonic crystals will be analyzed .

II. One Dimensional Photonic Crystal (Phc)

In a 1-D Photonic Crystal layers of different dielectric constant may be deposited or adhered together to form a band gap in a single direction .A Bragg grating is an example of this type of photonic crystal .This type of photonic crystal systems exhibits three important phenomena i) Photonic Band gap , ii)Localized mode iii) surface state ,because the index contrast is only along one direction , the band gaps and bound states are limited to that direction .By the help of this concept this characteristics analysis is being processed.

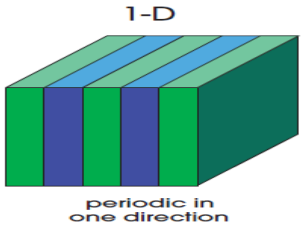

Fig (1)-1-D Photonic Crystal

III. Reason behind the choosing of Silicon Carbide (SiC) as a semiconductor material

SiC (wide forbidden energy gap of 2.86 eV@ 302 K) has been emerged as an attractive substrate for high power devices due to its larger band gap , higher break down strength , high thermal conductivity and high electron saturation drift velocity. Most important advantage of SiC over other wide band gap semiconductor is that SiC can be thermally oxidized to form an insulator Silicon die oxide. Although the refractive index of SiC is lower than that of a conventional semiconductor such as GaAs or Si , a wide photonic band gap , a broadband wave guide and a high quality nanocavity comparable to those of previous photonic crystals can be obtained in Silicon Carbide based photonic crystals, for above many reason in this analysis process we choose SiC.

Description

In this paper unit cell photonic crystal has been considered which has 2 layers. The refractive indices (n_1, n_2) of the two materials are related to the thickness of the layers (d_1, d_2) as

$n_1d_1=n_2d_2=\lambda_0/4$ …….. (1)

Where λ_0= Free space (vacuum) wavelength, whose value is taken here as 1550 nanometer, since it is the most important wavelength for optical communication.

When an electromagnetic wave with S-polarization incidents on a unit cell of two materials a and b, the reflection and transmission coefficient can be expressed as [2]

$$\frac{A_R}{A_I} = \frac{\sqrt{\epsilon_a/\mu_a}\cos\alpha - \sqrt{\epsilon_b/\mu_b}\cos\beta}{\sqrt{\epsilon_a/\mu_a}\cos\alpha + \sqrt{\epsilon_b/\mu_b}\cos\beta}$$

……(2)

$$\frac{A_T}{A_I} = \frac{2\sqrt{\epsilon_a/\mu_a}\cos\alpha}{\sqrt{\epsilon_a/\mu_a}\cos\alpha + \sqrt{\epsilon_b/\mu_b}\cos\beta}$$

…….... (3)

Where A is the complex amplitude of the electric field, α and β are angle of incidence and refraction at the interface.

Here S- polarized wave has its electric field vector confined perpendicular to the plane of incidence. Here electric field E is in the y direction, so $\tilde{E}$ = (0,A,0). Using S-polarization [equation (2) and (3)] we get the equation (4)

$$C_{m-1}e^{ik_mz_m\cos\propto_{m-1}} = \frac{\sqrt{\epsilon_{m-1}/\mu_{m-1}}\cos\propto_{m-1} - \sqrt{\epsilon_m/\mu_m}\cos\propto_m}{\sqrt{\epsilon_{m-1}/\mu_{m-1}}\cos\propto_{m-1} + \sqrt{\epsilon_m/\mu_m}\cos\propto_m} A_{m-1} \times e^{-ik_mz_m\cos\propto_{m-1}} + \frac{2\sqrt{\epsilon_m/\mu_m}\cos\propto_m}{\sqrt{\epsilon_{m-1}/\mu_{m-1}}\cos\propto_{m-1} + \sqrt{\epsilon_m/\mu_m}\cos\propto_m} C_m \times e^{ik_mz_m\cos\propto_m}$$

……..(4)

And

$$A_me^{-ik_mz_m\cos\propto_m} = \frac{2\sqrt{\epsilon_{m-1}/\mu_{m-1}}\cos\propto_{m-1}}{\sqrt{\epsilon_{m-1}/\mu_{m-1}}\cos\propto_{m-1} + \sqrt{\epsilon_m/\mu_m}\cos\propto_m} A_{m-1} \times e^{-ik_mz_m\cos\propto_{m-1}} + \frac{\sqrt{\epsilon_m/\mu_m}\cos\propto_m - \sqrt{\epsilon_{m-1}/\mu_{m-1}}\cos\propto_{m-1}}{\sqrt{\epsilon_{m-1}/\mu_{m-1}}\cos\propto_{m-1} + \sqrt{\epsilon_m/\mu_m}\cos\propto_m} C_m \times e^{ik_mz_m\cos\propto_m}$$

……...(5)

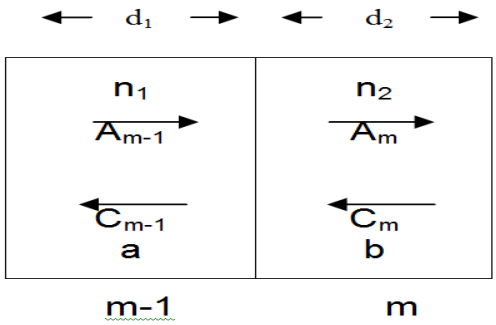

Fig-(2)- **Standard 2 layered unit cell Photonic Crystal**

a and b indicates the two layers with refractive indices n_1 and n_2.

From the figure 2, First layer is for denser material and other one is for rarer material. d_1 and d_2 are the thickness of each layer. C_m is the amplitude in the m^{th} layer for waves and C_{m-1} is for m-1 layer that is first layer.

A_m is the amplitude in the m^{th} layer for waves and A_{m-1} is the amplitude in the m-1 layer. From equation (4) & (5) it is possible to construct transfer matrix ,here cosine value is 0 for all cases (consider) and μ=1 in all cases but € value is changed for different material. Here m-1 layer signify the first layer and m is for second layer of an unit cell photonic crystal. By help of equation (4) and (5) first have to construct a standard unit cell whose two layers are made with Si and SiO2, after that just have to change the material from standard one and place SiC on that particular position and analyze the characteristics for different material combination where SiC is a common one.

The matrix form is like that

M=

$$\begin{bmatrix} a1 * \exp(-i.* km.* zm) & a2 * \exp(i.* km.* zm) \\ a2 * \exp(-i.* km.* zm) & a1 * \exp(i.* km.* zm) \end{bmatrix} \begin{bmatrix} b1 * \exp(-i.* km1.* zm1) & b2 * \exp(i.* km1.* zm1) \\ b2 * \exp(-i.* km1.* zm1) & b1 * \exp(i.* km1.* zm1) \end{bmatrix}$$

Here zm = d_2 and zm1 = d_1, the general form of equation for Transfer matrix M shown in below through which transmission coefficient can be achieved.

$$M = \begin{pmatrix} 1/t & r_1^*/t^* \\ r_1/t & 1/t^* \end{pmatrix} \quad \text{..... (6)}$$

If we apply the particular transmission coefficient for 10 numbers of unit cells then transmission coefficient of entire photonic crystal can be achieved.\

To apply 10 numbers of unit cells the standard matrix form of equation is stated below

$$M^N = \begin{pmatrix} 1/t_N & r_N^*/t_N^* \\ r_N/t_N & 1/t_N^* \end{pmatrix} \quad \text{.....(7)}$$

Computation of result using different parameters

Using equation (6) transmission coefficient has been computed using matlab. For computation this paper takes the following parameters.
Free space wavelength (λ_0) = 1550 nanometer (nm)
Number of unit cell (N) = 10
d_1 = Thickness of the first layer
d_2 = Thickness of the second layer
n_1 = Refractive index of the first layer
n_2 = Refractive index of the second layer

IV. Discussion of results

Silicon_Silica:

In case of Silicon and Silica the value of n_1 for Silicon is 3.5 and the value of n_2 for Silica is 1.5, so by using equation (1) thickness of the first layer (d_1) = 1550/4*3.5 = 110.71 nm and thickness for the second layer (d_2) = 1550/4*1.5 = 258.33 nm.

In Silicon_Silica based photonic crystal the stop band lies in between 1250 nm to 2100 nm (Approx), so the value of transmission coefficient is 0 within this range. We can find Stop band width = 850 nm. Here centre band gap is at 1680 nm. Pass band lies in between 550 nm to 1250 nm (Approx), so Pass band width = 1250-550= 700 nm. The choosing wavelength is 1550 nm but centre band gap lie is at 1680 nm. So our wavelength shifts towards the higher frequency range with respect to corresponding wavelength (λ_0). After 2120 nm (Approx) find another Pass band till investigate of our range 2400 nm.

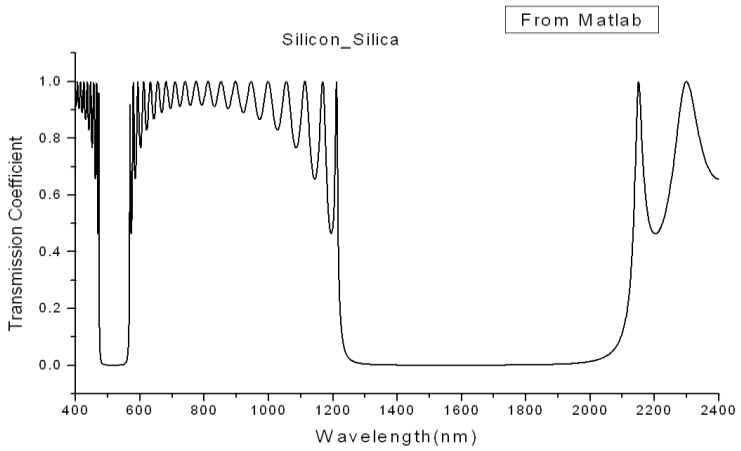

Fig3: Plot between
Wavelength(nm) Vs. Trasmission Coefficient in case of Silicon_Silica based photonic crystal containing number of unit cells (N) = 10

Silicon_Silicon Carbide:

In the case of Silicon and Silicon Carbide the value of n_1 for Silicon is 3.5 and the value of n_2 for Silicon Carbide is 2.55, so by using equation (1) thickness of the first layer (d_1) = 1550/4*3.5 = 110.71 nm and thickness for the second layer (d_2) = 1550/4*2.55 = 151.96 nm.

Here transmission coefficient value is not actually 0, its value is around 0.1. The reason behind is that the difference between the refractive index value of this two material is so small (3.50 - 2.55) = 0.95, so Stop band does not touches the 0 line. We find Pass band lies in between 550 nm to 1390 nm (Approx), so Pass band width= 840 nm. From graph it is clearly shown that centre band gap lie is at 1580 nm (Approx) but our working wavelength is 1550 nm. For this reason wavelength shifts towards the higher frequency range with respect to corresponding wavelength (λ_0). Starts from 1780 nm (Approx) here find another Pass band till investigate of our range 2400 nm.

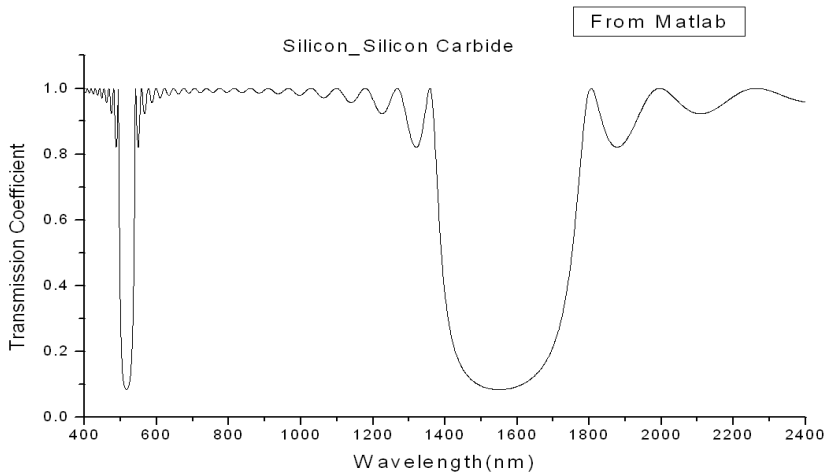

Fig4: Plot between Wavelength(nm) Vs. Transmission Coefficient in case of Silicon_Silicon Carbide based photonic crystal containing number of unit cells (N) = 10

Silicon_Silicon Carbide:

In that case transmission coefficient value is not actually 0, its value is around 0.1. The reason behind is that the difference between the refractive index value of this two material is so small (3.50 - 2.55) = 0.95, so Stop band does not touches the 0 line and has value (0.1). If we increase the number of unit cells from 10 to 30, then Stop band range is within 1410 nm to 1730 nm (Approx), so Transmission Coefficient value is actually 0 and Stop band width is 320 nm. Pass band lies in between 550 nm to 1410 nm (Approx), so Pass band width= 860 nm. From graph it is clearly shown that centre band gap lie is at 1580 nm (Approx) but our working wavelength is 1550 nm. For this reason wavelength shifts towards the higher frequency range with respect to corresponding wavelength (λ_0). Starts from 1730 nm (Approx) here find another Pass band till investigate of our range 2400 nm.

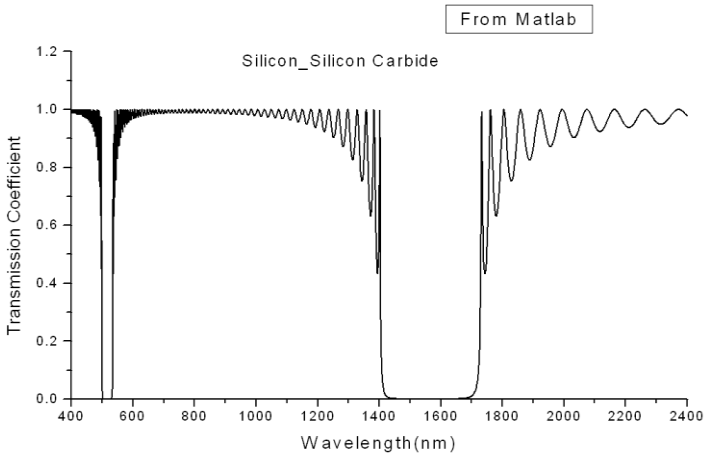

Fig5: Plot between Wavelength(nm) Vs. Transmission Coefficient in case of Silicon_Silicon Carbide based photonic crystal containing number of unit cells (N) = 30

Silicon Carbide_Air:

Here for Silicon Carbide and Air the value of n_1 for Silicon Carbide is 2.55 and the value of n_2 for Air is 1, so by using equation (1) thickness of the first layer (d_1) = 1550/4*2.55 = 151.96 nm and thickness for the second layer (d_2) = 1550/4*1 = 387.50 nm.

From this plot it is clearly shown that Stop band lies in between 1230 nm to 2180 nm (Approx). Within this Stop band range transmission coefficient value is 0, here Stop band width = 2180-1230 = 950 nm. Centre band gap is at 1680 nm. Pass band lies in between 550 nm to 1230 nm (Approx). So Pass band width = 1230 – 550 = 680 nm. We work with 1550 nm wavelength but here find centre band gap lie is at 1680 nm. So our wavelength shifts towards the higher frequency range with respect to corresponding wavelength (λ_0). After 2180 nm (Approx) we find another Pass band till investigate of our range 2400 nm.

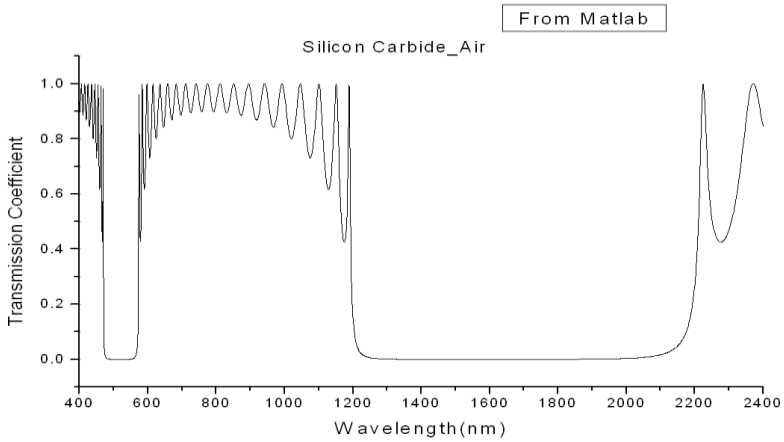

Fig6: Plot between Wavelength(nm) Vs. Transmission Coefficient in case of Silicon Carbide_Air based photonic crystal containing number of unit cells (N) = 10

Silicon Carbide_Silica:

In that case of Silicon Carbide and Silica the value of n_1 for Silicon Carbide is 2.55 and the value of n_2 for Silica is 1.5, so by using equation (1) thickness of the first layer (d_1) = 1550/4*2.55 = 151.96 nm and thickness for the second layer (d_2) = 1550/4*1.5 = 258.33 nm.

Here the value of transmission coefficient is not actually 0, its value is just above the 0 the reason is that the difference between the refractive index of that two material is so small (2.55 – 1.50) = 1.05, that's why it is not possible to achieve the Stop band. The Pass band lies in between 550 nm to 1320 nm (Approx), so the Pass band width is 1320 - 550 = 770 nm. In that case choosing wavelength is 1550 nm but the centre band gap lie is at 1600 nm. So wavelength shifts towards the higher frequency range with respect to corresponding wavelength (λ_0). After 1900 nm (Approx) the end range is 2400 nm within that region we find another Pass band lies.

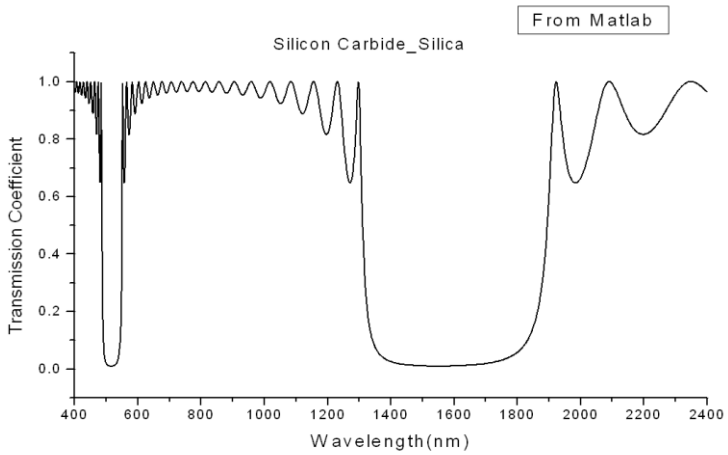

Fig7: Plot between Wavelength(nm) Vs. Transmission Coefficient in case of Silicon Carbide_Silica based photonic crystal containing number of unit cells (N) = 10

Silicon Carbide_Silica:

Here the value of transmission coefficient is not actually 0, its value is just above the 0 the reason is that the difference between the refractive index of that two material is so small (2.55 – 1.50) = 1.05, that's why it is not possible to achieve the Stop band. To achieve the Stop band we have to increase the number of unit cells (N) from 10 to 20, then we get the actual Transmission Coefficient value 0 within the Stop band range 1320 nm to 1870 nm (Approx), so Stop band width is 1870-1320= 550 nm. Pass band lies in between 550 nm to 1320 nm (Approx), so Pass band width is 770 nm. It is clearly shown that centre band gap lie is at 1600 nm (Approx) but our working wavelength is 1550 nm. For this reason wavelength shifts towards the higher frequency range with respect to corresponding wavelength (λ_0). Starts from 1870 nm (Approx) here find another Pass band till investigate of our range 2400 nm.

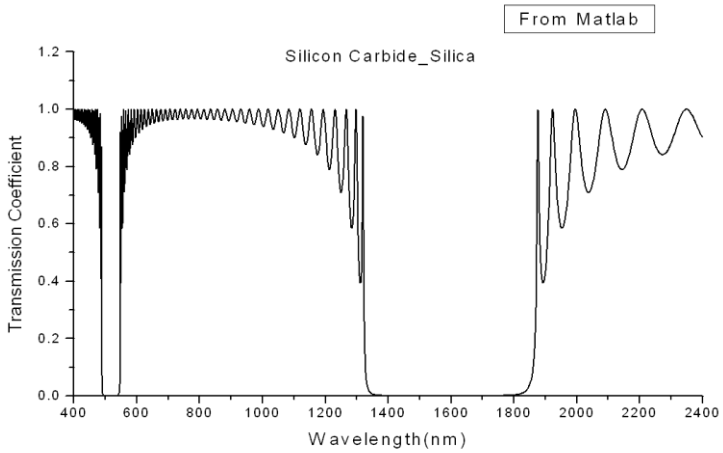

Fig8: Plot between

Wavelength(nm) Vs. Transmission Coefficient in case of Silicon Carbide_Silica based photonic crystal containing number of unit cells (N) = 20

V. Conclusion

From the below , combinations of different 2 layers photonic crystal(shown in table) it is become easier to compare the various characteristics and from below table it is clearly shown that for different material combinations the characteristics of SiC based photonic crystal has been varying. In case of stop band there is a large variation but in pass band the variation is not so large as of stop band .In this Silicon Carbide based 1D photonic crystal with 2 layered unit cell there are particular two types of semiconductor material combinations where selectivity of that two unit cell are not so good that's why firstly impossible to get stop band, after increasing the number of unit cell the selectivity will stand in a good position and then stop band is clearly shown.

Material	*Stop band width (nm) approx.*	*Pass band width (nm) approx.*	*Centre band gap (nm) approx.*	*Deviation of wavelength w.r.t. 1550 nm.*
Silicon_Silica	850	700	1680	130
Silicon_Silicon Carbide	320	840	1580	30
Silicon Carbide_Air	950	680	1680	130
Silicon Carbide_ Silica	550	770	1600	50

References

[1] J. D. Joannopoulos, S. G. Johnson, J. N. Winn, R. D. Meade, "Photonic Crystals Molding the Flow of Light", Princeton University Press, 2008.
[2] J. W. Haus, "Photonic Band gap Structures" in nanometer structures: Theory, Modelling and Simulation (Ed: A. Lakhtakia), PHI, New Delhi, 2007, P. 45.
[3] "Photonic crystal", http://en.wikipedia.org/wiki/Photonic_crystal

IOSR Journal of Electronics and Communication Engineering (IOSR-JECE)
e-ISSN: 2278-2834,p- ISSN: 2278-8735. Volume 5, Issue 6 (Mar. - Apr. 2013), PP 41-45
www.iosrjournals.org

A Review of BSS Based Digital Image Watermarking and Extraction Methods

Dr. Sangeeta Jadhav
Prof and Head of Information Technology Department, Army Institute of Technology ,Pune, India

Abstract :*The field of Signal Processing has witnessed the strong emergence of a new technique, the Blind Signal Processing (BSP) which is based on sound theoretical foundation. An offshoot of the BSP is known as Blind Source Separation (BSS). This digital signal processing techniques have a wide and varied potential applications. The term blind is indicative of the fact that both the source signal and the mixing procedures are unknown. One of the more interesting applications of BSS is in field of image data security/authentication where digital watermarking is proposed. Watermarking is a promising technique to help protect data security and intellectual property rights. The plethora digital image watermarking methods are surveyed and discussed here with their features and limitations. Thus literature survey is presented in two major categories-Digital image watermarking methods and BSS based techniques in digital image watermarking and extraction.*

Keywords – *BSP, BSS, Mixing Coefficient, Digital Image Watermarking, Watermark Extraction.*

I. Introduction

Research in image watermarking almost covers all media forms like audio, video, image text, and 3 D model and software codes. A digital watermark is a transparent, invisible information pattern that is inserted into a suitable component of the data source by using a specific computer algorithm. There are lot of similarities between information hiding, steganography and watermarking in distribution of electronic document. Information hiding involves the concealment of information so that an observer does not know about its existence. Steganography generally means "covered writing" where communications are carried out in secret. Watermarking is the embedding of content-dependent information. Information hiding covers both steganography and watermarking **[**1**]** .The blind digital image watermarking scheme does not require original image and watermark during extraction process. The watermarked image is viewed as linear mixture of sources *i.e.* original image and watermarks. In the proposed work BSS theory is used to form these linear mixtures in transmitter and blindly retrieve the robust watermark from the mixture in receiver. Thus instantaneous BSS problem is formulated for Digital image watermarking. Independent Component Analysis (ICA) is the most powerful and widely used technique for performing BSS.

In terms of embedding the watermark, there are two main methods. The first is to embed a random binary string into the cover image [2]and the second method is embed a grayscale or binary image watermark into the cover image [3,4]. The second method has the advantages in terms of robustness and copyright protection.

II. WATERMARKING TECHNIQUES

Watermarking techniques can be classifiedas shown in Figure 2.1 according to the application domain, type of document and human perception [5].

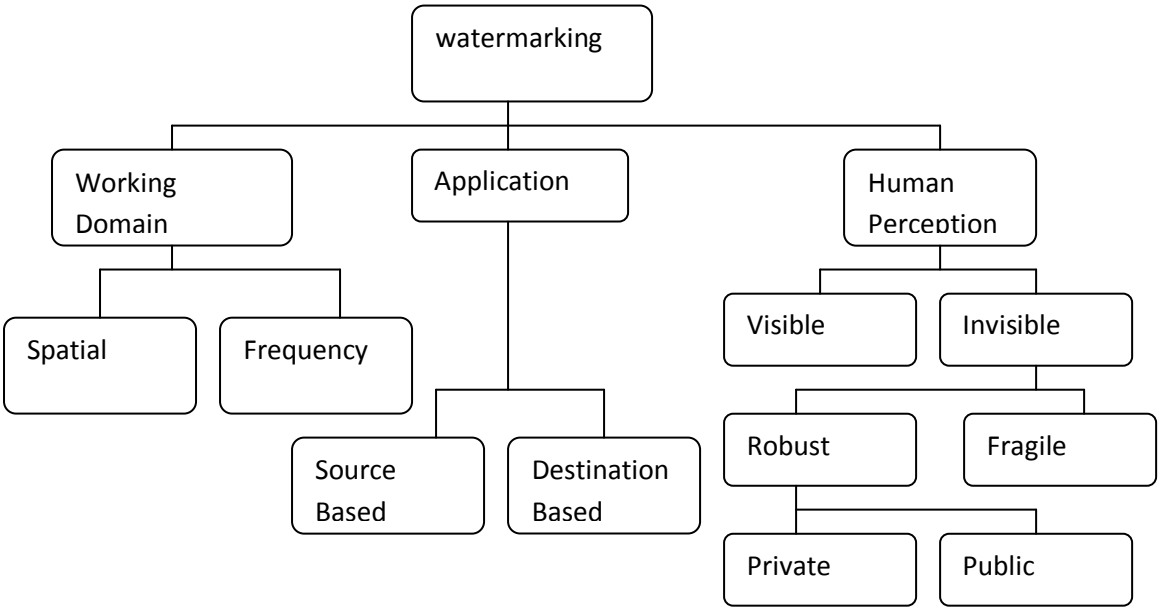

Figure 2.1: Classification of watermark techniques.

There are several ways of classifying watermarking methods as shown in Figure 2.2.4. Most widely adopted classification is based on watermark robustness. Under this classification watermark can be grouped into 3 types

- Robust watermarks :-These watermarks can resist non-malicious distortions[6] Application-wise, robust watermarks are suitable for copyright protection because they can resist common image processing operations
- Fragile watermarks:-These watermarks are easily destroyed by all image distortions. These watermarks can be used to detect tampering and authenticate an image because it is sensitive to changes [7]
- Semi-Fragile:- These watermarks can be destroyed by certain types of distortions while resisting other minor changes. These watermarks are usually applied in some special cases of authentication and tamper detection for example a semi -fragile watermarking scheme [8] for color image authentication using YST color space is presented where embedding space is created by setting the two LSB's of selected sub blocks to zero which will hold the authentication and recovery information

Depending on the availability of the original image, there are three watermark detection/extraction schemes: Non-blind, semi-blind, and blind.

- Non-blind schemes (also called non-public or non-oblivious watermarking) : Both the original image and the secret key(s) are needed
- Semi-blind schemes (also called semi-private or semi-oblivious watermarking) [9]: The secret key(s) and the watermark are needed
- Blind schemes (also called public or oblivious watermarking) [10]: Only the secret key(s) are needed

In nature , the process of watermark embedding is the same as some special kind of patterns or under-written images are added into the host image, we can consider it as a mixture of host image and watermark image, thus without host image the watermark detection is equal to blind source separation in the receiver [11,12].

III. General Watermarking Framework

A watermarking system is usually divided into three distinct steps, embedding, attacks and detection. The information to be embedded in a signal is called a digital watermark, although in some contexts the phrase digital watermark means the difference between the watermarked signal and the cover signal. The signal where the watermark is to be embedded is called the *host* signal.

1.1.1 Watermark embedding

It is also called watermark encoding. The watermark embedding algorithm embeds a watermark in the spatial and transformed domain of image.

Figure 3.1 shows a generic watermark embedding system. The input parameters for watermark encoder are original image, watermark to be embedded and the secret or public key.

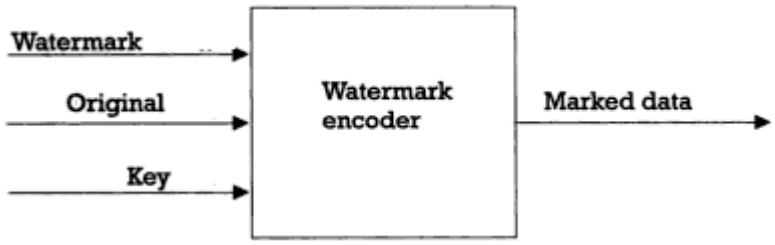

Figure 3.1: Generic Watermark Embedding Scheme

The output of the embedding process is always the watermarked data/image

1.1.2 Attacks

If any person makes a modification in transmitted signal, is called an *attack.*

In watermarking robustness against attacks is a major requirement. An attack is successful if the watermark cannot be detected anymore but the image is still intelligible and can be used for other purposes. With appropriate design objectively high robustness can be achieved. The attacks are classified into four categories

1. Simple attacks–These are conceptually simple attacks which attempt to impair the watermark by manipulation of the watermarked data. Examples include addition of noise, linear and nonlinear filtering, cropping *etc.*
2. Synchronization attacks-These attacks attempt to break the correlation by geometric distortion like rotation zooming *etc.* Watermark recovery becomes impossible for watermark detector due to this type of attacks.
3. Removal attacks- These attacks attempt to separate and remove the watermarks. Examples include denoising the watermarked image through median or high pass filtering.
4. Inversion attacks- Th Inversion attacks- These attacks attempt to confuse by producing fake original data which degrades the authority of watermark by embedding one or several additional watermarks .

3.1.3 Watermark Detection

This is also called extraction of watermark. It is an algorithm which is applied to the attacked signal to attempt to extract the watermark from it. If the signal was unmodified during transmission, then the watermark still is present and it may be extracted. In robust digital watermarking applications, the extraction algorithm should be able to produce the watermark correctly, even if the modifications were strong. In fragile digital watermarking, the extraction algorithm should fail if any change is made to the signal. A generic watermark detection scheme shown in Figure 3.2 needs a watermarked data and the secret key or public key.

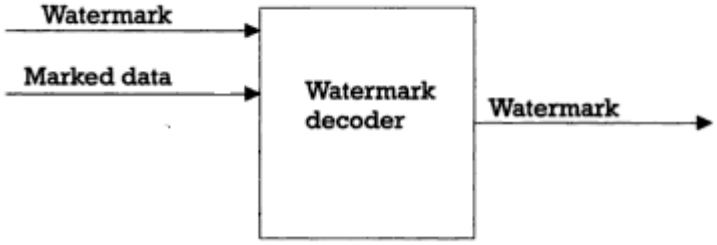

Figure 3.2: Generic Watermark Detecting Scheme

Figure 3.3:

For digital color image watermarking following requirements should be satisfied –

- Elements of digital content can be directly manipulated and information can be embedded in them.
- Watermark should be perceptually invisible. Alterations introduced in the image should not reduce its perceived quality.
- Deterioration of the quality of digital content is minimized.
- Watermarks are retained and detectable after the digital content is edited, compressed, or converted. Thus Watermark should be robust as much as possible against attacks or image processing operations that preserve a desired image quality.
- Processing required for watermarking and detection should be simple.

The Detection of the watermark should not require access to the original image data. This demand is necessary for avoiding time consuming search in large digital image libraries.

IV. Bss In Digital Image Watermarking

Applications of BSS in document security is attracting more researchers because this technique does not require any a-priory information . The application includes the BSS applied at added encryption level and the separation keys are used to control the BSS decryption. Combinations of approaches like combining wavelet fractal with BSS to realize the embedding, detection of watermark to improve the security.

In nature, the process of watermark embedding is the same as some special kind of patterns or under-written images are added into the host image, we can consider it as a mixture of host image and watermark image, thus without host image the watermark detection is equal to blind source separation in the receiver.

Theory of BSS along with RGB decomposition to embed and extract the watermark. By experimentation with various images the mixing matrices are determined by trial and error method[13]. A binary image is embedded into a wavelet approach sub-image. Fast ICA algorithm is used to extract the watermark and fixed mixing matrix is selected for forming watermarked mixtures. Ju Liu, Xingang Zhang *et al.* [14] discusses the watermarking scheme based on the combination of DWT and ICA and a random mixing matrix is used to form the mixtures of images which are used as approximate image of watermarked image and the other as the key. A robust audio watermarking [15] based on ICA and Singular Value Decomposition(SVD) where a random mixing matrix is used.

Spatial methods using BSS are discussed in previous literature like a blind watermark detection using ICA for Spread spectrum based image watermarking [16]. The digital image watermarking in wavelet domain and extraction using MLICA and in embedding a random key is used [17]. The watermark embedding is done in spatial domain using a secret key and extraction adopts ICA[18] where a global histogram approach is used to segment the video and ICA is used for each segment for watermarking.BSS based image watermarking [19] are discussed in previous literatures with fixed or random mixing matrices during embedding.

V. Challenges And Open Issues

Digital watermarking is a complex technology which involve many requirements and tradeoffs. This thesis has handled 3 major open issues regarding digital image watermarking

- Capacity- Related issues include the optimum amount of data, a method to embed and finally the extraction of watermark. In the proposed work the effort is taken to determine the optimum amount of data to be embedded in the cover image using the optimization technique and BSS theory.
- Robustness-This is the main requirement of digital watermarking in applications like copyright protection and content authentication. The presented work has been developed towards the robustness requirement and producing the promising results.
- Transparency- This feature of digital watermarking is required in most of the applications in real world. It is related to the issue of embedding of watermark in such a way that it should not perceptually degrade the data.

5.1. Applications and utility

Digital image watermarking has numerous applications in variety of fields. Some of the application fields are mentioned below.

The main applications fields of digital image watermarking are –

- Copyright Protection

Watermarking can be used to protect redistribution of copyright material over the untrusted network like Internet or peer-to-peer networks.

- Content Archiving

Watermarking can be used to insert digital object identifier or serial number to help archive digital contents like images, audio or video.

- Meta data Insertion

Meta-data refers to the data that describes data. Images can be labeled with its content and can be used in search engines. Audio files can carry the lyrics or the name of the singer. Medical X-rays could store patient records.

- Tamper Detection

Digital content can be detected for tampering by embedding fragile watermarks. If the fragile watermark is destroyed or degraded, it indicates the presence of tampering and hence the digital content can not be trusted. Tamper detection is very important for some applications that involve highly sensitive data like satellite imagery or medical imagery .

- Digital Fingerprinting

Digital fingerprinting is a technique used to detect the owner of the digital content .Finger prints are unique to the owner of the digital content . Hence a single digital object can have different fingerprints.

VI. CONCLUSION

The literature reviewed for digital image watermarking shows that there is lot of scope of improvement in the field of watermarking using Blind Source Separation (BSS). The embedding and extraction of watermark processes may be further modified so as to achieve high degree of imperceptibility and robustness.

Thus the presented work will be useful to develop aBSS based optimized system with variable values of mixing matrix for digital image watermarking.

References

[1] J.J. Eggers, R. Bauml, R Tzschoppe and J Huber, "Applications of Information hiding &digital watermarking" ECDL WS Generalized Documents Yr 2001,pp1-6.

[2] Wong Hon Wah, " Image Watermarking and data Hiding Techniques" Ph D Thesis , Hong-Kong Univ. ,Yr2003,pp1-70.

[3] Dr GN Swamy and B. Surekha, " A Spatial Domain Public Image Watermarking" International Journal of Security and Its Applications, Vol,5 No. 1,Yr 2011,pp 1-11.

[4] S. Radharani and Dr. ML valarmathi , " A Study on Watermarking Schemes for Image Authentication" International Journal of Computer Applications(0975-8887),vol-2-No 4, Yr 2010,pp 24-31.

[5] Peter Foris and DusanLevicky, "Adaptive Digital Image Watermarking Based on Combination of HVS Models" Radio Engineering Vol-18,No-3 Sep 2009,pp 317-323.

[6] Rajesh KannanMegalingam,MithunMuralidharan Nair, Rahul Srikumar ,VenkatKrishnanBalsubramanian and VineethSarma, VenugopalSarma," A Comparitive Study on Performance of Novel Robust Spatial Domain Digital Image Watermarking with DCT based watermarking" International Journal of Computer Theory and Engineering Vol-2,No-4, Yr 2010,pp 1793-8201.

[7] Hua Yuan and Xiao-Ping Zhang, "A Multiscale Fragile watermarkBased on the gaussian Mixture Model in the Wavelet Domain " IEEE proceedings of ICASSP,Yr-2004, pp III-413-416.

[8] M. Hamad Hassan. And S.A.M. Gilani, " A Semi -Fragile Watermarking Scheme for Color Image Authentication" World Academy of Science ,Engg. And Technology, Yr-2006, pp 36-38.

[9] JanuszKusyk and Ahmet M. Eskicioglu, "A Semi- Blind Logo Watermarking Scheme for Color Images by Comparison and Modification of DFT Coefficients",
Google Search: http://*citeseerx.ist.psu.edu*

[10] Xinde Sun and Shukui Bo, " A Blind digital Watermarking for Color Medical Images Based on PCA" IEEE, Yr-2010, pp421-427.

[11] Joachim J. Eggers, Jonathan K. Su and Bernd Girod, "Performance of a practical Blind Watermarking Scheme", proceedings of SPIE Vol 4314 Yr 2001, pp1-12.

[12] Peter H.W. Wong and Oscar C Au and YM Yeung," A Novel Blind Multiple Watermarking technique for Images" IEEE Transactions on Circuits and Systems for video Technology,vol-13,No.8,Yr-2003, pp813-830.

[13] Moilim Amir, AbdellahAdib and DrissAboutajdine, "Color Images Watermarking by Means of Independent Component Analysis",in IEEE transaction , yr-2007,pp 347-350.

[14] Ju Liu, Xingang Zhang and Jiande Sun, " A New Image watermarking Scheme Based on DWT and ICA" IEEE Int Conf. Neural Networks and Signal Processing ,Yr2003,pp 1489-1492.

[15] Xiao-Hong Ma Zhong-Jie Liang and Fu-Liang Yin "A digital audio Watermarking Scheme Based on Independent Component Analysis and Singular Value Decomposition" Proceedings of 5th International Conference on Machine Learning and Cybernetics ,Aug 2006,pp2434-2438.

[16] Hafiz Malik, AshfaqKhokhar and Rashid Ansari, " Improved Watermark Detection for Spread Spectrum Based Watrmarking using Independent Component Analysis" ACM, pp 102-111, Yr 2005.

[17] G. Thirugnanam and S. Arulselvi, " Maximum Likelihood ICA and Kernel ICA comparison for Wavelet Based Digital Image Watermarking", International Journal of Signal and Image Processing,Vol-1-2010/Issue1, Yr-2010,pp 12-17.

[18] SUN Jiande and Liu Ju, "A Blind Video Watermarking Scheme Based on ICA and Shot Segmentation." DOI: 10.1007/s11432-006-0302-9,Science in China: Series of Information Sciences 2006,Vol-49,No-3n302,pp 302-312.Yr-2006

[19] Ren Shijie,SuXin, YuHuishan and Niu Huijuan, " Blind Watermarking Based on Fast ICA and DWT", Proceedings of IWISA 2009,pp 256-259.

IOSR Journal of Electronics and Communication Engineering (IOSR-JECE)
e-ISSN: 2278-2834,p- ISSN: 2278-8735.Volume 5, Issue 6 (Mar. - Apr. 2013), PP 46-56
www.iosrjournals.org

Industrial Process Management Using LabVIEW

S.Venkatlakshmi[1], S.Vivekanandhan[2], S.Revathi[3], E.M.Shakthi Arul[4],
C.Paramasivam [5](Assistant Professor)
Department of ECE, K.S.Rangasamy College of Technology, Tiruchengode

***Abstract*:** *Nowadays process management is a tedious task in the industry. We plan to propose a LabVIEW based intelligent multi parameter monitoring system designed using RS232 and Microcontroller aids in the measurement and control of various Global Parameters. For data collection in the industry is a difficult task in real time execution of events with industrial process control and automation. We proposed two slaves for measuring various industrial parameters to monitor and control industrial process. Data acquired from each slave is processed and sent to Master that compile data received from different slaves and send this information to the system configured with LabVIEW platform. This enables us to view and track the online changes encountered in the particular parameter of all the parameters. One of the main advantages of this proposal is, it allows us to view all the parameter readings simultaneously on the front panel in LabVIEW. The Graph drawn on the front panel keeps on tracking the changes on the parameter. The parameters supported by this project includes: current, voltage, temperature, frequency, light intensity, logic switches, water level identifier, and alarm. This Project can be implemented in any of the process industries where there is a need for Simultaneous and fast acquiring of data and control.*

Keywords: *LabVIEW, RS232, Micro-controller, data acquisition*

I. INTRODUCTION

At present DAQ systems are widely popular in industry in the control and remote monitoring of system status and physiological parameters.The paper designed the virtual test platform for communication with measurement and control. After testing, the platform has high speed of data acquisition, is able to effectively deal with parameters of the object for testing and output the result, as well as can well communicate with other devices. The interaction with physical quantities to be measured is performing with specific hardware or PC standard interfaces [1].

Multiple embedded nodes are measuring various industrial parameters to monitor and control industrial process. Acquired data display at each node and sent to master processor that compile the acquired information and send to remote location [2].

G language LabVIEW can be effectively achieved a virtual panel in the personal computer. Virtual instrument panel has the virtual switches, buttons and knobs with the same function of real instrument. User operates the instrument through the friendly graphical interface, thus completing the measurement signal acquisition, analysis, judgment, display, and data access. The paper adds the value towards the low cost, less manufacturing time, ease of implementation with reliable measuring, controlling and data logging demands of industry [4].

II. SYSTEM DESIGN

2.1 DESIGN OF REAL TIME DATA ACQUISITION SYSTEM

Design of data acquisition system is demonstrated for measurement of parameters like temperature, light, voltage, current etc. by acquiring data using different sensors at different locations and communicating with the user using Ethernet module. System description divided into two parts, consisting of hardware and Software description.

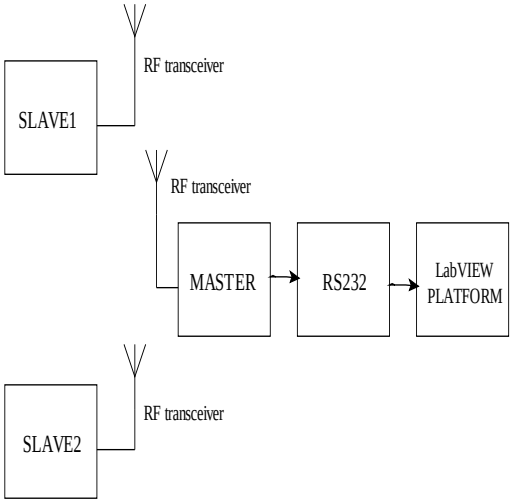

Figure1. Block diagram of Industrial process management

III. Hardware Description

In the design of real time data acquisition system, we used several sensors like LDR, temperature sensors that will observe the different parameters. The ADC for receiving the analog input and converts it into digital data that will be process by Slave controller. We have used PIC18F4550 as master controller. We are using master and slave method for realization of this DAQ system.

For slaves we have used 16 bit microcontroller name PIC18F4550. The slave takes the decision as per instruction stored in its program memory. The signal can be sent at faraway places by using Ethernet module and display waveforms of acquired signals on front panel designed with LabVIEW.

3.1 MICROCONTROLLER

Microcontrollers are small and cost effective but self-contained computer chips used for embedded applications in industrial and consumer electronics products. In this system, we are using PIC18F4550 microcontroller as slaves and also PIC18F4550 as master controller. The PIC18F4550 performs the major role in this project because we can connect this through the USB channel. The pin diagram was shown in Fig no 2.

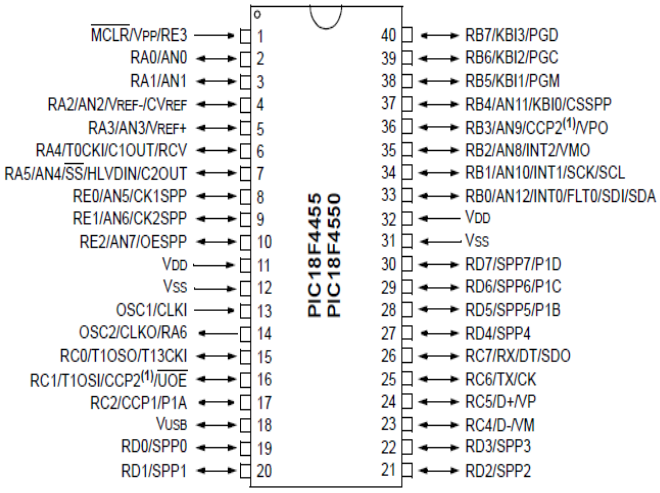

Figure2. Pin diagram of PIC18F4550

3.2 TEMPERATURE MEASUREMENT

The LM35 series are precision integrated-circuit temperature sensors, whose output voltage linearly calibrated directly in ˚ Celsius (Centigrade) i.e. Linear + 10.0 mV/˚C scale factor with 0.5˚C accuracy guarantee able (at +25˚C) and rated for full −55˚ to +150˚C range [1]. It operates from 4 to 30 volts and draws less than 60 μA. Schematic diagram of LM35 was shown in Figure 3.

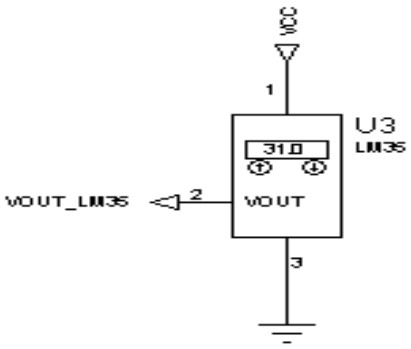

Figure 3.Schematic for LM35 IC temperature measurement

3.3 WATER LEVEL IDENTIFIER

The circuit indicates the amount of water in the tank head, but also gives an alarm when the tank is full [1].This circuit uses the widely available to show IC number CD4066 bilateral switch CMOS IC to the water level through LEDs.

If the water is empty the wires in the tank are open circuit and the 180K resistors pulls the switch to open the little switches and LEDs are off. When the water begins to fill the first connected to the reservoir in the S1 and the + supply are shorted by water. This closes the S1 and turns the LED1 ON. As the water further into the tank, LEDS2, 3 to 4 pm light gradually filled.

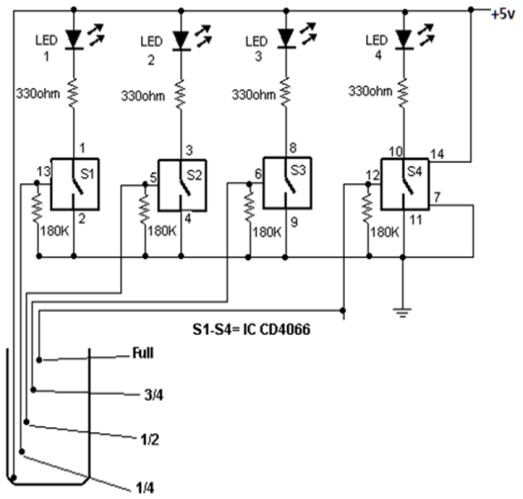

Figure4. Water level sensor circuit

3.4 LIGHT INTENSITY MEASUREMENT

A Light / Dark activated switch is a circuit which was shown Fig no.3.8 that will measure the light level and will turn on or off a relay accordingly. We use an LDR (Light Depended Resistor) to measure the light level.

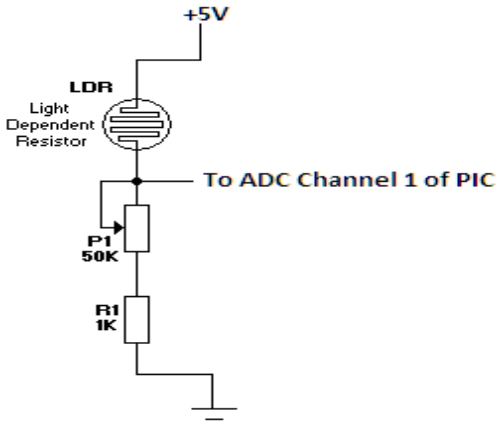

Figure5. Light/Dark activated relay circuit

The circuit is a simple transistor switch with the base of the transistor connected to a voltage divider [2]. The voltage divider has two resistors. The first is the 100K potentiometer plus the protective 1K resistor. The second resistor is the LDR. As light falls on the surface of the LDR, the LDR changes it's resistance. The more the light, the less the resistance of the LDR, the less the resistance, the less the voltage drop across it. The less the light, the more the resistance and thus the more the voltage drop across it. As the voltage drop increases, so does the VB of the 2N2222 transistor and therefore the ICE increases accordingly, until the time that the current is enough to actuate the relay.

The amount of light needed to actuate the relay can be changed by changing the 100K potentiometer. Basically, any change to the potentiometer will have an effect to the voltage drop of the LDR, as they are both members of the voltage divider described above. The 1N4001 diode is used to eliminate any back voltage when the relay is disarmed. It is very important to have this diode because without it, the transistor may be damaged. The circuit Figure no.3.8 b) dark activated relay senses darkness. As the light level decreases and LDR meets the maximum threshold resistance, the circuit automatically switches on the LED D1. A dark detector can be made using a variable resistor. The sensitivity of the circuit can be adjusted with a variable resistor.

High resistance→ more darkness to switch on the LED Low resistance→ less darkness to switch on the LED

As the light level increases and LDR meets the lowest threshold resistance, the circuit automatically turns on the LED D1. We can adjust the sensitivity using the preset VR1-10K.

Less resistance (vr1)→
Less darkness to switch off the LED
High resistance (vr1)→
More darkness to switch off the LED

3.5 ALARM

The design of alarm system used in Industrial process management is similar to the design used for fire alarm system in smart house [2]. It is divided into three parts; the first part is the signal that reaches from alarm sensors when its trigger threshold has been reached after any a specific danger in the industry. The second part is the output signal that sends after the processing of input signal, and final part is the controlling system and data processing by LabVIEW.

3.6 LOGIC SWITCHES

A microcontroller can't make any decisions on controlling something in the outside world without sensing something about it. The simplest thing for a microcontroller to check is the status of a switch. Switches can be used as operator controls. They can sense if a door is open or closed. A limit switch can detect if a part of a machine has reached a certain position. Switches can be used for many purposes, but they can be in only one of two states: On (closed) or off (open).

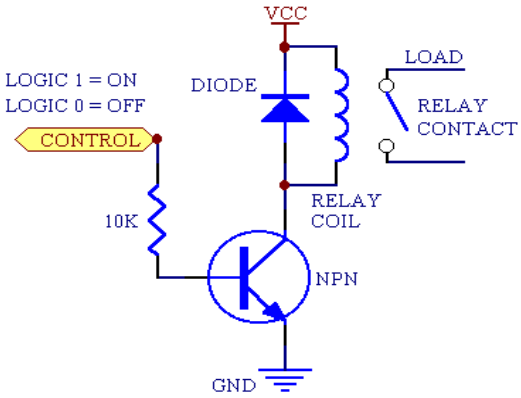

Figure7. Interfacing circuit of Microcontroller to logic Switches

Figure no 7 shows two common ways to interface switches to a microcontroller input. Input P0 uses R1 as a pull up. If SW1 is open, P0 will be high, and read as a logical 1. When SW1 is closed, pin P0 is shorted to ground, or 0V, and P0 will read as a logical 0.

3.7 VOLTAGE MEASUREMENT

Voltage is the difference of electrical potential between two points of an electrical or electronic circuit, expressed in volts. It measures the potential energy of an electric field to cause an electric current in an electrical conductor. Most measurement devices can measure voltage. Two common voltage measurements are direct current (DC) and alternating current (AC). Although voltage measurements are the simplest of the different types of analog measurements, they present unique challenges due to noise considerations.

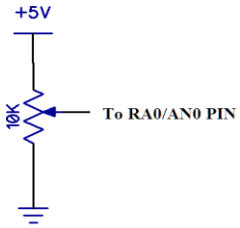

Figure 8.Voltage measurement circuit

3.8 CURRENT MEASUREMENT

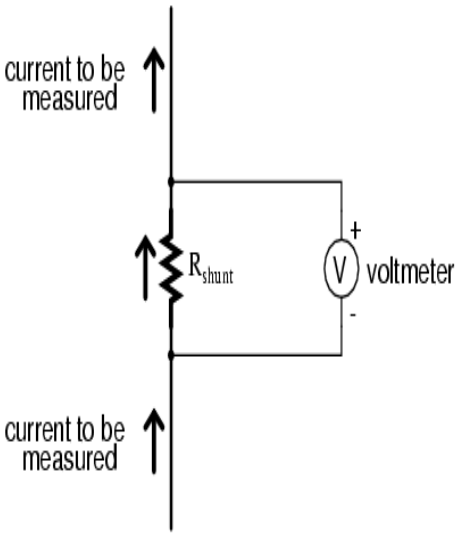

Figure9. Ammeter circuit

In ammeter designs, external resistors added to extend the usable range of the movement are connected in *parallel* with the movement rather than in series as is the case for voltmeters. This is because we want to divide the measured current, not the measured voltage, going to the movement, and because current divider circuits are always formed by parallel resistances. Taking the same meter movement in Fig no9 as the voltmeter example, we can see that it would make a very limited instrument by itself, full-scale deflection occurring at only 1µA.

3.9 FREQUENCY MEASUREMENT

In order to understand the effect of frequency on the various parameters; let us consider the following example. Consider a coil of negligible resistance and inductance 60mH, connected to 230V, 50 HZ 1phase supply.

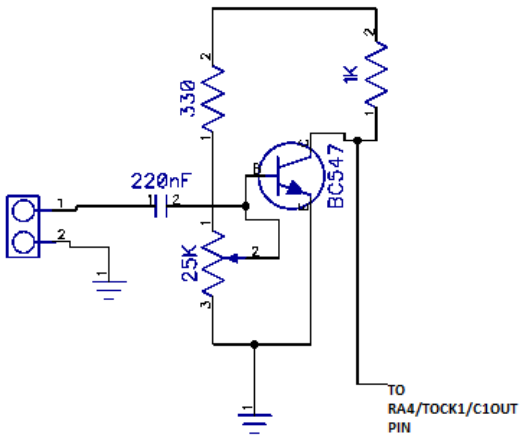

Figure 10.Frequency measurement circuit

IV. SOFTWARE DESCRIPTION Labview

LabVIEW front panel is designed for user interface to display waveforms of measured physical quantities, control number of byte counts, setting baud rate, selection of communication port number i.e. VISA resources name, error control techniques etc. S Graphical programming is used in LabVIEW and front panel along with its block diagram.

The virtual instrument designed in LabVIEW environment is able to receive binary equivalent of physical quantity from serial port connected to embedded board and display waveform on waveform chart, it also record the received values in a standard spreadsheet, then a application program running in PC.

4.1 LABVIEW SOFTWARE INTERFACE

Universal asynchronous receiver transmitter used here to interface computer through 9-pin RS232 port to display acquired signal waveform with front panel of LabVIEW platform. The LabVIEW front panel designed for user interface to display waveforms of measured physical quantities, control number of byte counts, setting baud rate, selection of communication port number i.e. VISA resources name, error control techniques etc.

Initializes the serial port specified by **VISA resource name** to the specified settings. Wire data to the **VISA resource name** input to determine the polymorphic instance to use or manually select the instance. VISA configure port representation diagram was shown in Figure 11.

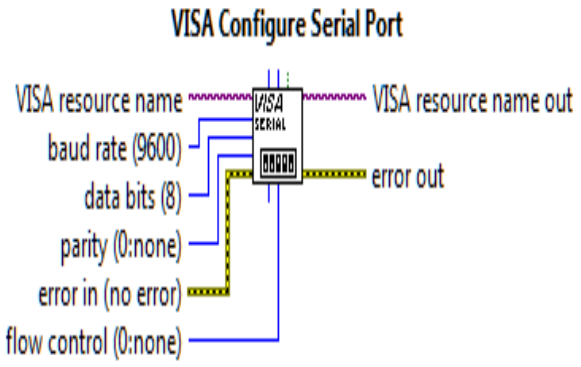

Figure 11.VISA configure serial port

`

4.2 BLOCK DIAGRAM

The programming in LabVIEW is graphical programming and performs in block diagram as shown in Figure11 The system has been implemented, tested successfully and achieved reliable transmission of data to the remote site and representation of waveform along with logging of data in excel sheet using LabVIEW.

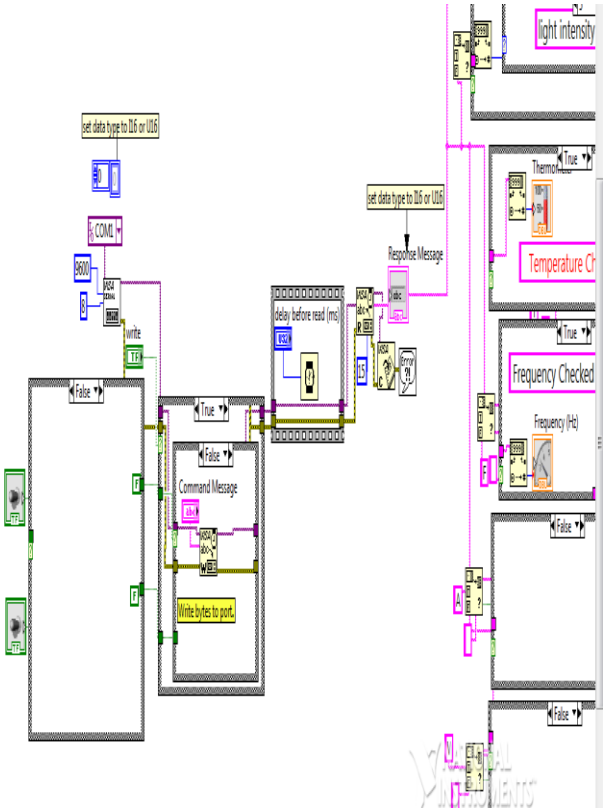

Figure11. Block diagram for serial communication in LabVIEW

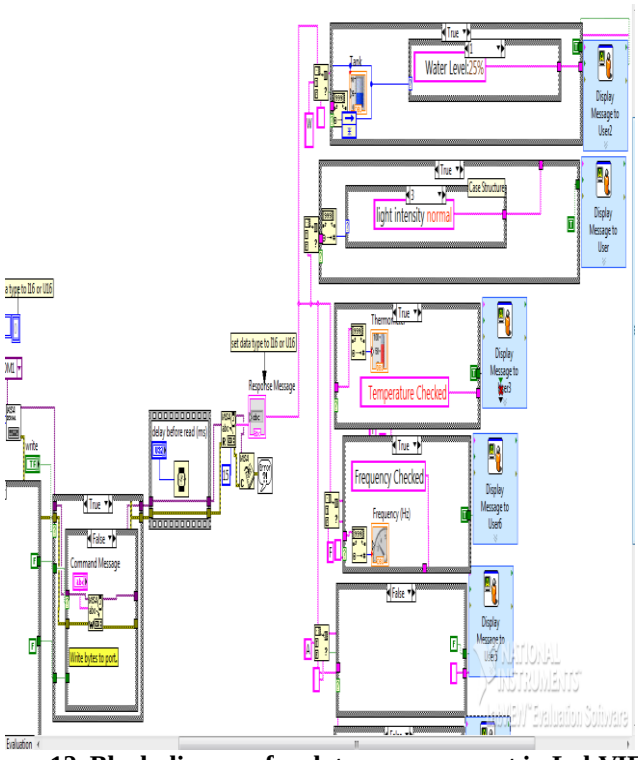

Figure 12. Block diagram for data measurement in LabVIEW

V. Results And Discussions

This project has been implemented, tested successfully and achieved reliable transmission of data to the remote site and representation of indications and controls with logging of data in excel sheet using LabVIEW.

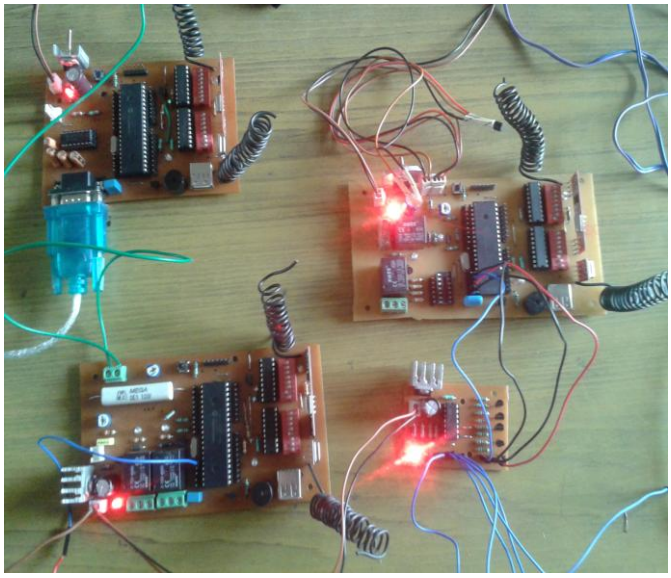

Figure13. Hardware part of industrial process management using LabVIEW

5.1 OUTPUT OF VARIOUS PARAMETERS IN LabVIEW

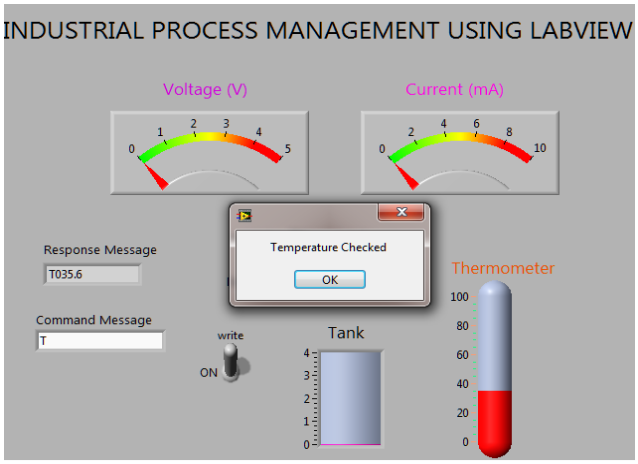

Figure 14.Output of Temperature measurement

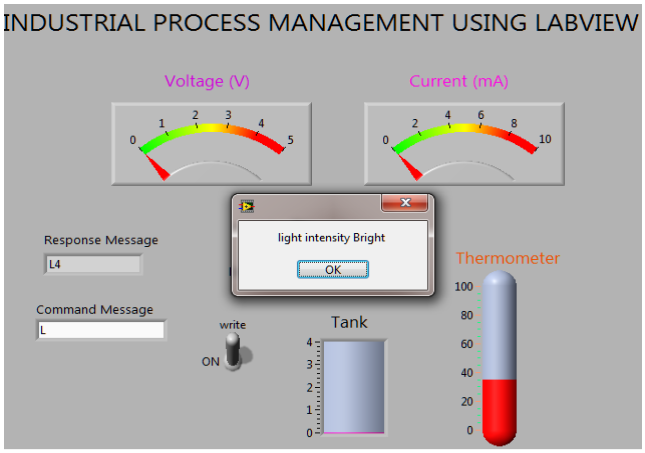

Figure 15.Output of Light intensity measurement

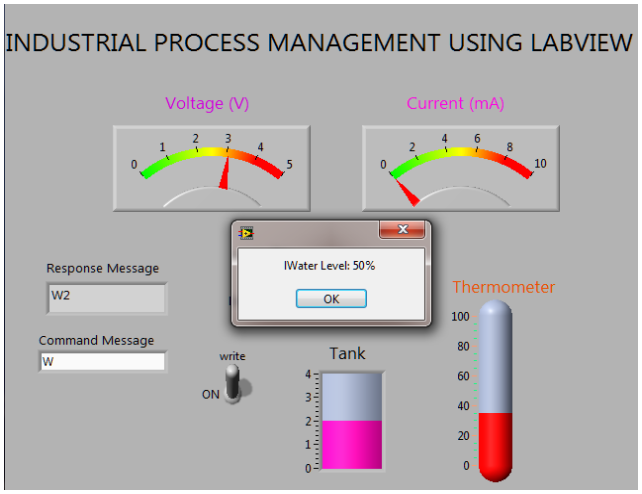

Figure 16. Output of water level measurement

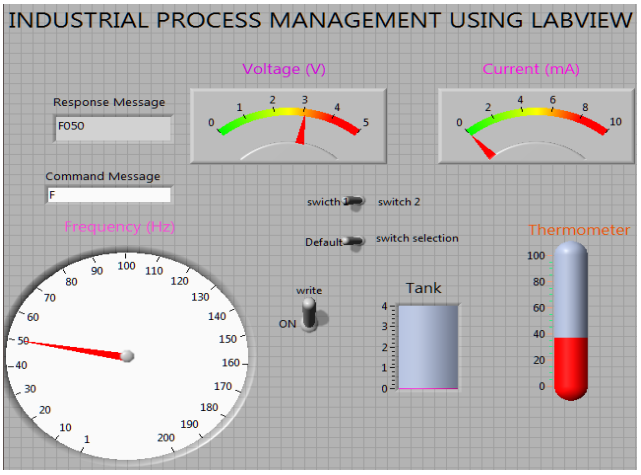

Figure 17.Output of Frequency measurement

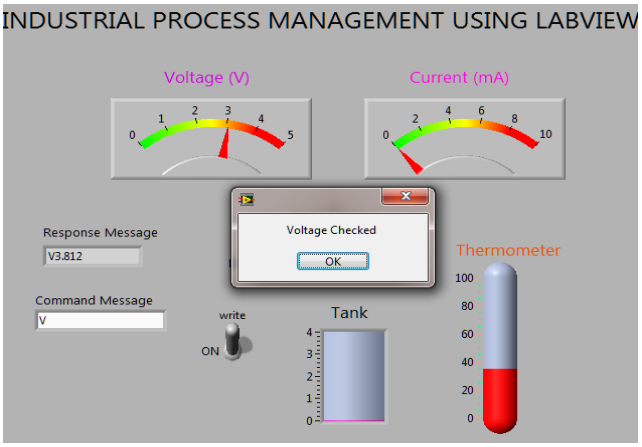

Figure 18. Output of Voltage measurement

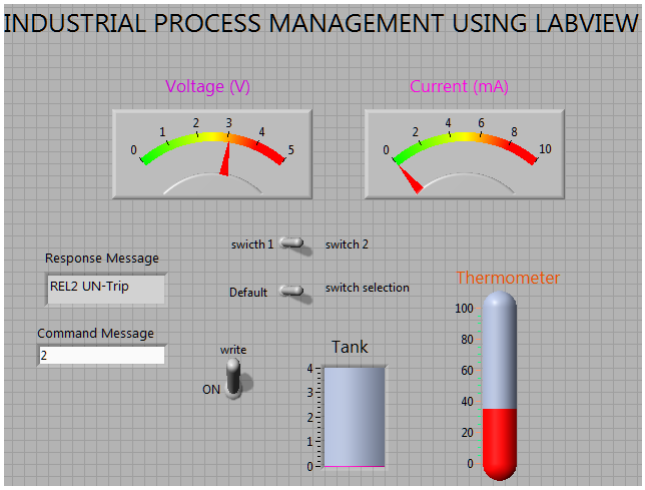

Figure 19. Output of Relay Circuit

VI. Conclusion

In this paper, master-node architecture for real time data acquisition and logging is demonstrated and implemented. Two slaves are measuring various industrial parameters to monitor and control industrial process. Acquired data display at each slave and sent to master processor that compile the acquired information and send to remote location using RS232 serial communication and simultaneously display and log into spreadsheet the variations in quantity under measurement to local and remote system configured with LabVIEW platform. In addition, the master processes this information and generates controls signals based on predefined cases or can receive the controlling action from remote controller to control the industrial application. The paper adds the

value simple approach for data acquisition, continuous monitoring of process parameters, less manufacturing time, ease of implementation with reliable measuring, controlling and data logging demands of industry.

References

[1] Mukesh Kumar, Sanjeev Sharma, Mansav Joshi **"Design of Real Time Data Acquisition with Multi Node Embedded Systems"** International Journal of Computer Applications (0975 – 8887) Volume 42– No.11, March 2012

[2] Basil Hamed **"Design & Implementation of Smart House Control Using LabVIEW"** International Journal of Soft Computing and Engineering (IJSCE) ISSN: 2231-2307, Volume-1, Issue-6, January 2012

[3] LabVIEW Software 2009 by National Instruments, http://www.ni.com.

[4] Amiya Ranjan Panda, Utpal Mandal, Hare Krishna Ratha **" Integrated Monitoring of Encoder Status Parameters and GUI based Remote Control Panel Using Lab view"**, 3rd International Journal of Computer Applications (0975 – 8887) Volume 43– No.3, April 2012.

[5] Baosheng Yang**,** Jianxin Li **,** Qian Zhang **"G Language Based Design of Virtual Experiment Platform for Communication with Measurement and Control"** on 2012 International Workshop on Information and Electronics Engineering (IWIEE)

[6] Wen Xinling, Zhao Cheng,"**Design and Simulation of Voltage Fluctuation Rate Monitor System Based on Virtual Instrument Technology"** in 2012 International Conference on Future Electrical Power and Energy Systems.

[7] Mukesh Kumar and Mansav Joshi, **"Design and Implementation of Embedding Web Server for Real Time Data Acquisition and Logging System"** 4th International Conference on Computer and Automation Engineering (ICCAE 2012), Mumbai, India, January 14-15, 2012.

[8] LabVIEW Graphical Programming by Gary W johnsion (TMH).

[9] Zhou Hongfu; Xiao Xinyan; Tang Yong, **"Serial Communication Interface Design Based on Lab VIEW and VC Mix Programming"**, 8th International Conference on Electronic Measurement & Instruments, (ICEMI2007) PP44-49, (in English) (ISTP/EI, INSPEC).

IOSR Journal of Electronics and Communication Engineering (IOSR-JECE)
e-ISSN: 2278-2834,p- ISSN: 2278-8735. Volume 5, Issue 6 (Mar. - Apr. 2013), PP 57-63
www.iosrjournals.org

Detection and Classification of Pests in Greenhouse Using Image Processing

Rupesh G. Mundada[1], Dr. V. V. Gohokar[2]
[1]*M.E.(Digital Electronics) 2nd year, Electronics & Tele-Communication Department, Shri Sant Gajanan Maharaj College of Engineering, Shegaon,*
[2]*Professor, Electronics & Tele-Communication Department, Shri Sant Gajanan Maharaj College of Engineering, Shegaon,*

Abstract: *The techniques of machine vision and digital image Processing are extensively applied to agricultural science and it have great perspective especially in the plant protection field, which ultimately leads to crops management. The paper proposes a software prototype system for early pest detection on the infected crops in greenhouse. Images of the infected leaf are captured by a camera with pan tilt and zoom and processed using image processing techniques to detect presence of pests. SVM classifier is used for classification. SVM classifier helps to detect the pests and in the classification of pest based on their features. Results show more precision in identifying the presence of pest at early stage.*
Keywords: *Early pest detection, feature extraction, image processing, pests, SVM (Support Vector Machine).*

I. INTRODUCTION

` In our country India larger portion of the population depends on agriculture. However, the cultivation of crops for optimum yield and quality produce is highly essential. A lot of research has been done on greenhouse agro systems and more generally on protected crops to control pests and diseases by biological means instead of pesticides. Research in agriculture is aimed towards increase of productivity and food quality at reduced expenditure and with increased profit, which has received importance in recent time. A strong demand now exists in many countries for non-chemical control methods for pests or diseases. In fact, in production conditions, greenhouse staff periodically observes plants and search for pests. This manual method is very time consuming. With the recent advancement in image processing techniques, it is possible to develop an autonomous system for disease classification of crops.

There are different crops which are cultivated under greenhouse e.g. Rose, Cucumber, Tomato, gerbera, Capsicum etc. Whiteflies, Thrips, aphids are the most common pests which attach on greenhouse crops.

White flies, thrips and aphids are very small in size. Normally the size of adult whitefly is 1/12 inch in length. The female of whitefly is sap-sucking pest may lay 150 eggs at the rate of 25 per day. The entire life cycle of whiteflies is 21-36 days.

Thrips are tiny, slender pest about 1/25-inch long in length. They range in colour from light brown to black. Thripes grows on flower plants and fruit plants.

Aphids are very small in size. Aphids are soft-bodied, sluggish pests. They form cluster in colonies on the leaves of the host plants. Their life span is 20 to 30 days.

The only way to stop the effect of these pests is pesticides. But excess use of the pesticides is very harmful to the crops, soil, air, water resources and the animals which came in contact with the pesticides. Pesticide residues have also been found in rain and groundwater. The use of pesticides decreases the general biodiversity in the soil. Excess of pesticides results in reduced nitrogen fixation and thus reduced crop yields. Animals may be poisoned by pesticides.

Early detection of pest or the initial presence of pests is a key-point for crop management. Improved crop protection strategies to prevent such damage and loss can increase production and make a substantial contribution to food security.

In this paper, we focus on early pest detection. This implies to regular observation the plants. Images are acquired using cameras. Then the acquired image has to be processed to interpret the image contents by image processing methods. The focus of this paper is on the interpretation of image for pest detection.

II. LITERATURE REVIEW

In this section we will discuss some methods which are presently used for the early detection of pests in greenhouse crops along with their advantages and disadvantages. The methods are explained below with their features and drawbacks.

A. Method with Static images.

The method of using static images is given by Paul Boissard, Sabine Moisan. In this method the image acquisition is done with the scanner. The next step is to perform image processing technique to detect the pests. The method has good accuracy and results but the biggest disadvantage of this method is to use scanner for image acquisition. Also the time required to generate the results is in hours. When we scan the image there may be a chance that the pests may fly away or there may be a chance of blurring of the image. Also there is a chance of improper scanning which leads the false information.

B. Method which use Sticky Traps.

The method of using sticky traps is given by Vincent Martin, Sabine Moisan Bruno Paris, and Olivier Nicolas. In this method the sticky traps are used to detect the pests. Sticky material which is on the sticky traps attracts the pests due to their properties. But to reach the sticky traps, the development of the pest must be completed i.e. the pest must fly but at that stage the damage is already done to the crops.

The drawback of these methods can be overcome by using pan tilt camera with zoom. The camera is continuously moving and used to capture the image so there is no problem flying away of pests and there is no false information. Also there is no need to reach the sticky trap.

III. PROPOSED METHOD

For this study, whiteflies are chosen because this pest requires early detection and treatment to prevent durable infection. Samples are collected by using the pan tilt camera with zoom in greenhouse as shown in Fig.2. Once the image is acquired the next step is to implement image processing technique in order to get the information about pest.

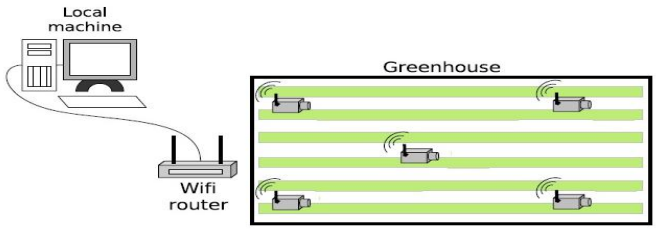

Figure 1: Overview of System

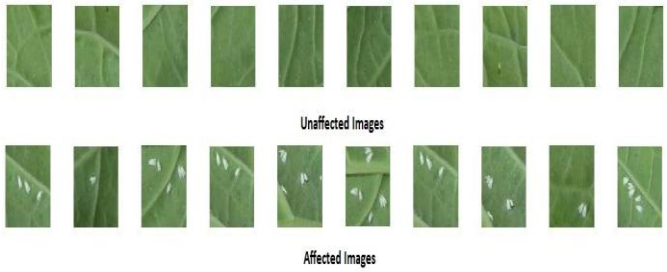

Figure 2: Database for the training of SVM

A. Methodology

1) Image acquisition

Every image processing application always begins with image acquisition. The images are captured by using a pan tilt camera with 20X zoom maintaining equal illumination to the object. All the images should be saved in the same format such as JPEG, TIF, BMP, PNG etc. The camera is interfaced with the system which will take the image captured by the camera as an input.

2) Image pre-processing

Image pre-processing creates an enhanced image that is more useful or pleasing to a human observer. The image preprocessing steps used in the system are: 1) Conversion of RGB image to gray image 2) Resizing of the image 3) Filtering of the image.

a) Conversion of RGB to gray image.

In RGB color model, each colour appears in its primary spectral components of red, green, and blue. The colour of a pixel is made up of three components; red, green, and blue (RGB), described by their corresponding intensities. RGB color image require large space to store. In image processing we have to process the three different channels. It consumes large time.

So we are going to convert the RGB image into gray scale image. The formula to covert RGB to gray is given below

$$I(x, y) = 0.2989*R + 0.5870*G + 0.1140*B$$

The information retained by gray scale image is enough for our method so we convert RGB image to gray scale image for image processing.

b) Resizing of the image.

The acquired image is resized according to the requirement of the system. The different methods available for image resizing are Nearest-neighbor interpolation, bilinear, and bicubic. In Nearest-neighbor interpolation the output pixel is assigned the value of the pixel that the point falls within. No other pixels are considered. In bilinear interpolation the output pixel value is a weighted average of pixels in the nearest 2-by-2 neighborhood. In bicubic interpolation the output pixel value is a weighted average of pixels in the nearest 4-by-4 neighborhood. Here in our system we are using bicubic interpolation as it generates more accurate results than any other method.

c) Filtering of the image

Filtering in image processing is a process that cleans up appearances and allows for selective highlighting of specific information. A number of techniques are available and the best options can depend on the image and how it will be used. Both analog and digital image processing may require filtering to yield a usable and attractive end result.

There are different types of filters such as low pass filters, high pass filters, median filters etc. The low pass filters are smoothening filters where as the high pass filters are sharpening filters. Smoothening filters are used for smoothening of the edges. Sharpening filters are used for enhancing the edges in the image.

In our system we are using smoothening filter. The purpose of smoothing is to reduce noise and improve the visual quality of the image. Spatial filters are applied to both static and dynamic images, whereas temporal images are applied only to dynamic images. The simplest smoothening filter is average filter. It consists of a 3X3 matrix of 1 and it is divided by 9.

3) Feature Extraction

In feature extraction we are considering some properties of the image. There are different properties like region properties, gray covariance matrix properties. From that he properties like entropy, mean, standard deviation, contrast, energy, Correlation and eccentricity are extracted from the image. They are compared and based on that the support vector machine is trained and used to classify the images.

Support Vector Machines (SVM's) are a relatively new learning method used for binary classification. The basic idea is to find a hyper plane which separates the d-dimensional data perfectly into its two classes. However, since example data is often not linearly separable, SVM's introduce the notion of a \kernel induced feature space" which casts the data into a higher dimensional space where the data is separable. Typically, casting into such a space would cause problems computationally, and with over fitting. The key insight used in SVM's is that the higher-dimensional space doesn't need to be dealt with directly (as it turns out, only the formula for the dot-product in that space is needed), which eliminates the above concerns. Furthermore, the VC-dimension (a measure of a system's likelihood to perform well on unseen data) of SVM's can be explicitly calculated, unlike other learning methods like neural networks, for which there is no measure. Overall, SVM's are intuitive, theoretically well- founded, and have shown to be practically successful. SVM's have also been extended to solve regression tasks (where the system is trained to output a numerical value, rather than \yes/no" classification).

The meaning of the properties which are stated above is given in following table

Entropy	A scalar value representing the entropy of grayscale image I. Entropy is a statistical measure of randomness that can be used to characterize the texture of the input image. Entropy is defined as -sum(p.*log2(p))

Mean	Returns the mean values of the elements along different dimensions of an array
Standard deviation	computes the standard deviation of the values in matrix or array
Eccentricity	Scalar that specifies the eccentricity of the ellipse that has the same second-moments as the region. The eccentricity is the ratio of the distance between the foci of the ellipse and its major axis length. The value is between 0 and 1. (0 and 1 are degenerate cases; an ellipse whose eccentricity is 0 is actually a circle, while an ellipse whose eccentricity is 1 is a line segment.) This property is supported only for 2-D input label matrices
Euler Number	Scalar that specifies the number of objects in the region minus the number of holes in those objects. This property is supported only for 2-D input label matrices. Regionprops uses 8-connectivity to compute the Euler Number measurement. To learn more about connectivity, see Pixel Connectivity.
Filled Area	Scalar specifying the number of on pixels in Filled Image.
Solidity	Scalar specifying the proportion of the pixels in the convex hull that are also in the region. Computed as Area/Convex Area. This property is supported only for 2-D input label matrices.
Gray Co-occurrence matrix	It creates a gray-level co-occurrence matrix (GLCM) from image I. graycomatrix creates the GLCM by calculating how often a pixel with gray-level (grayscale intensity) value i occurs horizontally adjacent to a pixel with the value j. (You can specify other pixel spatial relationships using the 'Offsets' parameter -- see Parameters.) Each element (i,j) in glcm specifies the number of times that the pixel with value i occurred horizontally adjacent to a pixel with value j.
Contrast	Returns a measure of the intensity contrast between a pixel and its neighbor over the whole image. It is computed by formula $\sum_{i,j} \lvert i-j \rvert^2 p(i,j)$
Energy	Returns the sum of squared elements in the GLCM. It is computed by formula

	$\sum_{i,j} p(i,j)^2$

Table 1: Definition of different Parameters

4) Disease classification and grading

The disease classification is done by the support Vector machine classifier. The two categories are formed such as affected leaf and unaffected leaf. Based on this the data provided to train the support vector machine. From above table we can clearly see that there is a variation in standard deviation and contrast. So we will consider the standard deviation and contrast for training the support vector machine.

5) Detection

The input image is given to the support vector machine. As the support vector machine is trained with the data collected from our data base which we have collected. The features of the input image are extracted and given as an input to the support vector machine; Based on the comparison with the parameters of database support vector machine generates the output.

6) Identification of Pests

If the leaf is found to be infected then the next step is to find out the type of pest. Here we are classifying them into two categories which are whiteflies and aphids.

For identification, after the averaging filtering, a special type of mask is used. Then the filtered image is convolved with the mask. Then extracting the region properties and gray co-occurrence matrix properties the classification is done in two types, whiteflies and aphids. For identification we are considering region properties like standard deviation and contrast. For deciding the category we are using SVM classifier again. The database which is provided for the training of second SVM is shown in figure. 3

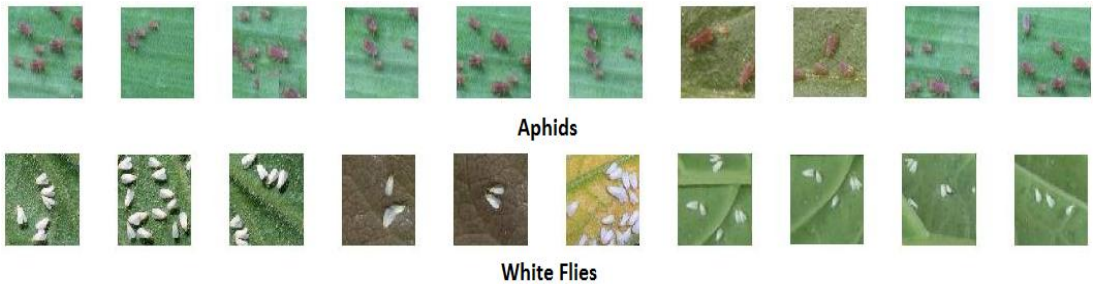

Figure 3: Database for classification

IV. FLOWCHART

The flow chart for the propose system is given in fig.4. The flowchart gives the complete idea about the system.

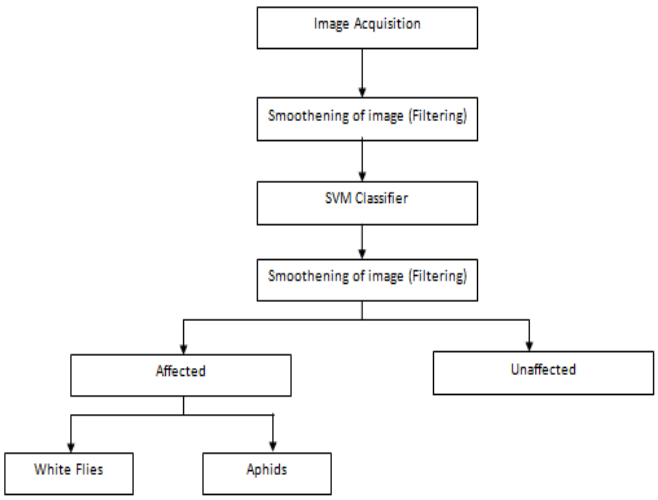

Figure 4: Flowchart of the system

V. RESULTS

The results obtained by performing the operations are shown below. The different parameters which are calculated for given data base are shown in table 2. The graph of the different parameters is also shown in fig. 5 and from the analysis of that we have decided to choose Standard deviation and contrast as deciding or classification factors. The graph shown in fig. 6 shows that the training to the SVM is done with 100% accuracy. We have divided it into two categories affected and unaffected. Here 1 represents unaffected and 0 represents affected. Also further the affected category is divided into two classes, aphids and whiteflies. For this classification we have used one more SVM classifier. The different properties which decide that they are whiteflies or aphids are shown in table 3. The graph for different properties is shown in figure 6. Based on this the SVM is trained and input image of affected leaf is given to the second support vector machine which will generate the output as 1 or 0 based on the parameters of the input image. 1 is for aphids and 0 is for whitefly.

Parameters	Entropy	Mean	Standard deviation	Contrast	Correlation	Eccentricity
Unaffected Images	5.111022	128.9804	8.784494	0.099495	0.788207687	0.08005621
	5.704047	122.7276	13.36848	0.088384	0.817424865	0.0369198
	5.356719	119.6399	11.23865	0.065354	0.775523552	0.06858617
	4.956636	118.4778	7.785343	0.053232	0.666828028	0.08068627
	5.266736	107.8553	10.09207	0.06	0.661228997	0.24282954
	5.335025	99.7185	10.26094	0.094747	0.7433882	0.11856729
	4.750367	120.2329	6.788967	0.04899	0.759140928	0.05610738
	5.552168	118.4309	11.68626	0.063838	0.825014884	0.07377056
	4.706327	120.4082	6.939394	0.044646	0.774875913	0.06434045
Affected Images	5.169737	120.4206	19.33133	0.18697	0.713766094	0.10776177
	5.743359	124.3191	17.72068	0.100303	0.849842034	0.06283355
	5.849869	93.6361	16.42084	0.112828	0.841796732	0.18596007
	5.703574	125.1937	17.29079	0.123232	0.830376481	0.08401726
	5.826912	127.2926	17.94776	0.113232	0.844825531	0.05584843
	5.902958	126.3397	18.74501	0.105556	0.85344753	0.12640911
	6.084404	131.414	21.01807	0.128182	0.859443699	0.86873436
	5.825271	127.2334	17.8611	0.115051	0.841136478	0.08528723
	5.809195	126.9435	18.45275	0.120606	0.842934082	0.03635498
	5.336148	110.0158	13.31124	0.14101	0.816806901	0.05226187
	5.540607	136.7816	17.02995	0.123131	0.808520036	0.0907478

Table 2: Different Parameters

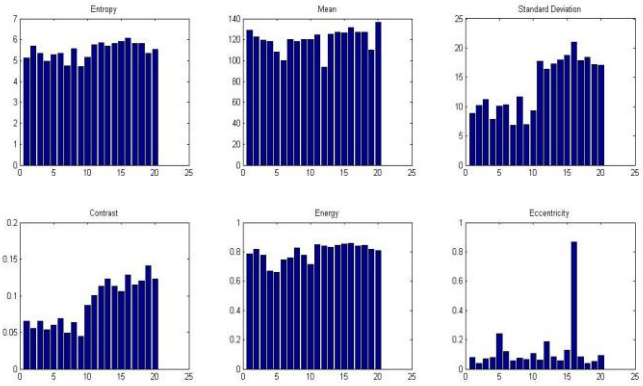

Figure 5: Graph of different Parameters

Parameters	Entropy	Standard Deviation	Contrast	Eccentricity	Euler's Number
Affected with Aphids	0.241974	0.1958067	0.040022	0.47946715	112
	0.241974	0.1958067	0.040789	0.303154	124
	0.244457	0.1970767	0.040899	0.5103298	115
	0.243465	0.1965699	0.040899	0.29788011	111
	0.241974	0.1958067	0.039912	0.47548961	109
	0.242968	0.1963159	0.041009	0.36370833	99
	0.24693	0.1983371	0.042105	0.56804004	84
	0.243465	0.1965699	0.041228	0.50649518	98
	0.243465	0.1965699	0.042544	0.3016139	113
	0.243961	0.1968235	0.041667	0.31537708	111
Affected with Whiteflies	0.327893	0.2377087	0.069956	0.51147809	76
	0.357723	0.251445	0.07182	0.418625	44
	0.305539	0.2271689	0.066667	0.45601103	63
	0.301057	0.2250285	0.060855	0.39285678	106
	0.285105	0.2173283	0.049452	0.39021232	110
	0.296089	0.2226441	0.064474	0.59140669	75
	0.28741	0.218449	0.056031	0.32758873	146
	0.280933	0.2152929	0.055811	0.54562806	178
	0.281398	0.2155203	0.055044	0.39666599	151
	0.275793	0.2127727	0.054167	0.50532207	160

Table 3: Different Parameters to decide Aphids or whiteflies.

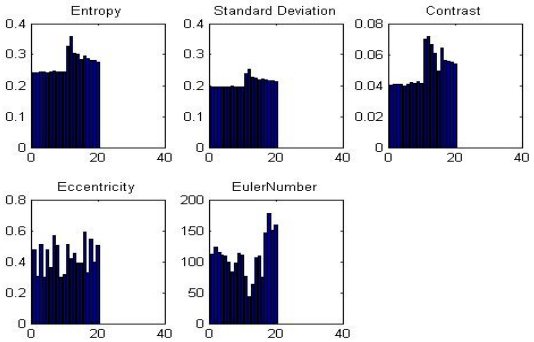

Figure 6: Graph of different Parameters

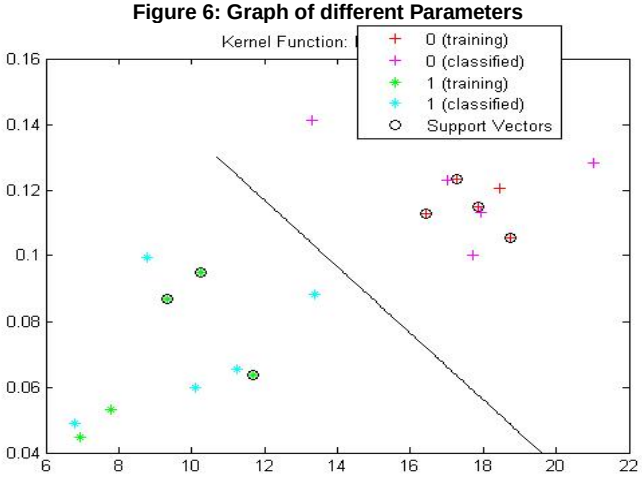

Figure 7: output of the SVM.

VI. CONCLUSION

Image processing technique plays an important role in the detection of the pests. Our first objective is to detect whiteflies, aphids and thrips on greenhouse crops. We propose a novel approach for early detection of pests. To detect objects we use pan tilt camera with zoom. So without disturbing the pests we are able to take the image. It illustrates the collaboration of complementary disciplines and techniques, which led to an automated, robust and versatile system. The prototype system proved reliable for rapid detection of pests. It is rather simple to use and exhibits the same performance level as a classical manual approach. Our goal is to detect the pests as early as possible and reduce the use of pesticides.

REFERENCES

[1]. Martin,V.Thonnat,. "A Learning Approach For Adaptive Image Segmentation." In Proceedings of IEEE Trans.Computers and Electronics in Agriculture.2008.
[2]. Vincent Martin and Sabine Moisan, "Early Pest Detection in Greenhouses". INRIA Sophia Antipolis M´editerrann´ee, PULSAR team 2004 route des Lucioles, BP93
[3]. Jayamala K. Patil1 , Raj Kumar, "Advances In Image Processing For Detection Of Plant Diseases" Journal Of Advanced Bioinformatics Applications and Research ISSN 0976-2604 Vol 2, Issue 2, June-2011, pp 135-141
[4]. Ikhlef Bechar and Sabine Moisan, "On-line counting of pests in a greenhouse using computer vision". published in "VAIB 2010 - Visual Observation and Analysis of Animal and Insect Behavior (2010)"
[5]. Paul Boissarda, Vincent Martin, "A cognitive vision approach to early pest detection in greenhouse crops". computers and electronics in agriculture 6 2 (2 0 0 8) 81–93
[6]. B.Cunha."Application of Image Processing in Characterisation of Plants." IEEE Conference on Industrial Electronics.2003.
[7]. Santanu Phadikar, Jaya Sil."Rice Disease Identification Using Pattern Recognition Techniques." IEEE 10th International Conference On I.T.E.2007.
[8]. Rafael C. Gonzalez, Richard E. Woods. "Digital Image Processing'',2nd edition, Pearson education (singapore) pte.ltd.2003.
[9]. T.F.Burks, S.A.Shearer and F.A. Payne, "Classification of weed species using color texture features and discriminant analysis," Trans. ASAE, vol.43, no.2, pp.441–448, Apr. 2000.
[10]. R.Pydipati, T.F. Burks and W.S. Lee, "Identification of citrus disease using color texture features and discriminant analysis," Comput. Electron. Agric., vol.52, no.1, pp.49-59, June 2006.
[11]. Laaksonen, J.Koskela, M.Oja, E. , "Self-organizing maps for content-based image retrieval," International Joint Conference on Neural Networks, vol.4, pp.2470-2473 ,1999.
[12]. R.M. Haralick, K. Shanmugam and I.Dinstein, "Textual features for image classification," IEEE Trans. Syst. Man Cybern., vol.3, no.6, pp. 610–621, Nov. 1973
[13]. H. Ritter and T.Kohonen. "Self-organizing semantic maps", Biological Cybernetics, vol.61, pp.241-254, 1989.

IOSR Journal of Electronics and Communication Engineering (IOSR-JECE)
e-ISSN: 2278-2834,p- ISSN: 2278-8735. Volume 5, Issue 6 (Mar. - Apr. 2013), PP 64-73
www.iosrjournals.org

Performance Analysis and Comparative Study of Cognitive Radio Spectrum Sensing Schemes

Prabhat Prakash Singh[1], Divya Kumar[2]
[1 2](Electronics & Communication Department, College of Engineering & Technology, Moradabad, U.P., INDIA)

Abstract : *In cognitive radio, spectrum sensing is an emergent technology to find available and unused spectrum for increasing spectrum utilization and to overcome spectrum scarcity problem without harmful interference to licensed users. Cooperative spectrum sensing is used to give reliable performance in terms of detection probability and false alarm probability as well as in order to reduce fading, noise and shadowing effects on cognitive radio users. In this paper according to detection performance and complexity various cooperative spectrum sensing schemes have been discussed. We have analyzed spectrum sensing with different fusion rules and their comparative behavior has also been studied. Furthermore, we introduced AND-OR fusion rules in 2-bit and 3-bit hard combination schemes.*

Keywords *- Cognitive radio, cooperative spectrum sensing, energy detector, spectrum sensing, hard combination*

I. INTRODUCTION

Radio spectrum is a very scarce and important resource for wireless communication systems. The tremendous growth in wireless communications has contributed to a huge demand on the deployment of new wireless services in both the licensed and unlicensed frequency spectrum. Recently, a Cognitive Radio (CR) access technology has been proposed as a promising solution for improving the efficiency of spectrum usage by adopting dynamic spectrum resource management concept [4], [13].

The main functions of a cognitive radio can be addressed as follows [14]:

- Spectrum sensing is the process of a cognitive radio sensing the channel and determining if a primary user is present, detecting the spectrum holes
- Spectrum management is selecting the best available channel (for a cognitive user) over the available channels.
- Spectrum sharing is the allocation of available frequencies between the cognitive users.
- Spectrum mobility is the case when a secondary user rapidly allocates the channel to the primary user when a primary user wants to retransmit again.

Among these functions, spectrum sensing is the one that has driven most interest. The role of spectrum sensing in the CR system is to locate unoccupied spectrum segments as quickly and accurately as possible. Inaccurate or delayed sensing results deter communication of the primary user occupying the spectrum. Thus, spectrum sensing speed and accuracy are extremely important. From a CR system commercialization standpoint, minimizing hardware complexity as well as power consumption is also critical.

Spectrum scarcity problem [1],[2] due to the growth of demand for the spectrum, is suggested to be solved by increasing the spectrum utilization which can be done by allowing cognitive users (unlicensed users) to occupy the spectrum band when the primary users (licensed users) do not use it. CR system [3], [4] can be suggested to use the spectrum band efficiently. In spectrum sensing [5] there are several sensing methods. One from these methods is the energy detection [6], [7]. Other methods were described briefly in Ref. [4], [8], [9]. Energy detection will be used here due to its simplicity and no need for any prior information about the primary users' signals. Therefore, it has been thoroughly studied both in local spectrum sensing [6],[7],[8],[9],[10] and cooperative spectrum sensing [11],[12],[13],[14].In cooperative spectrum sensing, local spectrum sensing information from multiple CRs are combined for Primary User (PU) detection. In centralized CR network, a common receiver plays a key role in collecting these information and detecting spectrum holes which were described in details in [12].

Cooperative spectrum sensing was proposed to overcome noise uncertainties, fading and shadowing in primary user signal detection. It can be as a solution to hidden node problem and decrease sensing time as well [15]. In this technique, CR users/nodes are collaborated to sense spectrum hole and detect PUs signal. Then, with or without sharing local detection information among users, they forward them to data fusion centre. The fusion centre decides the final result in accordance with the decision rules whether primary signal is present or absent.

The paper is organized as follows: Section 2 reviews spectrum sensing schemes. In section 3, we provide comparison of spectrum sensing schemes. Conclusion is presented in Section 4.

II. SPECTRUM SENSING SCHEMES

Several methods have been proposed to perform local spectrum sensing [14], [16], [17], and [18]. The following section highlights three of the most relevant methods from the literature [18]: 1) energy detection based spectrum sensing, 2) cyclostationary-based spectrum sensing, and 3) matched filtering. A brief overview of each technique is provided below along with the relative advantages and disadvantages of each.

2.1 Energy Detection Based Spectrum Sensing

Due to its low complexity and computational cost, energy detection based spectrum sensing is the most common spectrum sensing method [16]. It is performed by comparing the received energy of the signal against a predefined energy detection threshold to determine the presence or absence of the user in the frequency band of interest [16], [17], [19]. The energy of the received signal is determined by squaring and integrating the received signal strength (RSS) over the observation time interval [14], [16], [19]. The energy detection threshold is determined using the noise variance of the environment [14]. Thus, small errors in the noise variance estimation can cause significant performance degradation [14]. Energy detection based spectrum sensing is the optimal detection method for zero-mean constellation signals when no information is known in advance about the user occupying the channel [14], [19]. However, energy detection based spectrum sensing cannot distinguish the type of user occupying the frequency band [14], [16]. In addition, under low signal-to-noise ratio (SNR) conditions, energy detection performs poorly [14], [16].

The principle of energy detection is shown in fig. 1. Energy detector has a band-pass filter which limits the bandwidth of the received signal to the frequency band of interest, a square law device which squares each term of the received signal and a summation device which adds all the squared values to compute the energy.

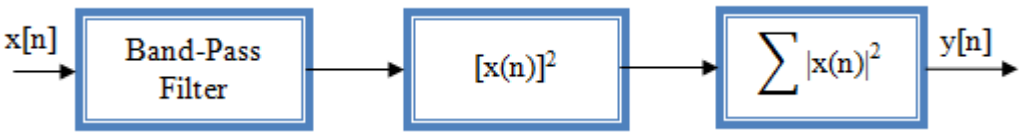

Figure 1: Energy Detector-based Sensing

The energy is calculated as:

$$E = \sum_{n=0}^{N} |x(n)|^2 \quad (1)$$

The Energy is now compared to a threshold for checking which hypothesis turns out to be true.

$$E > \lambda \Rightarrow H_1$$
$$E < \lambda \Rightarrow H_0 \quad (2)$$

The probability of detection (P_d) and probability of false alarm (P_{fa}) can be given as :

$$P_d = Q_m\left(\sqrt{2\gamma}, \sqrt{\lambda}\right) \quad (3)$$

Where $Q_m(a, b)$ is generalized Marcum Q-function.

$$P_f = \frac{\Gamma(m,\lambda/2)}{\Gamma(m)} \quad (4)$$

Where Γ (a) is the complete gamma function and Γ (a,b) is the incomplete gamma function. γ and λ represents SNR and detection threshold respectively.

1.2 Cyclostationary-Based Spectrum Sensing

Given the disadvantages of energy detection based spectrum sensing, cyclostationary-based spectrum sensing offers an attractive alternative [14], [16]. By exploiting the cyclostationary features of the received signal [16], cyclostationary-based spectrum sensing is capable of discriminating which type of user is present [14], [16] and detecting the presence of a user under low SNR conditions [14]. Such benefits come at the cost of additional hardware complexity and a lengthier detection process when compared to energy detection based spectrum sensing [14]. Cyclostationary features are the result of periodicity in the received signal or its statistical properties [16]. As such, detection is accomplished by finding the unique cyclic frequency of the spectral correlation function of the received signal [14], [16]. The spectral correlation function is determined by taking the Fourier transform of the cyclic autocorrelation function.

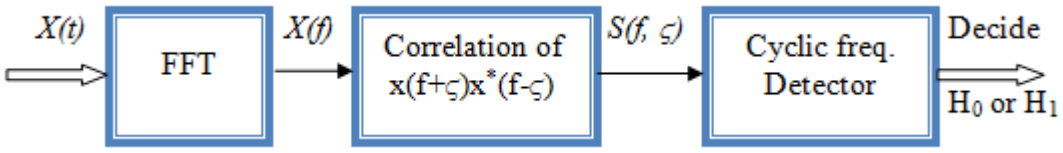

Figure 2: Cyclostationary-based Sensing

1.3 Matched Filter Detection

The Matched Filter is used to maximize the signal to noise ratio (SNR). This method incorporates a filter matched to the primary user's signal at the cognitive radio receiver. Obviously, this method is optimal in the sense that it maximizes the SNR, minimizing the decision errors. However, this method is not practical since it requires the cognitive user to know the primary user's signalling type.

It is a linear filter and prior knowledge of the primary user signal is very essential for its operation. The operation performed is equivalent to a correlation. Matched filter correlates the signal with time shifted version and compares between the final output of matched filter and predetermined threshold will determine the PU presence.

1.4 Waveform-Based Sensing

Known patterns are usually utilized in wireless systems to assist synchronization or for other purposes. Such patterns include preambles, midambles, regularly transmitted pilot patterns, spreading sequences *etc*. A preamble is a known sequence transmitted before each burst and a midamble is transmitted in the middle of a burst or slot. In the presence of a known pattern, sensing can be performed by correlating the received signal with a known copy of itself [24], [25], [27]. This method is only applicable to systems with known signal patterns, and it is termed as waveform-based sensing or coherent sensing. In [24], it is shown that waveform based sensing outperforms energy detector based sensing in reliability and convergence time. Furthermore, it is shown that the performance of the sensing algorithm increases as the length of the known signal pattern increases.

1.5 Radio Identification Based Sensing

A complete knowledge about the spectrum characteristics can be obtained by identifying the transmission technologies used by primary users. Such identification enables cognitive radio with a higher dimensional knowledge as well as providing higher accuracy [26]. For example, assume that a primary user's technology is identified as a Bluetooth signal. Cognitive radio can use this information for extracting some useful information in space dimension as the range of Bluetooth signal is known to be around 10 meters. Furthermore, cognitive radio may want to communicate with the identified communication systems in some applications.

For radio identification, feature extraction and classification techniques are used in the context of European transparent ubiquitous terminal (TRUST) project [33]. The goal is to identify the presence of some known transmission technologies and achieve communication through them. The two main tasks are initial mode identification (IMI) and alternative mode monitoring (AMM). In IMI, the cognitive device searches for a possible transmission mode (network) following the power on. AMM is the task of monitoring other modes while the cognitive device is communicating in a certain mode.

In radio identification based sensing, several features are extracted from the received signal and they are used for selecting the most probable primary user technology by employing various classification methods. In [20], [34], features obtained by energy detector based methods are used for classification. These features include amount of energy detected and its distribution across the spectrum. Channel bandwidth and its shape are used in [35] as reference features. Channel bandwidth is found to be the most discriminating parameter among others. For classification, radial basis function (RBF) neural network is employed. Operation bandwidth and centre frequency of a received signal are extracted using energy detector based methods in [26]. These two features are fed to a Bayesian classifier for determining the active primary user and for identifying spectrum opportunities. The standard deviation of the instantaneous frequency and the maximum duration of a signal are extracted using time-frequency analysis in [22], [23], [36], [37] and neural networks are used for identification of active transmissions using these features. Cycle frequencies of the incoming signal are used for detection and signal classification in [30]. Signal identification is performed by processing the (cyclostationary) signal features using hidden Markov model (HMM). Another cyclostationarity based method is used in [28], [29] where spectral correlation density (SCD) and spectral coherence function (SCF) are used as features. Neural network are utilized for classification in [29] while statistical tests are used in [28].

III. COMPARISON OF SENSING SCHEMES

A basic comparison of the sensing methods given in this section is presented in Fig. 3. Waveform-based sensing is more robust than energy detector and cyclostationarity based methods because of the coherent processing that comes from using deterministic signal component [24]. However, there should be a priori information about the primary user's characteristics and primary users should transmit known patterns or pilots.

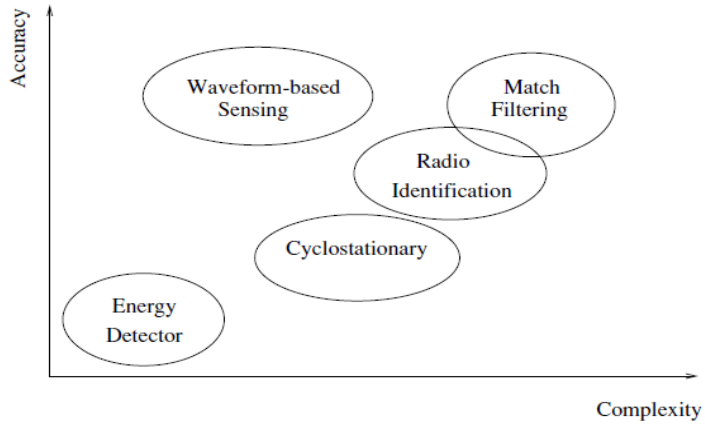

Figure 3: Main sensing methods in terms of their sensing accuracies and complexities.

The performance of energy detector based sensing is limited when two common assumptions do not hold [24]. The noise may not be stationary and its variance may not be known. Other problems with the energy detector include baseband filter effects and spurious tones [27]. It is stated in literature that cyclostationary-based methods perform worse than energy detector based sensing methods when the noise is stationary. However, in the presence of co-channel or adjacent channel interferers, noise becomes non-stationary. Hence, energy detector based schemes fail while cyclostationarity-based algorithms are not affected [32]. On the other hand, cyclostationary features may be completely lost due to channel fading [31], [39]. It is shown in [39] that model uncertainties cause an SNR wall for cyclostationary based feature detectors similar to energy detectors [38]. Furthermore, cyclostationarity based sensing is known to be vulnerable to sampling clock offsets [32].

IV. RESULT AND DISCUSSION

As described earlier, cooperative technique was proposed to combat noise uncertainty, fading, and shadowing. These all can cause sensing errors such as false detection and miss-detection. False detection senses idle channel as a busy channel and CR users refrain to transmit data. On the other hand, miss detection senses busy channel as an idle channel and cause CR users collide to PU transmission.

There are three rules commonly used in hard decision combining based cooperative spectrum sensing. OR rule decides primary user is present when at least one user detects primary user signal while AND rule decides primary user is present if all cognitive radio users forward their bit-1 local detections. MAJORITY rule decides primary user is present when X out of N secondary users detect primary user present. Through computer simulation, we model cooperative spectrum sensing and obtain numerical results.

First we have discussed the relationship of the probability of detection (P_d) and probability of false alarm (P_{fa}) based on AND rule, OR rule and MAJORITY rule. The simulation conditions are shown below: the number of cognitive users is 5, constant losses are 1, the probability of false alarm (p_{fa}) of each single cognitive user is p_{fa} =0.1 and SNR=15dB.

Fig.4 shows Complementary ROC of Cooperative sensing with AND fusion rule under AWGN. AND rule has lower probability of false alarm (P_{fa}) , but also has lower probability of detection (P_d).

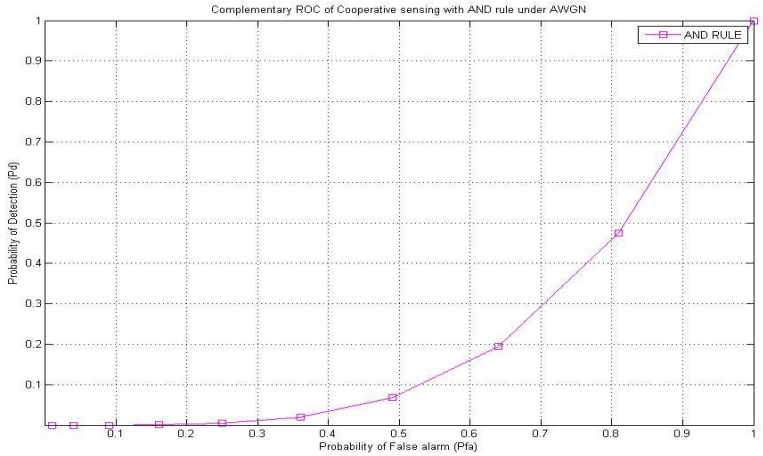

Figure 4: Complementary ROC of Cooperative sensing with AND fusion rule under AWGN

Fig.5 shows Complementary ROC of Cooperative sensing with OR fusion rule under AWGN. OR rule has high probability of detection (P_d) but also has high probability of false alarm (P_{fa}).

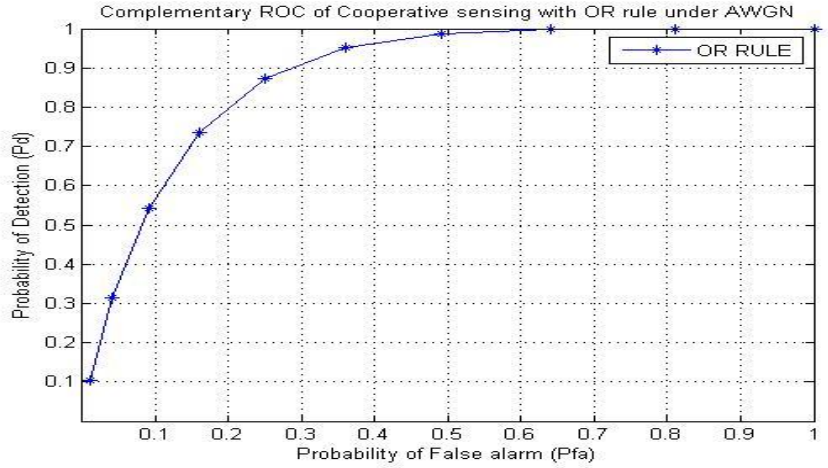

Figure 5: Complementary ROC of Cooperative sensing with OR fusion rule under AWGN

Now, OR and AND rule are studied. We define P_{fa} values from 0.1-1.0. The information of local detection from each cognitive radio users are forwarded to data fusion centre and combined to obtain final decision. The simulation is performed by using probability of detection as a metric at different SNR values.

Fig.6 describes the probability of detection by employing AND and OR rule. We assume 5 CR users are collaborated to detect primary user signal. As shown in the figure that OR rule has better probability of detection than AND rule. The data fusion centre decides H1 when at least there is one CR user detects primary user signal for OR rule while in AND rule, all local detection of CR users must be H1 to decide the presence of primary user signal. From fig.6 it is clear that as probability of false alarm (P_{fa}) is low, OR fusion rule has better probability of detection (P_d) than AND fusion rule. The reason is that data fusion centre decides H_1 i.e. primary user is present when at least there is one CR user detects primary user signal for OR fusion rule while in AND fusion rule, all local detection of CR users must be H_1 i.e. primary user is present to decide the presence of primary user signal. As probability of false alarm (P_{fa}) increases OR and AND fusion rules show similar results. At SNR values less than 10dB OR fusion rule exhibits better detection performance than AND fusion rule.

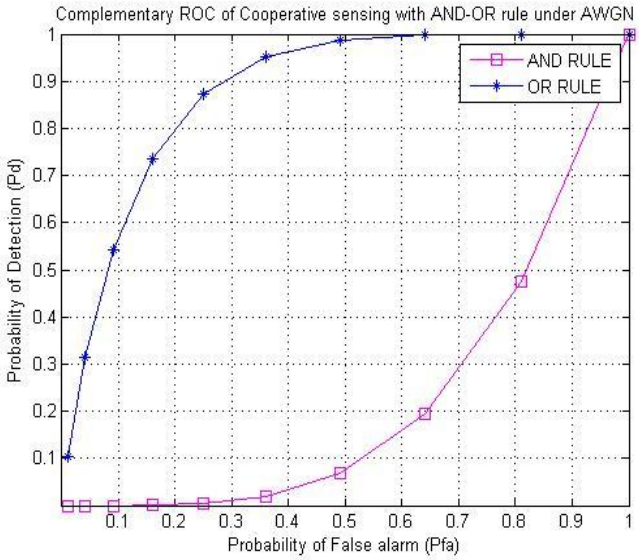

Figure 6: Probability of detection for AND and OR rule.

Then, In Fig.7 we evaluate probability of detection with different number of cognitive radio users in each decision fusion rule. Number of 5 and 10 collaborated users is implemented for this evaluation.We used here two important spectrum sensing detection parameters i.e. Probability of Missed Detection (P_{md}) and Probability of False alarm (P_{fa}).

A missed detection occurs when a primary signal is present in the sensed band and the spectrum sensing algorithm selects hypothesis H_0, which may result in harmful interference to primary users. On the other hand, a false alarm occurs when the sensed spectrum band is idle and the spectrum sensing algorithm selects hypothesis H_1, which results in missed transmission opportunities and therefore in a lower spectrum utilization. Based on these definitions, the performance of any spectrum sensing algorithm can be summarized by means of two probabilities:

The probability of missed detection
$P_{md} = P (H_0=H_1)$,
and the probability of false alarm
$P_{fa} = P (H_1=H_0)$

In Fig.7 we have used two different number of cognitive users n=5 and n=20.All the results obtained after 1000 run of simulations. As number of cognitive users increases, both fusion rules show different results. At low false alarm values OR fusion rule shows better results for number of cognitive users n=20 than number of cognitive users n=5.Probability of missed detection (P_{md}) also decreases for number of cognitive users n=20.So total detection probability (P_d) increases accordingly.

At low false alarm values AND fusion rules shows almost similar characteristics for both number of cognitive users i.e. n=5 and n=20.But as values for false alarm increases it shows better performance for number of cognitive users n=5 than number of cognitive users n=20.It means Probability of missed detection(P_{md}) increases as number of cognitive users increases according to Probability of false alarm(P_{fa}).For AND fusion rule total detection probability(P_d) decreases with increment of number of cognitive users(n).

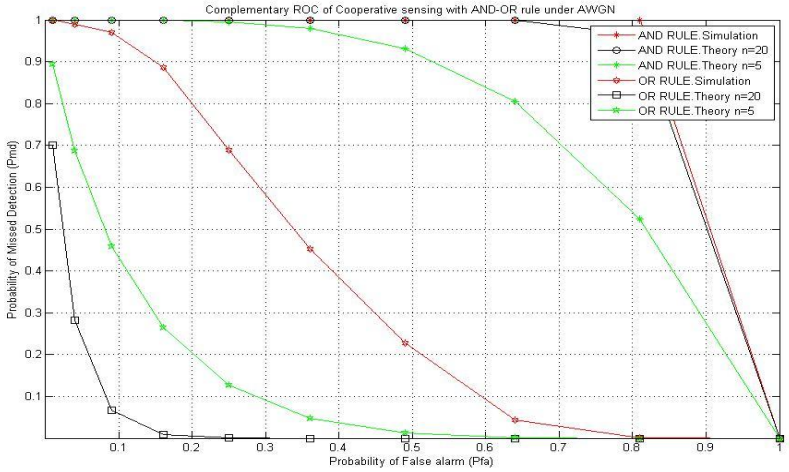

Figure 7: Probability of detection for AND and OR rule for different no. of secondary users

Fig.8 describes the probability of detection by employing AND, OR and MAJORITY rules. We assume 5 CR users are collaborated to detect primary user signal. As shown in the figure that OR rule has better probability of detection than AND and MAJORITY rules. The data fusion centre decides H1 when at least there are X out of N. CR users detect primary user signal for MAJORITY rule.When comparing the performances of all fusion rules, performance of the MAJORITY fusion rule is considerably worse but much better than the performance of the AND rule. It clearly seen that performance of MAJORITY fusion rule lies between OR fusion rule and AND fusion rule. At low values of Probability of false alarm (P_{fa}), OR fusion rule exhibits best results over MAJORITY and AND fusion rules. Probability of detection (P_d) for OR rule is also much better than other fusion rules at low false alarm values. For better primary user detection, Probability of detection (P_d) should be maximum and Probability of false alarm (P_{md}) should be minimum so that spectrum could be utilized efficiently. AND fusion rule shows worst performance among all fusion rule as final decision of primary user presentation depends on all cognitive users while in OR fusion rule one cognitive user is sufficient for final decision making. Final decision can be obtained in MAJORITY fusion rule by k out of n rule.

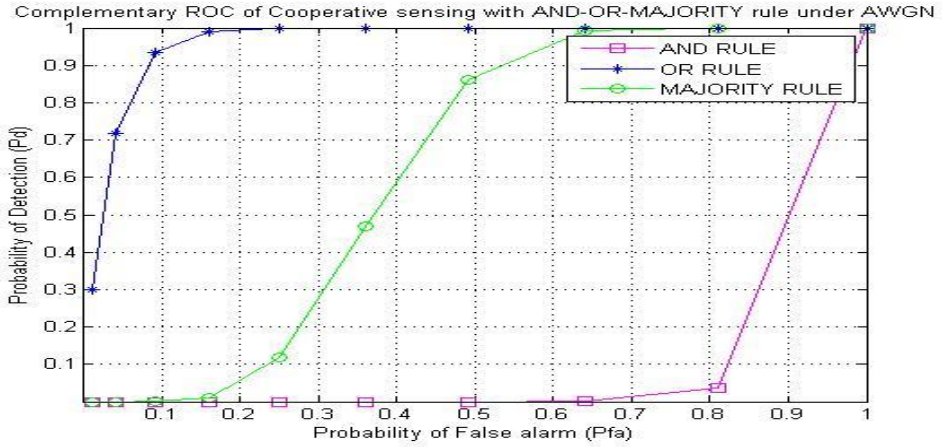

Figure 8: Probability of detection for AND, OR and MAJORITY rule.

The main idea behind the 2-bit hard combination scheme is to divide the whole range of observed energy into more than two regions and to assign different weights to these regions [18]. By doing this, nodes that observe higher energies in upper regions have greater weights than nodes that observe lower energies in lower regions [6]. Using the main idea of the 2-bit hard combination scheme proposed in [18], in 3-bit case the whole range of observed energy is divided into more than four regions. In particular, seven thresholds are used to divide the whole range of observed energy into eight regions. Each node sends to the decision maker a 3-bit information that indicates the region in which it's observed energy fell.

Fig.9 represents 2-bit and 3-bit combination comparison at SNR=-10dB. Comparing both hard combination schemes, 3-bit combination schemes shows better probability of detection (P_d) in terms of

probability of false alarm (P_{fa}) over 2-bit combination schemes.3-bit combination scheme has low false alarm value than 2-bit combination scheme but when we consider probability of detection (p_d), 3-bit combination scheme outperforms than 2-bit combination scheme due to low false alarm value for particular probability of detection (P_d).

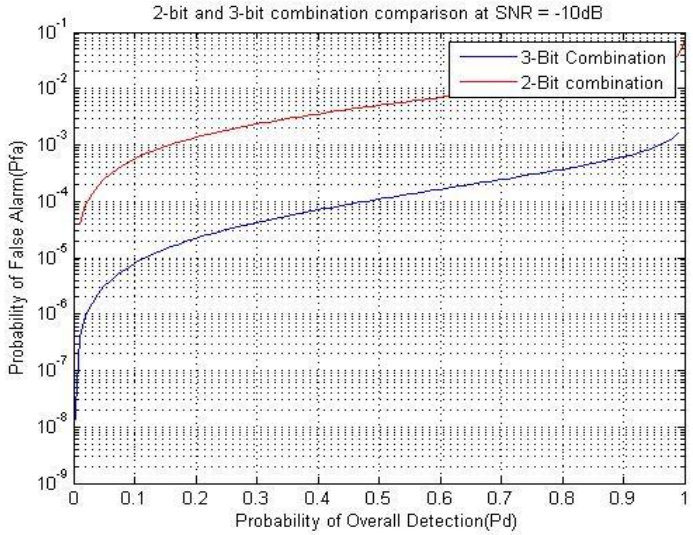

Figure 9: 2-bit and 3-bit combination comparison at SNR=-10dB

At low probability of detection (P_d), 2-bit OR combination scheme has highest false alarm value than 2-bit AND combination schemes and both 3-bit combination schemes. When probability of detection (P_d) increases for both 2-bit and 3-bit combination schemes, 3-bit combination AND and OR schemes show less false alarm values than other two of 2-bit combination schemes as shown in fig. 10.

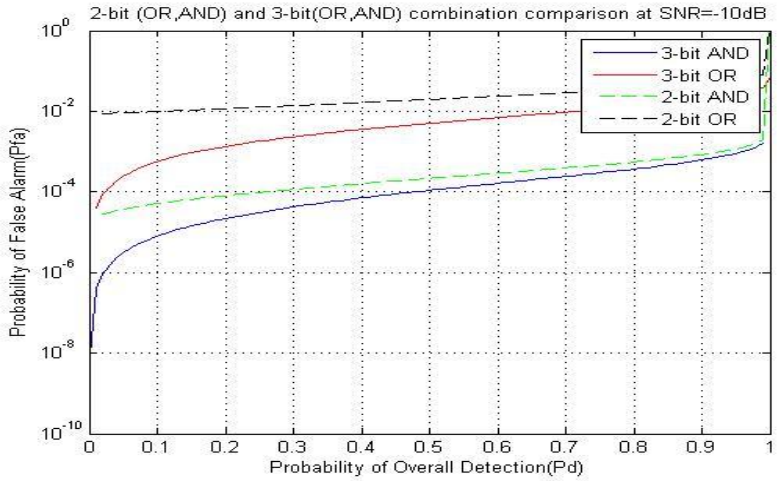

Figure 10: 2-bit (OR, AND) and 3-bit (OR, AND) combination comparison at SNR=-10dB

V. CONCLUSION

Spectrum Is A Very Valuable Resource In Wireless Communication Systems, And It Has Been A Focal Point For Research And Development Efforts Over The Last Several Decades. Cognitive Radio, Which Is One Of The Efforts To Utilize The Available Spectrum More Efficiently Through Opportunistic Spectrum Usage, Has Become An Exciting And Promising Concept. One Of The Important Elements Of Cognitive Radio Is Sensing The Available Spectrum Opportunities. Several Sensing Methods Are Studied.

The numerical results OR rule can improve probability of detection than AND rule and MAJORITY rule. Cooperative technique is more effective when received SNR in cognitive radio users is low due to fading and shadowing.

There are several ideas for future work from this thesis. First, simulation models can be improved. Multipath fading effects could be added and their effects on the performance of the fusion rules could be investigated. Instead of generating the RF signals in MATLAB, actual transmitted signals could be collected in

the field. The 3-bit hard combination scheme could be compared with the 2-bit hard combination scheme with actual signal collected in the field. In the simulation results, probability of detection could be illustrated as a detection performance measure.

REFERENCES

[1] Federal Communications Commission, *Spectrum Policy Task Force Report*, FCC Document ET Docket No. *02-155*, Nov. 2002.

[2] *Notice of Proposed Rulemaking on Cognitive Radio*, Federal Communications Commission (FCC) Std.No.*03-322*, Dec.2003.

[3] J. Mitola, *Cognitive Radio: An Integrated Agent Architecture for Software Defined Radio*, Ph.D. Thesis, KTH, Stockholm, Sweden, 2000.

[4] S. Haykin, Cognitive Radio: Brain-Empowered Wireless Communications, *IEEE J. Select. Areas Comm.*, vol. *23*, no. *2*, Feb. 2005, pp. 201-220.

[5] A.Sahai and D.Cabric, A Tutorial on Spectrum Sensing: Fundamental Limits and Practical Challenges, *IEEE DySPAN2005*, Baltimore, MD, Nov.2005.

[6] H. Urkowitz, Energy Detection of Unknown Deterministic Signals, *in Proc. Of IEEE*, vol. *55*, April 1967, pp. 523-531.

[7] F. F. Digham, M. S. Alouini, and M. K. Simon, On the Energy Detection of Unknown Signals over Fading Channels, *IEEE Transactions on Communications*, vol. *55*, no. *1*, Jan. 2007.

[8] D. Cabric, S.M. Mishra, and R.W. Brodersen, Implementation Issues in Spectrum Sensing for Cognitive Radios, *IEEE Asilomar Conf. on Signals*, Systems and Computers, vol. 1, Nov. 2004, pp. 772-776.

[9] H. Tang, Some Physical Layer Issues of Wide-Band Cognitive Radio Systems, *IEEE Int. Conf. on Wireless Networks, Comm.. and Mobile Computing*, Nov. 2005, pp. 151-159.

[10] R. Tandra and A. Sahai, Fundamental Limits on Detection in Low SNR under Noise Uncertainty, *IEEE Int. Conf. on Wireless Networks, Comm.. and Mobile Computing*, vol. *1*, June 2005, pp. 464-469.

[11] Geng Wang ,*Performance of Collaborative Spectrum Sensing in a Cognitive Radio System*, Master Thesis, The University of British Columbia, 2009.

[12] Khaled Ben Letaief, and Wei Zhang, Cooperative Communications for Cognitive Radio Networks, *Proceedings of the IEEE*, vol. *97*, Issue: *5*, May 2009.

[13] Mitola, J., III, Cognitive radio for flexible mobile multimedia communications, *in Proc. IEEE Int. Workshop on Mobile Multimedia Comm..*, 1999.

[14] K. Ben Letaief and Wei Zhang, Cooperative Communications for Cognitive Radio Networks, *Proceedings of the IEEE*, vol. *97*, no. 5, May 2009, pp. 878–893.

[15] Yucek, T. & Arslan, H., A Survey of Spectrum Sensing Algorithm for Cognitive Radio Applications, *IEEE Communications Surveys & Tutorials*, *11(1)*,First Quarter 2009.

[16] T. Yucek and H. Arslan, A survey of spectrum sensing algorithms for cognitive radio applications, *IEEE Communications Surveys & Tutorials*, vol. *11*, no. *1*, First Quarter 2009, pp. 116-130.

[17] V. Sönmezer, M. Tummala, J. McEachen, and A. Adams, Cooperative wideband spectrum sensing using radio frequency sensor networks, *Proc. 2010 Conference Record of the Forty Fourth Asilomar Conference on Signals, Systems and Computers*, 2010, pp. 951–955.

[18] Jun Ma, Guodong Zhao, and Ye Li, Soft Combination and Detection for Cooperative Spectrum Sensing in Cognitive Radio Networks, *IEEE Transactions on Wireless Communications*, vol. *7*, no. *11*, November 2008, pp. 4502–4507.

[19] Wei Zhang, R. K. Mallik, and K. Ben Letaief, Cooperative Spectrum Sensing Optimization in Cognitive Radio Networks, *Proc. IEEE International Conference on Communications*, 2008, pp. 3411–3415.

[20] G. Vardoulias, J. Faroughi-Esfahani, G. Clemo, and R. Haines, Blind radio access technology discovery and monitoring for software defined radio communication systems: problems and techniques, *in Proc. Int. Conf. 3G Mobile Communication Technologies, London*, UK, Mar. 2001, pp. 306–310.

[21] G. Ganesan and Y. Li, Agility improvement through cooperative diversity in cognitive radio, *in Proc. IEEE Global Telecomm. Conf. (Globecom)*, vol. *5*, St. Louis, Missouri, USA, Nov./Dec. 2005, pp. 2505–2509.

[22] A. F. Cattoni, I. Minetti, M. Gandetto, R. Niu, P. K. Varshney, and C. S. Regazzoni, A spectrum sensing algorithm based on distributed cognitive models, *in Proc. SDR Forum Technical Conference*, Orlando, Florida, USA, Nov. 2006.

[23] M. Gandetto and C. Regazzoni, Spectrum sensing: A distributed approach for cognitive terminals, *IEEE J. Select. Areas Commun.*vol. *25*, no. *3*, Apr. 2007, pp. 546–557.

[24] H. Tang, Some physical layer issues of wide-band cognitive radio systems, *in Proc. IEEE Int. Symposium on New Frontiers in Dynamic Spectrum Access Networks*, Baltimore, Maryland, USA, Nov. 2005, pp. 151–159.

[25] A. Sahai, R. Tandra, S. M. Mishra, and N. Hoven, Fundamental design tradeoffs in cognitive radio systems, *in Proc. of Int. Workshop on Technology and Policy for Accessing Spectrum*, Aug. 2006.

[26] T. Y¨ucek and H. Arslan, Spectrum characterization for opportunistic cognitive radio systems, *in Proc. IEEE Military Commun. Conf.*, Washington, D.C., USA, Oct. 2006, pp. 1–6.

[27] S. t. B. S. M. Mishra, R. Mahadevappa, and R. W. Brodersen, Cognitive technology for ultra-wideband/WiMax coexistence, *in Proc. IEEE Int. Symposium on New Frontiers in Dynamic Spectrum Access Networks*, Dublin, Ireland, Apr. 2007, pp. 179–186.

[28] M. Oner and F. Jondral, Cyclostationarity based air interface recognition for software radio systems, *in Proc. IEEE Radio and Wireless Conf.*, Atlanta, Georgia, USA, Sept. 2004, pp. 263–266.

[29] A. Fehske, J. Gaeddert, and J. Reed, A new approach to signal classification using spectral correlation and neural networks, *in Proc. IEEE Int. Symposium on New Frontiers in Dynamic Spectrum Access Networks*, Baltimore, Maryland, USA, Nov. 2005, pp. 144–150.

[30] K. Kim, I. A. Akbar, K. K. Bae, J.-S. Um, C. M. Spooner, and J. H. Reed, Cyclostationary approaches to signal detection and classification in cognitive radio, *in Proc. IEEE Int. Symposium on New Frontiers in Dynamic Spectrum Access Networks*, Dublin, Ireland, Apr. 2007, pp. 212–215.

[31] P. D. Sutton, J. Lotze, K. E. Nolan, and L. E. Doyle, Cyclostationary signature detection in multipath rayleigh fading environments, *in Proc. IEEE Int. Conf. Cognitive Radio Oriented Wireless Networks and Comm.. (Crowncom)*, Orlando, Florida, USA, Aug. 2007.

[32] A. Tkachenko, D. Cabric, and R. W. Brodersen, Cyclostationary feature detector experiments using reconfigurable BEE2, *in Proc. IEEE Int. Symposium on New Frontiers in Dynamic Spectrum Access Networks*, Dublin, Ireland, Apr. 2007, pp. 216–219.

[33] T. Farnham, G. Clemo, R. Haines, E. Seidel, A. Benamar, S. Billington, N. Greco, N. Drew, T. Le, B. Arram, and P. Mangold, IST-TRUST: A perspective on the reconfiguration of future mobile terminals using software download, *in Proc. IEEE Int. Symposium on Personal, Indoor and Mobile Radio Comm.*, London, UK, Sept. 2000, pp. 1054–1059.
[34] M. Mehta, N. Drew, G. Vardoulias, N. Greco, and C. Niedermeier, Reconfigurable terminals: an overview of architectural solutions, *IEEE Comm. Mag*., vol. *39*, no. *8*, 2001, pp. 82– 89.
[35] J. Palicot and C. Roland, A new concept for wireless reconfigurable receivers, *IEEE Comm. Mag*., vol. *41*, no. 7, 2003, pp. 124–132.
[36] M. Gandetto, M. Guainazzo, and C. S. Regazzoni, Use of time frequency analysis and neural networks for mode identification in a wireless software-defined radio approach, *EURASIP Journal on Applied Signal Processing*, vol. *2004*, 2004, pp. 1778–1790.
[37] M. Gandetto, M. Guainazzo, F. Pantisano, and C. S. Regazzoni, A mode identification system for a reconfigurable terminal using Wigner distribution and non-parametric classifiers, *in Proc. IEEE Global Telecomm. Conf. (Globecom)*, vol. *4*, Dallas, Texas, USA, Nov./Dec. 2004, pp. 2424–2428.
[38] R. Tandra and A. Sahai, Fundamental limits on detection in low SNR under noise uncertainty, *in Proc. IEEE Int. Conf. Wireless Networks, Comm. and Mobile Computing*, vol. *1*, Maui, HI, June 2005, pp. 464–469.
[39] R. Tandra and A. Sahai, SNR walls for feature detectors, *in Proc. IEEE Int. Symposium on New Frontiers in Dynamic Spectrum Access Networks*, Dublin, Ireland, Apr. 2007, pp. 559–570.

IOSR Journal of Electronics and Communication Engineering (IOSR-JECE)
e-ISSN: 2278-2834,p- ISSN: 2278-8735. Volume 5, Issue 6 (Mar. - Apr. 2013), PP 74-79
www.iosrjournals.org

Comparison of TCP congestion control mechanisms Tahoe, Newreno and Vegas

Digvijaysinh B Kumpavat[1], Prof. Paras S Gosai[2], Prof. Vyomal N Pandya[3]
[1](Research student, Department of EC engineering, Govt.Engg. College, Surat, Gujarat, India)
[2](Asso. Prof., Department of EC engineering, Govt.Engg. College, Surat, Gujarat, India)
[3](Asst. Prof., Department of EC engineering, CKPCET, Surat, Gujarat, India)

***Abstract*:** *The widely used reliable transport protocol TCP, is an end to end protocol designed for the wireline networks characterized by negligible random packet losses. This paper represents exploratory study of TCP congestion control principles and mechanisms. Modern implementations of TCP contain four intertwined algorithms: slow start, congestion avoidance, fast retransmit, and fast recovery. In addition to the standard algorithms used in common implementations of TCP, this paper also describes some of the more common proposals developed by researchers over the years. We also study, through extensive simulations, the performance characteristics of four representative TCP schemes, namely TCP Tahoe, New Reno and Vegas under the network conditions of bottleneck link capacities for wired network.*

***Keywords* -** *Congestion avoidance, Congestion control mechanisms, Newreno, Tahoe, TCP, Vegas.*

I. Introduction

The standard algorithms in TCP implementations today can be found in RFC 2001[4]. This reference document specifies four standard congestion control algorithms that are now in common use. The four algorithms, Slow Start, Congestion Avoidance, Fast Retransmit and Fast Recoveries are described below.

1.1 Slow start

Slow Start, a requirement for TCP software implementations is a mechanism used by the sender to control the transmission rate, otherwise known as sender-based flow control. This is accomplished through the return rate of acknowledgements from the receiver. When a new connection is established, the congestion window is initialized to one segment. Each time an ACK is received, the congestion window is increased by one segment. The sender can transmit up to the minimum of the congestion window and the advertised window. The congestion window is flow control imposed by the sender, while the advertised window is flow control imposed by the receiver. The former is based on the sender's assessment of perceived network congestion; the latter is related to the amount of available buffer space at the receiver for this connection. The sender can transmit the minimum of the congestion window and the advertised window of the receiver, which is simply called the transmission window. The sender starts by transmitting one segment and waiting for its ACK. When that ACK is received, the congestion window is incremented from one to two, and two segments can be sent. When each of those two segments is acknowledged, the congestion window is increased to four. This provides an exponential growth, although it is not exactly exponential because the receiver may delay its ACKs, typically sending one ACK for every two segments that it receives. At some point the capacity of the internet can be reached, and an intermediate router will start discarding packets. This tells the sender that its congestion window has gotten too large.

1.2 Congestion avoidance

Congestion can occur when data arrives on a big pipe (a fast LAN) and gets sent out a smaller pipe (a slower WAN). Congestion can also occur when multiple input streams arrive at a router whose output capacity is less than the sum of the inputs. Congestion avoidance is a way to deal with lost packets. In the Congestion Avoidance algorithm a retransmission timer expiring or the reception of duplicate ACKs can implicitly signal the sender that a network congestion situation is occurring. The sender immediately sets its transmission window to one half of the current window size (the minimum of the congestion window and the receiver's advertised window size), but to at least two segments. If congestion was indicated by a timeout, the congestion window is reset to one segment, which automatically puts the sender into Slow Start mode. If congestion was indicated by duplicate ACKs, the Fast Retransmit and Fast Recovery algorithms are invoked.

1.3 Fast retransmit

When a duplicate ACK is received, the sender does not know if it is because a TCP segment was lost or simply that a segment was delayed and received out of order at the receiver. Typically no more than one or two

duplicate ACKs should be received when simple out of order conditions exist. If however more than two duplicate ACKs are received by the sender, it is a strong indication that at least one segment has been lost. The TCP sender will assume enough time has lapsed for all segments to be properly re-ordered by the fact that the receiver had enough time to send three duplicate ACKs.

When three or more duplicate ACKs are received, the sender does not even wait for a retransmission timer to expire before retransmitting the segment (as indicated by the position of the duplicate ACK in the byte stream). This process is called the Fast Retransmit algorithm and was first defined in [5]. Immediately following Fast Retransmit is the Fast Recovery algorithm.

1.4 Fast recovery

It is an improvement that allows high throughput under moderate congestion, especially for large windows. The receipt of the duplicate ACKs tells TCP more than just a packet has been lost. Since the receiver can only generate the duplicate ACK when another segment is received, that segment has left the network and is in the receiver's buffer.

The fast retransmit and fast recovery algorithms are usually implemented together as follows. [4]

1. When the third duplicate ACK in a row is received, set ssthresh to value:

ssth = min (cwnd/2 , 2 MSS) (1)

Retransmit the missing segment. Set cwnd to ssthresh plus 3 times the segment size. This inflates the congestion window by the number of segments that have left the network and which the other end has cached.

2. Each time another duplicate ACK arrives, increment cwnd by the segment size. This inflates the congestion window for the additional segment that has left the network. Transmit a packet, if allowed by the new value of cwnd:

cwnd = ssth + no. of dupacks received (2)

3. When the next ACK arrives that acknowledges new data, set cwnd to ssthresh (the value set in step 1). This ACK should be the acknowledgment of the retransmission from step 1, one round-trip time after the retransmission. Additionally, this ACK should acknowledge all the intermediate segments sent between the lost packet and the receipt of the first duplicate ACK. This step is congestion avoidance, since TCP is down to one-half the rate it was at when the packet was lost.

II. Congestion Control Mechanisms

Here we will discuss three congestion control mechanisms.

2.1 TCP Tahoe

TCP Tahoe added the *slow-start*, *congestion avoidance*, and *fast retransmit* algorithms to TCP. TCP Tahoe is briefly described in [8]. With fast retransmit, when a packet is lost, instead of waiting for the retransmission timer to expire, if *tcprexmtthresh* (usually three) duplicate ACKs are received, the sender infers a packet loss and retransmits the lost packet. The sender now sets its *ssthresh* to half the current value of *cwnd* (maintained in bytes) and begins again in the slow-start mode with an initial window of 1. The slow start phase lasts till the *cwnd* reaches *ssthresh* and then congestion avoidance takes over. In this phase, the sender increases its *cwnd* linearly by *cwnd* for every new ACK it receives. Note that with TCP Tahoe the sender might retransmit packets which have been received correctly. Timeouts are used as the means of last resort to recover lost packets. On receiving three *dupacks* Tahoe starts Fast retransmit phase in which it retransmits packet and set *ssth* to half of *cwnd* and then enters in *slow start* phase by setting *cwnd* to one segment.

2.2 TCP Newreno

Standard TCP schemes such as Reno are simple and effective for reliable data transfer in wired networks, where packet loss due to bit errors is rare. TCP newreno [1] have similar slow-start, congestion avoidance and fast retransmit- recovery algorithm as Reno. During the slow-start phase, the sender increases its congestion window *cwnd* by one with each acknowledgment (ACK) received, until the slow-start threshold *ssth* is reached and the congestion avoidance phase takes over. In congestion avoidance, the sender increases its *cwnd* linearly by 1/ *cwnd* with each ACK received. Upon receiving triple duplicate ACKs (TD), the sender infers a packet loss and retransmits the lost packet, i.e. fast retransmit. The sender then sets *ssth* to *cwnd* / 2 , halves its *cwnd* and activates the fast recovery algorithm. In fast recovery, upon receiving a duplicate ACK, by assuming that a packet has left the networks, the sender sends/retransmits a packet to maintain the link to the receiver full. Upon receiving a *partial ACK*, the sender retransmits the first unacknowledged packet. When an ACK acknowledges all the packets transmitted before the fast retransmit triggered, the sender exits fast recovery and sets the congestion window *cwnd* to the slow-start threshold *ssth*. Then the sender enters the congestion avoidance phase.

In the case of multiple packets dropped from a single window of data, the first new information available to the sender comes when the sender receives an acknowledgement for the retransmitted packet (that is

the packet retransmitted when Fast Retransmit was first entered). If there had been a single packet drop, then the acknowledgement for this packet will acknowledge all of the packets transmitted before Fast Retransmit was entered (in the absence of reordering). However, when there were multiple packet drops, then the acknowledgement for the retransmitted packet will acknowledge some but not all of the packets transmitted before the Fast Retransmit. We call this packet a partial acknowledgment. Which is described in [2].

2.3 TCP Vegas

Vegas is an implementation of TCP that achieves between 37 and 71 % better throughput [3]on the Internet, with one-fifth to one-half the losses, as compared to the implementation of TCP in the Reno distribution. There are three techniques that Vegas employs to increase throughput and decrease losses.

2.3.1 New retransmission mechanism

TCP Vegas introduces three changes that affect TCP's (fast) retransmission strategy. First, TCP Vegas measures the RTT for every segment sent. The measurements are based on fine-grained clock values. Using the fine-grained RTT measurements, a timeout period for each segment is computed. When a duplicate acknowledgement (ACK) is received, TCP Vegas checks whether the timeout period has expired. If so, the segment is retransmitted. Second, when a non-duplicate ACK that is the first or second after a fast retransmission is received, TCP Vegas again checks for the expiration of the timer and may retransmit another segment. Third, in case of multiple segment loss and more than one fast retransmission, the congestion window is reduced only for the first fast retransmission.

2.3.2 Congestion avoidance mechanism

TCP Vegas does not continually increase the congestion window during congestion avoidance. It controls *cwnd* by observing changes of RTTs (Round Trip Time) of segments that the connection has sent before. If observed RTTs become large, TCP Vegas recognizes that the network begins to be congested, and throttles *cwnd* down. If RTTs become small, on the other hand, TCP Vegas determines that the network is relieved from the congestion, and increases *cwnd*.

In congestion avoidance phase, the *cwnd* is updated as shown in [6]:

$$Cwnd\ (t+t_A) = \begin{cases} cwnd(t)+1, & \text{if} \quad diff < \alpha/base\_rtt \\ cwnd(t), & \text{if} \quad \alpha/base\_rtt < diff < \beta/base\_rtt \\ cwnd(t)-1, & \text{if} \quad \beta/base\_rtt < diff \end{cases} \qquad (3)$$

$$diff = cwnd(t)/base\_rtt - cwnd/rtt$$

where *rtt* is an observed round trip time, *base_rtt* is smallest value of observed RTTs, and α and β are some constant values.

2.3.3 Modified slow-start mechanism

A similar congestion detection mechanism is applied during slow-start to decide when to change to the congestion avoidance phase. To have valid comparisons of the expected and the actual throughput, the congestion window is allowed to grow only every other RTT.

In [3], an additional algorithm is presented, which tries to infer available bandwidth during slow-start from ACK spacing. However, this algorithm was marked experimental, and it was not used in the evaluation of TCP Vegas.

III. Simulation Environment

This section describes the simulation environment used to investigate the influence of the various congestion control mechanism in TCP. Here we used simulator ns-2 for better scheduling event and controlled environment.

3.1 Network topology

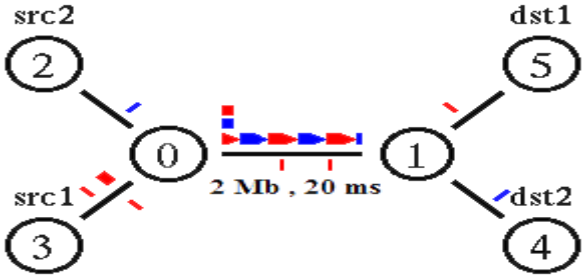

Figure 1 Network topology

The network model that we will use in the analysis is depicted in Fig. 1. The model consists of two sources (srcl, src2), two destinations (dst1, dst2), two intermediate nodes (or routers) (node 0 and node 1), and links interconnecting between the end stations and routers. We consider two connections; Connection 1 from src1 to dst1, which is assigned TCP traffic, and Connection 2 from src2 to dst2, which is assigned UDP traffic. Both connections are established via Node 0 and Node 1, and the link between Node 0 and Node 1 is shared between two connections. The bandwidth of the shared bottleneck link is 2 Mbps. The buffer size of Node 0 is 10 [segments]. The propagation delays between srci and dsti is 40 ms (i=1,2)**.**

IV. Simulation for Congestion window versus time

Congestion window of TCP changes based on change in its basic algorithms for every TCP variant. Simulation result of congestion window describes slow start, congestion avoidance, fast retransmit and fast recovery algorithms in TCP variants.

4.1 TCP Tahoe

Fig. 2 shows *cwnd* vs time for TCP tahoe for network topology defined as above.

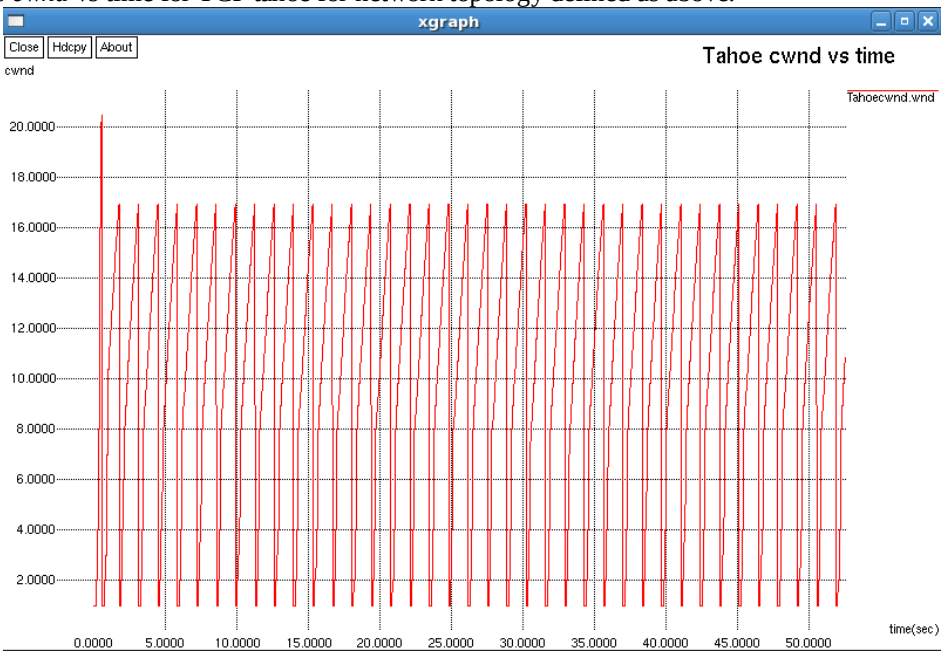

Figure 2 cwnd vs. Time for TCP Tahoe

As shown in Fig. 2 TCP Tahoe *cwnd* is exponentially increased in slow start phase up to *ssth.* In congestion avoidance phase *cwnd* is increased linearly and after receiving three *dupacks* TCP enters in fast retransmit phase. The *ssth* is now set to the half of *cwnd* and congestion window is set to the one segment and TCP enters in slow start phase.

4.2 TCP Newreno:

Fig. 3 shows *cwnd* vs time for TCP Newreno for network topology defined as above.

As shown in Fig. 3 TCP Tahoe *cwnd* is exponentially increased in slow start phase up to *ssth.* In congestion avoidance phase *cwnd* is increased linearly and after receiving three *dupacks* TCP enters in fast retransmit

phase. The *ssth* is now set to the half of *cwnd* and congestion window is set to the value *ssth*, that is, half of the previous *cwnd*. So TCP enters in congestion avoidance phase after retransmission.

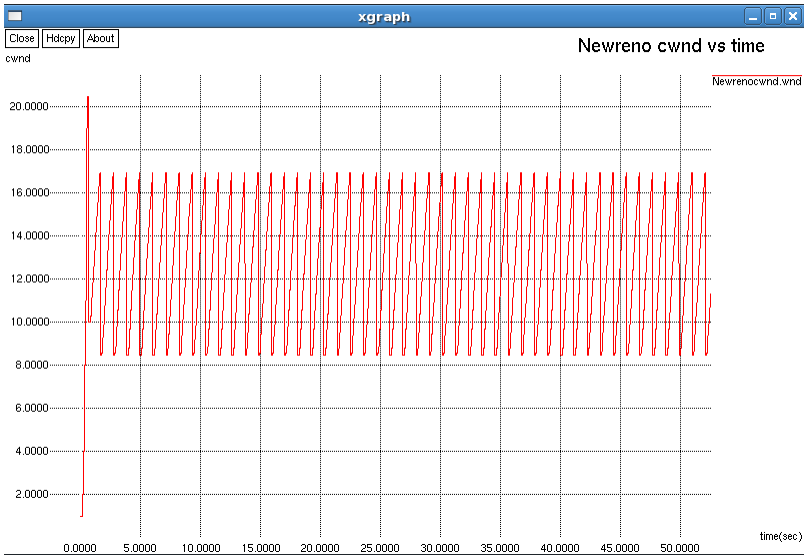

Figure 3 cwnd vs. Time for TCP Newreno

4.3 TCP Vegas:

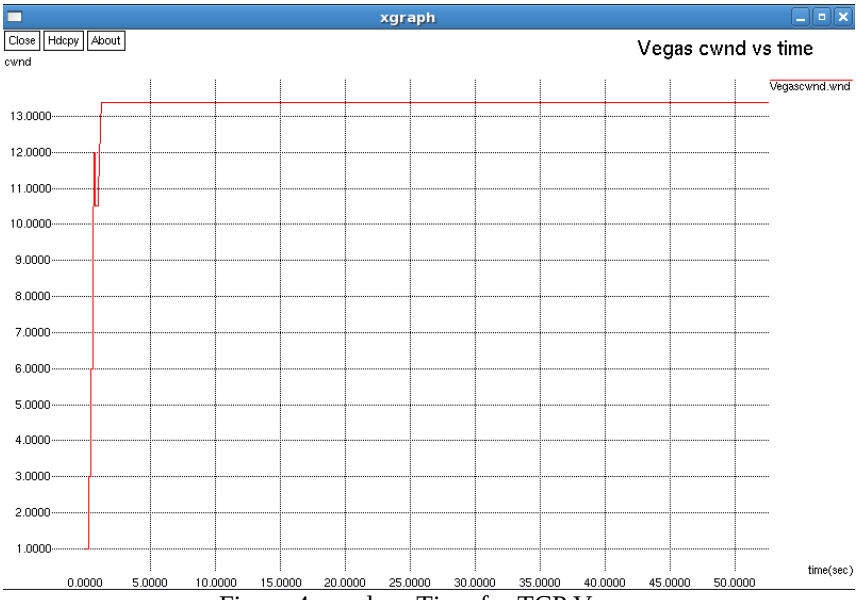

Figure 4 cwnd vs. Time for TCP Vegas

Fig. 4 shows *cwnd* vs time for TCP Vegas for network topology defined as above. As shown in Fig.4 *cwnd* of TCP vegas increase by rate half than TCP Tahoe and Newreno in slow start phase. In congestion avoidance phase *cwnd* is set to constant value as *cwnd* is controlled according to network traffic prediction based on observed RTT values.

V. Throughput vs time

Fig. 5 shows throughput vs time graph of TCP Tahoe, Newreno and Vegas. As we can see that throughput value increases abruptly initially, but then throughput is constant with time which indicates that packets delivery per RTT epoch is constant i.e same number of packets are delivered by network in certain amount of cyclic period of time.

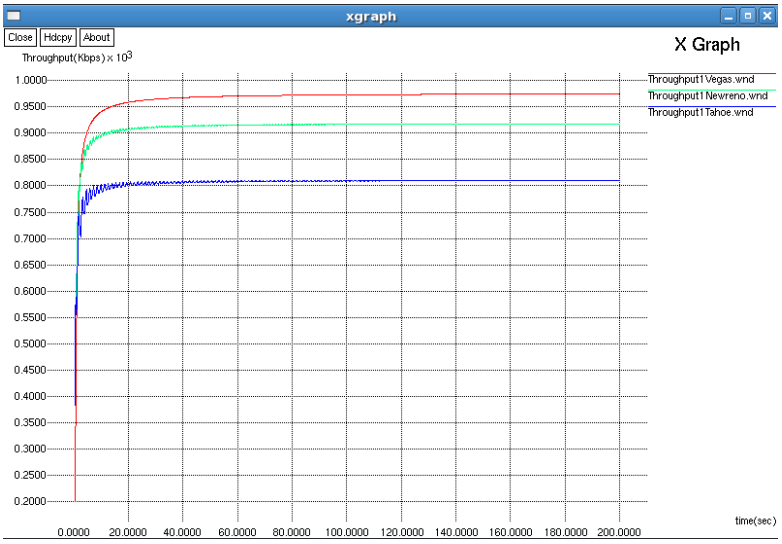

Figure 5 Comparison of TCP Tahoe, Newreno and Vegas throughput vs time

As shown in Fig. 5 TCP Vegas (indicated by RED line) has highest value of throughput, which is 974.803 Kbps for given topology. This due to its wise changes in slow start, congestion avoidance and retransmission algorithms. TCP Newreno (indicated by GREEN line) is next to TCP Vegas. Throughput of Newreno is 918.249 Kbps, which is degraded as compared to Vegas due to throttling of congestion window. TCP Tahoe (indicated by BLUE line) has lowest value of throughput, which is 810.187 Kbps for given topology, as it starts from slow start phase every time after retransmission.

VI. Conclusion

In this paper, we have evaluated the performance characteristics of various TCP congestion control schemes under the wired network conditions with bottleneck end-to-end link capacities, and both type of traffic TCP and UDP. We can conclude based on throughput calculation that TCP vegas gives highest performance as it can change its congestion window based on network traffic situation. However in wireless network the whole scenario may differ. This is because any packet loss over the wireline links is mainly on account of congestion unlike wireless links where packet losses can result both due to congestion and random losses. Since, TCP does not distinguish between congestion losses and random losses, the throughput of a TCP connection over a wireless link may suffers.

References

[1] Kai Xu, Ye Tian, Nirwan Ansari, Improving TCP performance in integrated wireless communications networks, Elsevier Computer Networks 47, 2005, 219-237

[2] T. Henderson, S. Floyd and A. Gurtov, The Newreno Modification to TCP's Fast Recovery Algorithm, RFC 6582, April 2012, 1-16

[3] Lawrence S. Brakmo and Larry L. Peterson, TCP Vegas: End to End Congestion Avoidance on a Global Internet, IEEE Journal on Selected Areas In Communication ,13 (8), October 1995, 1465-1480

[4] W. Stevens, TCP Slow Start, Congestion Avoidance, Fast Retransmit, and Fast Recovery Algorithms, RFC 2001, January 1997, 1-7

[5] Van Jacobson, Congestion Avoidance and Control. Computer Communications Review, 18 (4), August 1988, 314-329.

[6] G. Hasegawa, M. Murata, and H. Miyahara, Fairness and stability of the congestion control mechanism of TCP, Proceedings of IEEE INFOCOM'99, March 1999, 1329–1336.

[7] Paul Meeneghan and Declan Delaney, An Introduction to NS, Nam and Otcl scripting, Department of Computer Science, National University of Ireland, Maynooth, 2004-05.

[8] B. Sikdar, S. Kalyanaraman and K. S. Vastola, Analytic Models for the Latency and Steady-State Throughput of TCP Tahoe, Reno, and SACK, IEEE/ACM Transactions On Networking, 11(6), December 2003, 959-971.

IOSR Journal of Electronics and Communication Engineering (IOSR-JECE)
e-ISSN: 2278-2834,p- ISSN: 2278-8735. Volume 5, Issue 6 (Mar. - Apr. 2013), PP 80-87
www.iosrjournals.org

Design of MEMS capacitive accelerometer with different perforated proof- mass for enhancement of performance

Kamran Akhtar, Dr.A. Vimala Juliet
Instrumentation and control Engineering SRM University Kattankulathur. Tamilnadu.
Instrumentation and control Engineering SRM University Kattankulathur. Tamilnadu

Abstract:- *This work represents a study of perforated proof mass of a micro fabricated accelerometer with different perforation shapes, by application of load stress and displacement is measuredto know the deflection and flexibility of the proof mass. Perforation shapes of proof mass of capacitive accelerometer affects the sensitivity and other performance parameters of accelerometer.Eigen frequency analysis is done to know the stress and displacement distribution on vibrating proof mass which are used to measure and compare the sensitivity and mechanical strength of proof mass. As a result of this study it has been found that the proof mass with perforation shape of nozzle/diffuser is the most efficient perforation shape to get better performance from an capacitive micro fabricated accelerometers.*
Keywords:- *Accelerometer, Eigen frequency, MEMS, perforation.*

I. Introduction

Accelerometer is a device used to detect magnitude and direction of the proper acceleration (or g-force), as a vector quantity, and can be used to sense orientation (because direction of weight changes), coordinate acceleration, vibration, shock, and falling in a resistive medium.. Different types of accelerometer are available such as capacitive, piezo-resistive, tunnelling, thermal etc., studies and research on these accelerometer have proved that capacitive accelerometers are more efficient and widely used.Capacitive accelerometer is one of the earliest inertialinstruments studied intensively in MEMS (Micro-Electro-Mechanical Systems) field since 1980s because of its simple structure and easy integration with integrated circuit. Perforation is done to reduce the air damping which has significant effect on the performance Proof mass of capacitive accelerometer will act as movable plates which causes change in distance between the plates so capacitance will change. This change in capacitance will be measured as acceleration.

II. Device Description

Proof mass of accelerometer is act as a movable plates when load is applied, proof mass moves causes change in capacitance which can be measured as acceleration.Proof mass with different perforation has different stress and displacement distribution means flexibility and sensitivity of proof mass changes with perforation shapes.
d is distance between the plates when load is applied this distance will change accordingly capacitance will change.
Capacitance C is defined as:-

$$C=€A/d.$$

€ iselectrical permittivity of dielectric medium and is defined as $€=€_0€r$,for air as dielectric medium $€=€_0$.

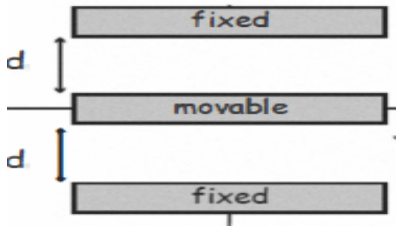

Fig.Equivalent model of capacitive accelerometer

Accelerometer can be modelled as system composed of proof mass,spring,damper.This system can be expressed as:-

$$F=ma=md^2z/dt^2+bdz/dt+kz$$

Where z id displacement,k is spring constant,b is damping coefficient and m is mass of proof mass, a is applied stress. Poly-silicon is used in proof mass as well as in fixed plates since poly -silicon has excellent mechanical and yield strength. *1kpa*loadis applied along negative z-axis.

Table1:- Model dimension.

	Length in µm	Width in µm	Height in µm
Proof mass	5000	5000	100
Square hole	1000	1000	100
Anchor	1500	1500	100
Beam	5000	1500	100
Shin	3000	500	100

III. Simulation

All the simulations are done in COMSOL(multi physics), version 4.3and version 4.3a

1) Proof mass with square perforation:-

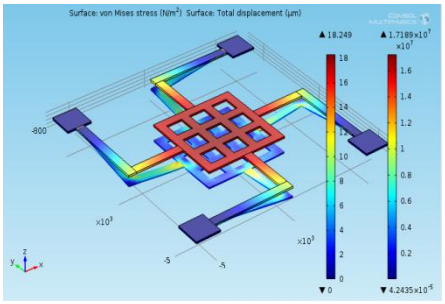

Fig.1:-Proof mass with square perforation

2) Proof mass with cylindricalperforation:-
Radius of circular hole=500µm

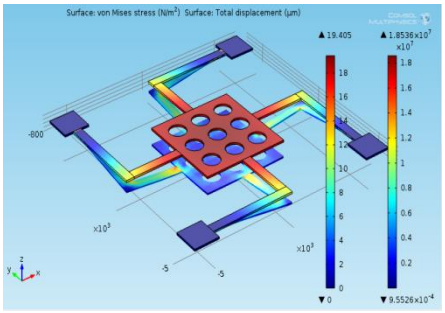

Fig. 2.Proof mass with cylindrical perforation

3) Proof mass with nozzle and diffuser perforation:-

Nozzle a-semi axis =500 µm
Nozzle b-semi axis =500 µm
Height =100µm
Ratio=0.5

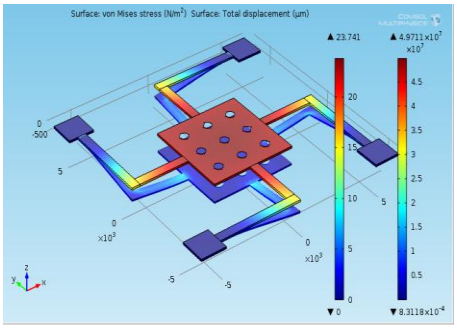

Fig. 3.Proof mass with nozzle diffuser perforation

4) Proof mass with pyramidal perforation:-
Base length 1=1000µm
Base length 2=1000µm
Height= 100µm
Ratio = 0.5

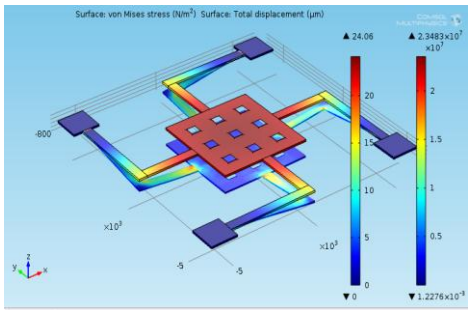

Fig. 4.Proof masswith pyramidal perforation

Table2:- Maximum stress and displacement values On the proof mass of different perforations

Perforation	Stress in N/m^2	Displacement in µm
Square	1.71E7	18.25
Circle	1.85E7	19.40
Nozzle diffuser	4.97E7	23.74
Pyramidal	2.34E7	24.06

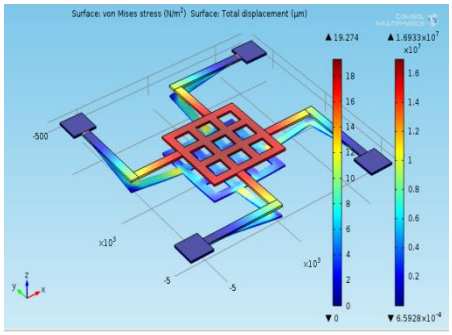

Fig.5:-Proof mass with square perforation and changed beam position change Stress and displacement values will be change if We change the spring position of the proof mass

Table3:- Stress and displacement values with change spring position

Perforation	Stress in N/m^2	Displacement in µm
Square	1.69E7	19.27
Circle	2.27E7	21.36
Nozzle diffuser	2.63E7	26.32
Pyramidal	2.35E7	25.03

IV. Eigen Frequency Analysis

In this analysis proof mass vibrates in six different modes at six different frequencies. These frequencies decides the maximum stress and maximum displacement of the proof mass.
These frequencies depend on the model design.

1. Proof mass with cylindrical perforation

Table4:- Stress and displacement values at six modes.

Modes	Frequency In Hz	Stress in N/m^2	Displacement in micro meter
Mode1	2111.25	2.28E12	2.35E6
Mode2	4436.62	5.46E12	3.51E6
Mode3	4438.59	5.54E12	3.53E6
Mode4	8231.76	8.50E12	4.43E6
Mode5	9971.85	1.11E13	4.58E6
Mode6	13094.56	1.88E13	4.17E6

2. Proof mass with square perforation*:-*

Table 5:- Stress and displacement values at six modes.

Modes	Frequency In Hz	Stress in N/m^2	Displacement in micro meter
Mode1	4385.68	5.98E12	4.37E6
Mode2	4385.95	5.94E12	4.36E6
Mode3	8339.22	8.34E12	4.46E6
Mode4	10062.45	10.4E12	4.64E6
Mode5	12997.44	2.35E13	5.65E6
Mode6	13010.51	2.40E13	5.57E6

3. Proof mass with pyramidal perforation

Table 6:- Stress and displacement values at six modes.

Modes	Frequency inHz	Stress in N/m^2	Displacement In micro meter
Mode1	2173.43	2.28E12	2.31E6
Mode2	4477.34	5.30E12	3.56E6
Mode3	4478.34	5.40E12	3.56E6
Mode4	7887.52	8.23E12	4.58E6
Mode5	9721.36	9.572E12	4.66E6
Mode6	13010.51	2.40E13	5.57E6

4. Proof mass with nozzle diffuser perforation

Table7:- Stress and displacement values at six modes

Modes	Frequency In Hz	Stress in N/m^2	Displacement in micro meter
Mode1	2028.33	3.29E12	2.31E6
Mode2	4376.26	5.80E12	3.88E6
Mode3	4379.78	5.88E12	3.79E6
Mode4	8875.34	27.52E12	4.63E6
Mode5	10375.38	16.62E12	4.76E6
Mode6	13199.45	28.87E12	5.73E6

V. Eigen Frequency Analysis With Spring Position Change

1. Proof mass with cylindrical perforation*:-*

Table8:- Stress and displacement distribution.

Modes	Frequency inHz	Stress in N/m^2	Displacement In micro meter
Mode1	1938.65	6.01E12	3.38E6
Mode2	4401.89	6.29E12	4.66E6
Mode3	4624.24	6.53E12	4.67E6
Mode4	8305.56	9.31E12	5.57E6
Mode5	9871.19	12.5E12	5.69E6
Mode6	12415.23	19.67E12	5.74E6

2. Proof mass with nozzle diffuser perforation

Table9:- Stress and displacement distribution.

Modes	Frequency inHz	Stress in N/m^2	Displacement In micro meter
Mode1	1940.33	2.5E12	2.25E6
Mode2	4453.56	7.2E12	4.24E6
Mode3	4453.99	7.72E12	4.25E6
Mode4	8246.52	1.31E13	5.5E6
Mode5	9931.05	1.54E13	5.5E6
Mode6	12630.53	3.01E13	6.35E6

3. Proof mass with square perforation:-

Table 10:- Stress and displacement values at six modes.

Modes	Frequency inHz	Stress in N/m^2	Displacement In micro meter
Mode1	2121.60	2.30E12	2.42E6
Mode2	4645.65	6.47E12	4.30E6
Mode3	4648.61	6.54E12	4.33E6
Mode4	7851.48	8.35E12	4.88E6
Mode5	9817.13	10.34E12	4.88E6
Mode6	12979.01	23.38E12	5.77E6

4. Proof mass with pyramidal perforation:-

Table11:- Stress and displacement distribution.

Modes	Frequency inHz	Stress in N/m^2	Displacement In micro meter
Mode1	2019.17	2.56E12	2.57E6
Mode2	4560.45	6.46E12	4.33E6
Mode3	4562.98	6.50E12	4.34E6
Mode4	8346.18	8.86E12	4.57E6
Mode5	10196.20	1.23E13	4.76E6
Mode6	13056.83	2.4E13	5.40E6

VI. Graphical Representation

Stress distribution

1. Proof mass with circular perforation:-

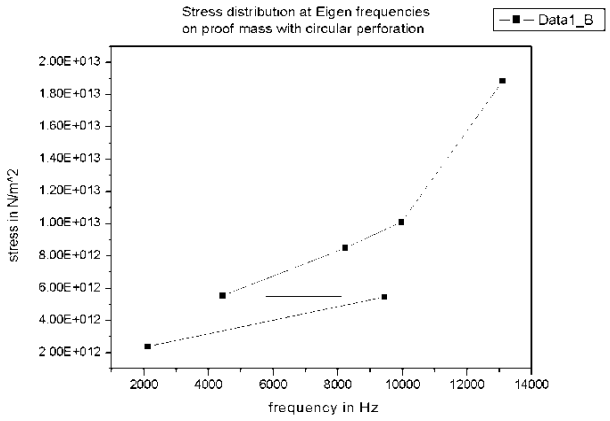

2. Proof mass with square perforation

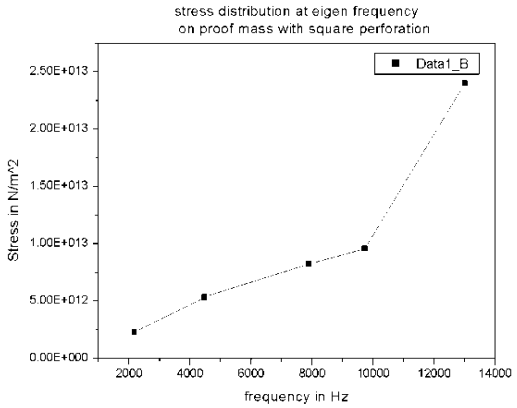

3. Proof mass with nozzle diffuser perforation

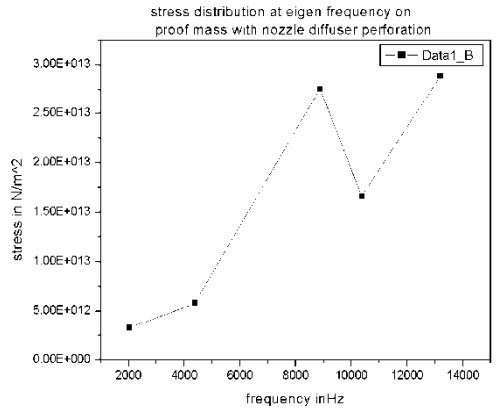

4. Proof mass with pyramidal perforation

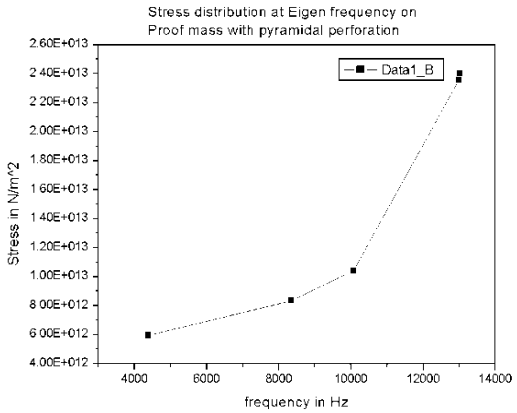

Displacement distribution

1. Proof mass with circular perforation

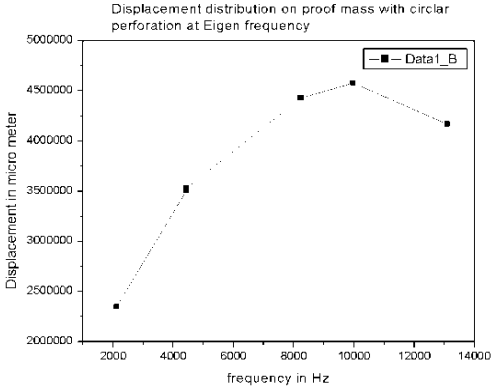

2. Proof mass with square perforation

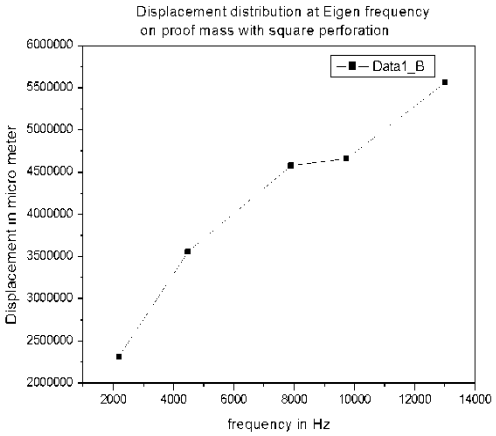

3. Proof mass with nozzle diffuser perforation

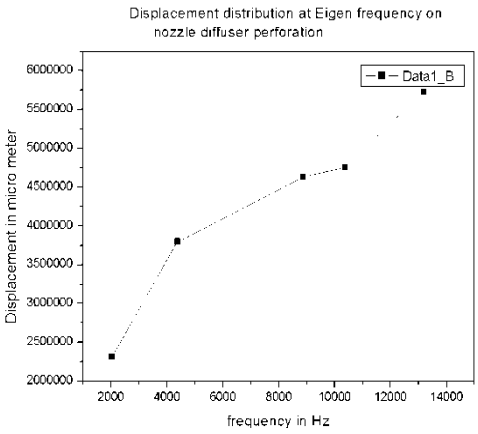

4. Proof mass with pyramidal perforation

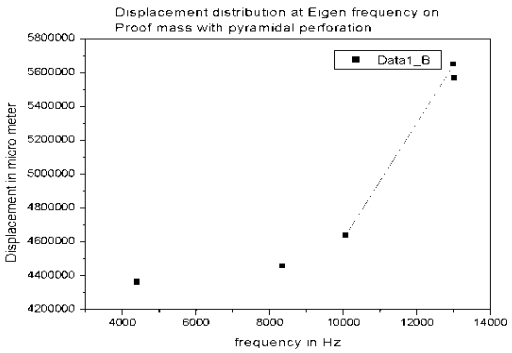

VII. Result

In the same perforated proof mass if position of spring changes maximum displacement and maximum stress will also change.Maximum stress is observed in proof mass with *nozzle-diffuse* perforation.Minimum stress is observed in proof mass with *square* perforation when spring position changes.Maximum displacement is observed in proof mass with*nozzle-diffuser*perforation when spring position changes.Minimum displacement isobserved in proof mass with *square* perforation.

VIII. Conclusion.

Maximum Stress and maximum displacement in nozzle diffuser perforation shows that it is more sensitive to stress and displacement on application of load. Minimum stress and displacement in square perforation shows that it is less sensitive to stress and displacement on application of load. So nozzle –diffuser perforated proof mass is more sensitive as well as has better mechanical strength.

References

[1] Inn am *etal*"School of Mechanical and Aerospace Engineering, Seoul National University, San 56-1, Shilim-Dong, Kwanak-Gu, Seoul, South Korea "School of Electrical Engineering and Computer Science", Seoul National University, Seoul, South Korea.2004

[2] Isaac G.Macwan*et al* "Department of Electrical and Computer Engineering, University of Bridgeport", Bridgeport, CT 06604. 2005

[3] BanibrataMukherjee*et al*, "Department of Electrical Engineering Institute of Technology, Kharagpur",Kharagpur-721302.

[4] Jiri *et al* "Sensor for automotve Technology"*Wiley-VCH GmbH &Co, 2003*

[5] G.K.Fedder,"SimulationofMicroelectromechanicalsystem"*Ph.D thesis* University of California Berkeley.

[6] E.Peeters,S. Vergote,B.Puers and W.Sansen,"A highly symmetrical capacitive micro-accelerometer with singledegree-of-freedom response"J.Miceomech. Microeng

[1] E. Peeters, S. Vergote, B. Puers and W. Sansen," A highly symmetrical capacitive micro-accelerometer with single degree-of-freedom response" J.Micromech. Microeng.2 (1992) 104-112

IOSR Journal of Electronics and Communication Engineering (IOSR-JECE)
e-ISSN: 2278-2834,p- ISSN: 2278-8735. Volume 5, Issue 6 (Mar. - Apr. 2013), PP 88-96
www.iosrjournals.org

Comparative Analysis of Varios Diversity Techniques for Ofdm Systems

Reena[1] M.Tech., Sahasha Namdeo[2] M.Tech.
(Maharishi Dayanand University, Rohtak, India)

Abstract: *In this paper, three transmit diversity techniques are proposed that use extra transmit antennas to obtain additional diversity. An analytical expression for the signal-to-noise ratio (SNR) and bit-error-rate at the output of a three-branch maximal ratio combining, equal gain combining and selection diversity system is given. The three branches are assumed to be Rayleigh fading, correlated with the BPSK modulation. Measurements of the signal-to-noise ratio and bit-error-rate after selection, equal gain combining and maximal ratio combining were made in Rayleigh fading channels and compared with the analytical results. Also presented are the exact analytical average probabilities of bit error for coherent binary phase-shift keying for three-branch maximal ratio combining, equal gain combining and selective diversity for Rayleigh fading channel. All these three branches is compared on the basis of signal to noise ratio and bit error rate with the increasing no. of receiver. This work confirms the benefits of choosing the maximal ratio combining instead of equal gain combining and selection diversity by measuring the performances of these three branches for SNR and BER.*

Keywords *- BPSK, EGC, LOS, MRC, PDF, RF, SNR,BER*

I. Introduction

Antenna diversity, also known as space diversity, is any one of several wireless diversity schemes that uses two or more antennas to improve the quality and reliability of a wireless link. Often, especially in urban and indoor environments, there is no clear line-of-sight (LOS) between transmitter and receiver. Instead the signal is reflected along multiple paths before finally being received. Each of these bounces can introduce phase shifts, time delays, attenuations, and distortions that can destructively interfere with one another at the aperture of the receiving antenna. In most scattering environments, antenna diversity is a practical, effective and, hence, a widely applied technique for reducing the effect of multipath fading [1].

Antenna diversity is especially effective at mitigating these multipath situations. This is because multiple antennas offer a receiver several observations of the same signal. Each antenna will experience a different interference environment. Thus, if one antenna is experiencing a deep fade, it is likely that another has a sufficient signal. Collectively such a system can provide a robust link. While this is primarily seen in receiving systems (diversity reception), the analog has also proven valuable for transmitting systems (transmit diversity) as well.

The classical approach is to use multiple antennas at the receiver and perform combining or selection and switching in order to improve the quality of received signal. The problem with this system is the cost, size and power of the remote units. The use of multiple antennas and RF chains (selections and switching circuits) makes the remote units larger and more expensive. As a result, diversity techniques have almost exclusively applied to base stations to improve their reception quality. Base station often serves hundreds to thousands of remote units. It is economical to add equipments to base stations rather than the remote units. For this reason, transmit diversity schemes are very attractive. For instance, one antenna and one transmit chain may be added to base station to improve the reception quality of all the remote units in that the station's coverage area [2].

Inherently an antenna diversity scheme requires additional hardware and integration versus a single antenna system but due to the commonality of the signal paths a fair amount of circuitry can be shared. Also with the multiple signals there is a greater processing demand placed on the receiver, which can lead to tighter design requirements. Typically, however, signal reliability is paramount and using multiple antennas is an effective way to decrease the number of drop-outs and lost connections.

Diversity techniques are used to improve the performance of the radio channel without any increase in the transmitted power[5].

II. Selection Diversity

Selection Processing presents only one antenna's signal to the receiver at any given time [5]. The antenna chooses the best SNR among the received signals. In the figure 1 shown below the receiver selects the signal having max SNR.

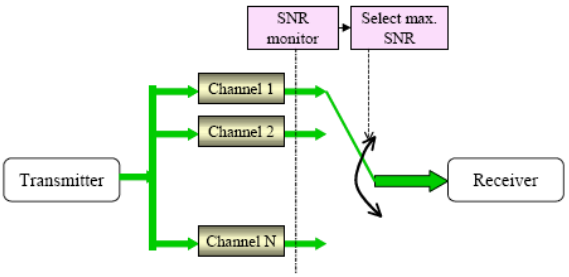

Fig 1.Selection Diversity

In **selection diversity**, we will assume that the channel is a flat fading Rayleigh multipath channel and the modulation is BPSK.

1. We have N receive antennas and one transmit antenna.
2. The channel is flat fading – In simple terms, it means that the multipath channel has only one tap. So, the convolution operation reduces to a simple multiplication.
3. The channel experienced by each receive antenna is randomly varying in time. For any receiving antenna, each transmitted symbol gets multiplied by a randomly varying complex number h_i. As the channel under consideration is a Rayleigh channel, the real and imaginary parts of h_i are Gaussian distributed having mean 0 and variance 1/2.
4. The channel experience by each receive antenna is independent from the channel experienced by other receive antennas.
5. On each receive antenna, the noise n has the Gaussian probability density function with

$p(n) = \frac{1}{\sqrt{2\pi\sigma^2}} e^{\frac{-(n-\mu)^2}{2\sigma^2}}$ with μ=0 and $\sigma^2 = \frac{N_0}{2}$

The noise on each receive antenna is independent from the noise on the other receive antennas.

6. At each receive antenna, the channel h_i is known at the receiver. For example, on any receiving antenna, equalization is performed at the receiver by dividing the received symbol y_i by the apriori known h_i i.e.

$\hat{y} = \frac{y_i}{h_i} = \frac{h_i x + n_i}{h_i} = x + \tilde{n_i}$

where $\tilde{n_i} = \frac{n_i}{h_i}$ is the additive noise scaled by the channel coefficient.

7. In the presence of channel h_i, the instantaneous bit energy to noise ratio at any receive antenna is $\frac{|h_i|^2 E_b}{N_0}$.

For notational convenience, let us define,

$\gamma_i = \frac{|h_i|^2 E_b}{N_0}$

we know that, if h_i is a Rayleigh distributed random variable, then h_i^2 is a chi-squared random variable with two degrees of freedom. The pdf of γ is

$p(\gamma_i) = \frac{1}{(E_b/N_0)} e^{\frac{-\gamma_i}{(E_b/N_0)}}$

III. Equal-Gain Combining Diversity

Various techniques are known to combine the signals from multiple diversity branches. In Equal Gain Combining, each signal branch weighted with the same factor, irrespective of the signal amplitude. However, co-phasing of all signal is needed to avoid signal cancellation[18].

Thus, EGC is simpler to implement than Maximum Ratio Combining (MRC). The adaptively controller amplifiers / attenuators are not needed. Moreover, no channel amplitude estimation is needed.

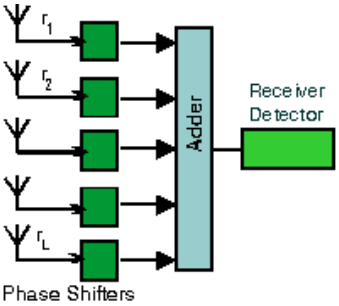

Figure: *2*- branch Equal Gain Combining antenna diversity receiver (L = 5).

The average SNR improvement of EGC is typically about 1 dB worse than with MRC, but still much better than without diversity.

Receiver diversity is a form of space diversity, where there are multiple antennas at the receiver. The presence of receiver diversity poses an interesting problem – how do we use '*effectively*' the information from all the antennas to demodulate the data[11].

1. We have N receive antennas and one transmit antenna.
2. The channel is flat fading – In simple terms, it means that the multipath channel has only one tap. So, the convolution operation reduces to a simple multiplication.
3. The channel experienced by each receive antenna is randomly varying in time. For any receiving antenna, each transmitted symbol gets multiplied by a randomly varying complex number h_i. As the channel under consideration is a Rayleigh channel, the real and imaginary parts of h_i are Gaussian distributed having mean $\mu_{h_i} = 0$ and $\sigma_{h_i}^2 = \frac{1}{2}$
4. The channel experience by each receive antenna is independent from the channel experienced by other receive antennas.
5. On each receive antenna, the noise n has the Gaussian probability density function with $p(n) = \frac{1}{\sqrt{2\pi\sigma^2}} e^{\frac{-(n-\mu)^2}{2\sigma^2}}$ with μ=0 and $\sigma^2 = \frac{N_0}{2}$

The noise on each receive antenna is independent from the noise on the other receive antennas.

6. At each receive antenna, the channel h_i is known at the receiver.
7. In the presence of channel h_i, the instantaneous bit energy to noise ratio at any receiving antenna is $\frac{|h_i|^2 E_b}{N_0}$.

For notational convenience, let us define,

$$\gamma_i = \frac{|h_i|^2 E_b}{N_0}$$

we know that, if h_i is a Rayleigh distributed random variable, then h_i^2 is a chi-squared random variable with two degrees of freedom. The pdf of γ_i is

$$p(\gamma_i) = \frac{1}{(E_b/N_0)} e^{\frac{-\gamma_i}{(E_b/N_0)}}$$

IV. Maximum Ratio Combining Diversity

Various techniques are known to combine the signals from multiple diversity branches. In Maximum Ratio combining each signal branch is multiplied by a weight factor that is proportional to the signal amplitude[11]. That is, branches with strong signal are further amplified, while weak signals are attenuated.

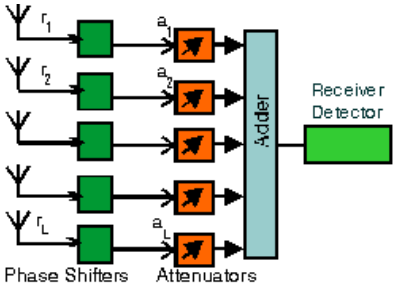

Figure: *3*-branch antenna diversity receiver (L = 5). With MRC, the attenuation/amplification factor is proportional to the signal amplitude $a_i = r_i$ for each channel *i*.

Receiver diversity is a form of space diversity, where there are multiple antennas at the receiver. The presence of receiver diversity poses an interesting problem – how do we use '*effectively*' the information from all the antennas to demodulate the data[14].

In Maximal Ratio Combining**,** we will assume that the channel is a flat fading Rayleigh multipath channel and the modulation is BPSK.

We use the same constraints as defined in the Selection Diversity and Equal Gain Combining (EGC). Then repeat the same.

1. We have N receive antennas and one transmit antenna.
2. The channel is flat fading – In simple terms, it means that the multipath channel has only one tap. So, the convolution operation reduces to a simple multiplication.
3. The channel experienced by each receive antenna is randomly varying in time. For any receiving antenna, each transmitted symbol gets multiplied by a randomly varying complex numberh_i. As the channel under consideration is a Rayleigh channel, the real and imaginary parts of h_i are Gaussian distributed having mean $\mu_{h_i} = 0$ and variance $\sigma_{h_i}^2 = \frac{1}{2}$
4. The channel experience by each receive antenna is independent from the channel experienced by other receive antennas.
5. On each receive antenna, the noise n has the Gaussian probability density function with

$p(n) = \frac{1}{\sqrt{2\pi\sigma^2}} e^{\frac{-(n-\mu)^2}{2\sigma^2}}$ with μ=0 and $\sigma^2 = \frac{N_0}{2}$

The noise on each receive antenna is independent from the noise on the other receive antennas.

6. At each receive antenna, the channel h_i is known at the receiver.
7. In the presence of channel h_i, the instantaneous bit energy to noise ratio at the receiving antenna is $\frac{|h_i|^2 E_b}{N_0}$.

For notational convenience, let us define,

$\gamma_i = \frac{|h_i|^2 E_b}{N_0}$

V. Proposed Methodology:

BER:

V.I.I Selection Diversity

(a) Generate random binary sequence of +1′s and -1′s.
(b) Multiply the symbols with the channel and then add white Gaussian noise.
(c) At the receiver, find the receive path with maximum power.
(d) Chose that receive path, equalize (divide) the received symbols with the known channel.
(d) Perform hard decision decoding and count the bit errors.
(e) Repeat for multiple values of E_b/N_0 and plot the simulation and theoretical results.

V.I.II Maximal Ratio Combining

(a) Generate random binary sequence of +1′s and -1′s.
(b) Multiply the symbols with the channel and then add white Gaussian noise.
(c) Chose that receive path, equalize the received symbols per maximal ratio combining.
(d) Perform hard decision decoding and count the bit errors.
(e) Repeat for multiple values of $E_b/N_0$and plot the simulation and theoretical results.

V.I.III Equal Gain Combining

(a) Generate random binary sequence of +1′s and -1′s.
(b) Multiply the symbols with the channel and then add white Gaussian noise.
(c) At the receiver, for each receive path, equalize by compensating with the known channel phase.
(d) Accumulate the equalized symbols from all the receive paths
(d) Perform hard decision decoding and count the bit errors
(e) Repeat for multiple values of $E_b/N_0$and plot the simulation and theoretical results.

V.I.IV Simulation Result

In this work , we have observed the bit error rate and signal to noise ratio performances with the different receiver diversity technique, which is shown below-

V.I.IV.A BER

a) In the figure shown below the result for BER for selection diversity with Eb/No are taken. It can be clearly observed that BER is much better, when there are two receivers, which clearly shows that as the no. of receiver increases BER improves.

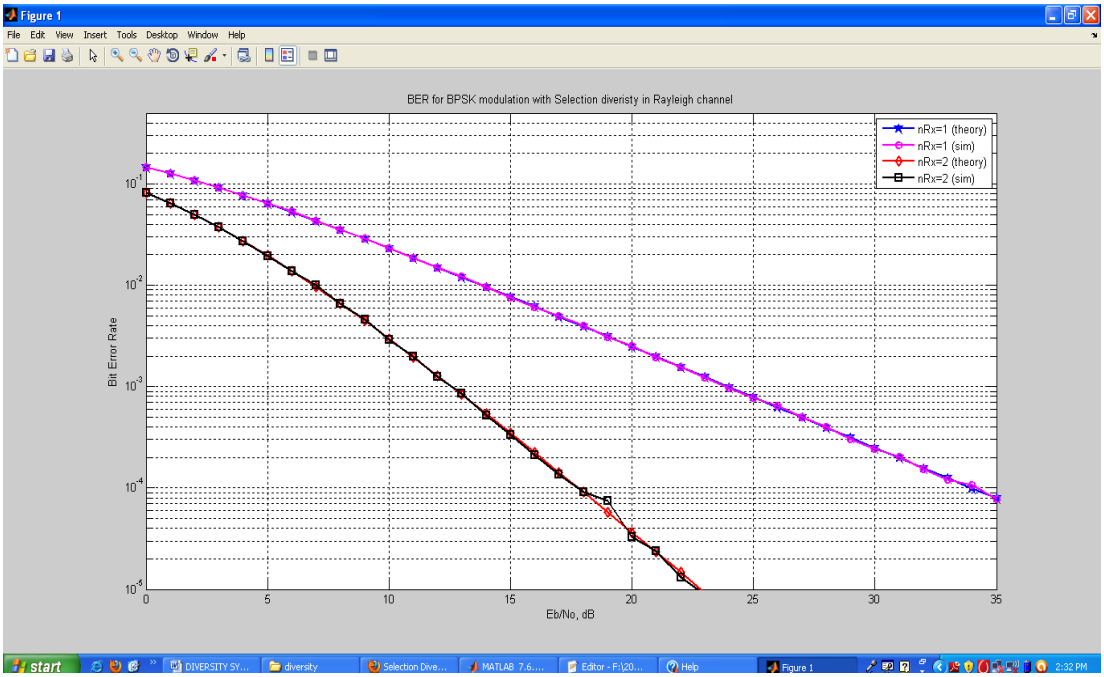

Fig: BER Vs Eb/No for selection diversity

b) In the figure shown below the result for BER for Equal Gain Combining with Eb/No are taken. It can be clearly observed that BER is much better, when there are two receivers, which clearly shows that as the no. of receiver increases BER improves.

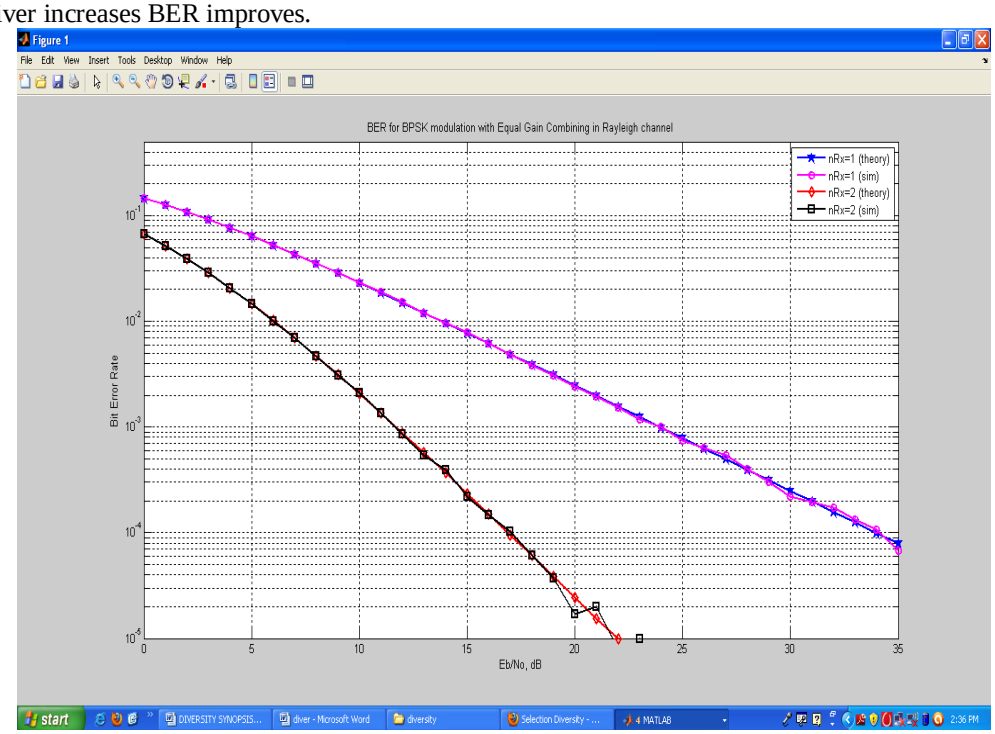

Fig: BER Vs Eb/No for Equal Gain Combinig

c) In the figure shown below the result for BER for Maximal Ratio Combining with Eb/No are taken. It can be clearly observed that BER is much better, when there are two receivers, which clearly shows that as the no. of receiver increases BER improves.

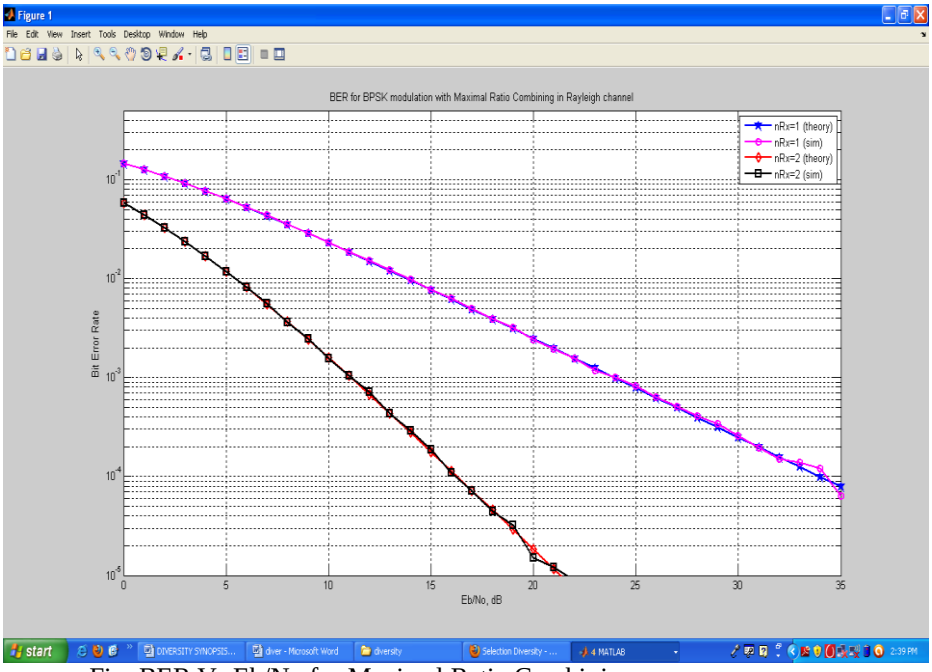

Fig: BER Vs Eb/No for Maximal Ratio Combining

V.I.V Result Comparison:

In the figure below, plot of the BER with the Eb/No for all the three techniques have been shown. This clearly shows that BER in case of MRC is much better than that of Equal Gain combining and selection diversity. If the value of Eb/No is 5 then it can be observed from the below figure the value of bit error rate is lesser for Maximal Ratio Combining diversity technique as compare to Equal Gain Combining and Selection diversity technique and BER value for Equal Gain Combining is more than the Selection diversity technique.

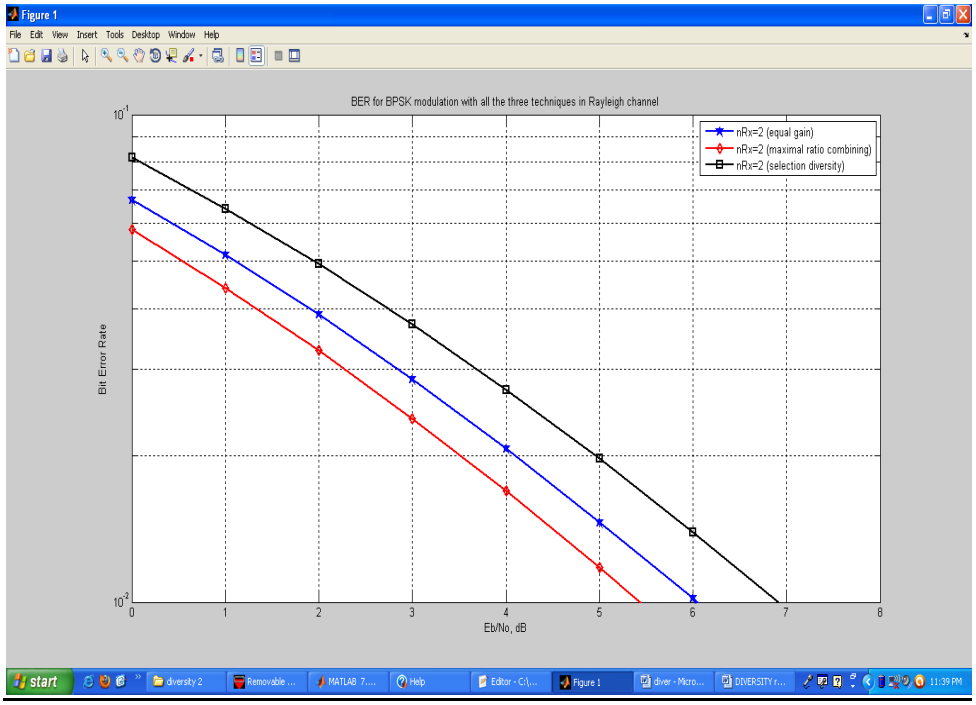

Fig: BER Comparison

V.I.IV.B Signal to noise ratio

Performance of different receiver diversity technique is shown below. In which it can be seen the changes in the value of SNR with the no. of receiving antenna.

a) In the figure shown below the result for SNR for selection diversity with no. of receivers are taken. It can be clearly observed that SNR is much better, when no. of receiving antennas increases. which clearly shows that as the no. of receiving antenna increases SNR improves.

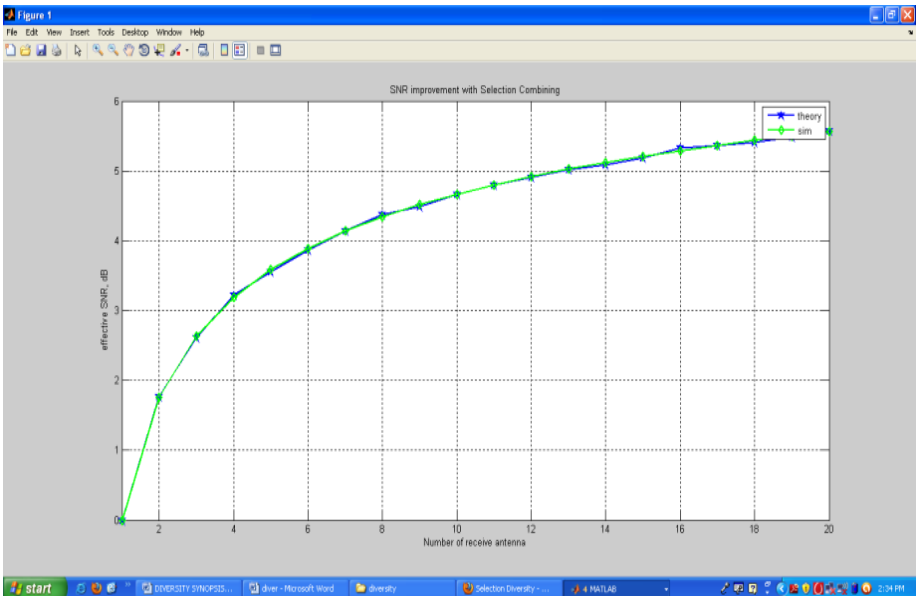

Fig: SNR for selection diversity

a) In the figure shown below the result for SNR for Equal Gain Combining with no. of receiving antenna are taken. It can be clearly observed that SNR is much better, when no. of receiving antenna increases.

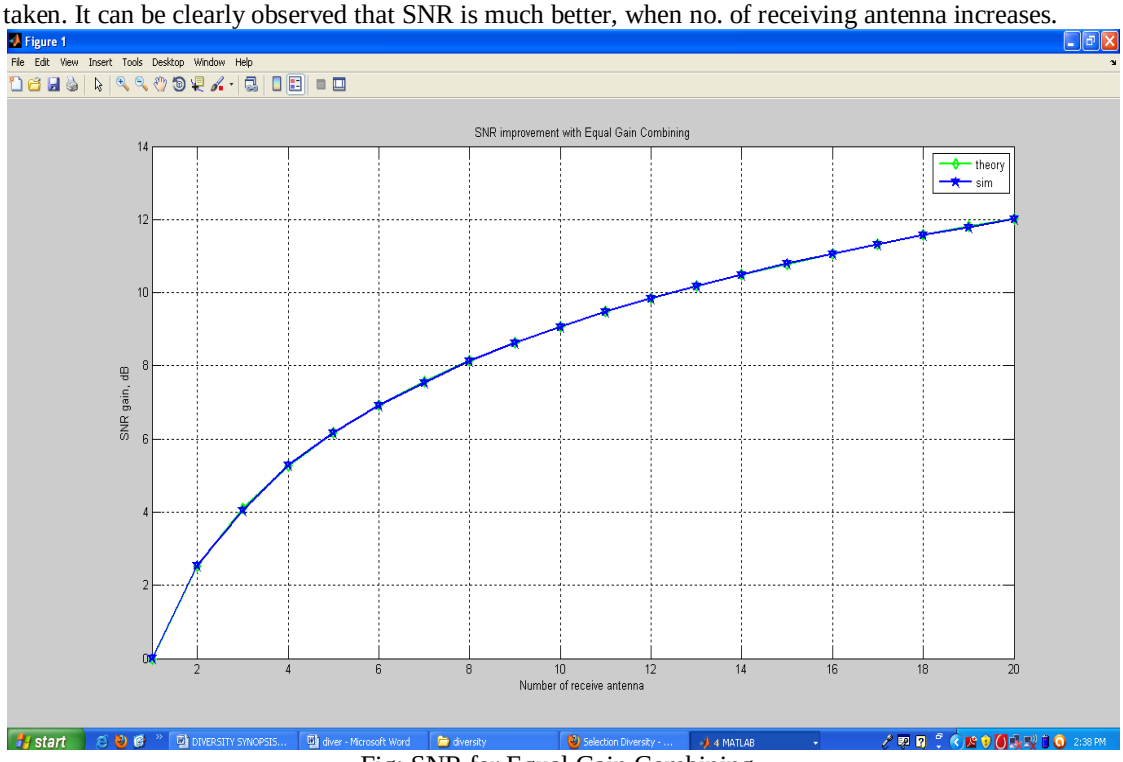

Fig: SNR for Equal Gain Combining

a) In the figure shown below the result for SNR for Maximal Ratio Combining with no. of receiving antenna are taken. It can be clearly observed that SNR is much better, when no. of receiving antenna increases. which clearly shows that as the no. of receiving antenna increases SNR improves.

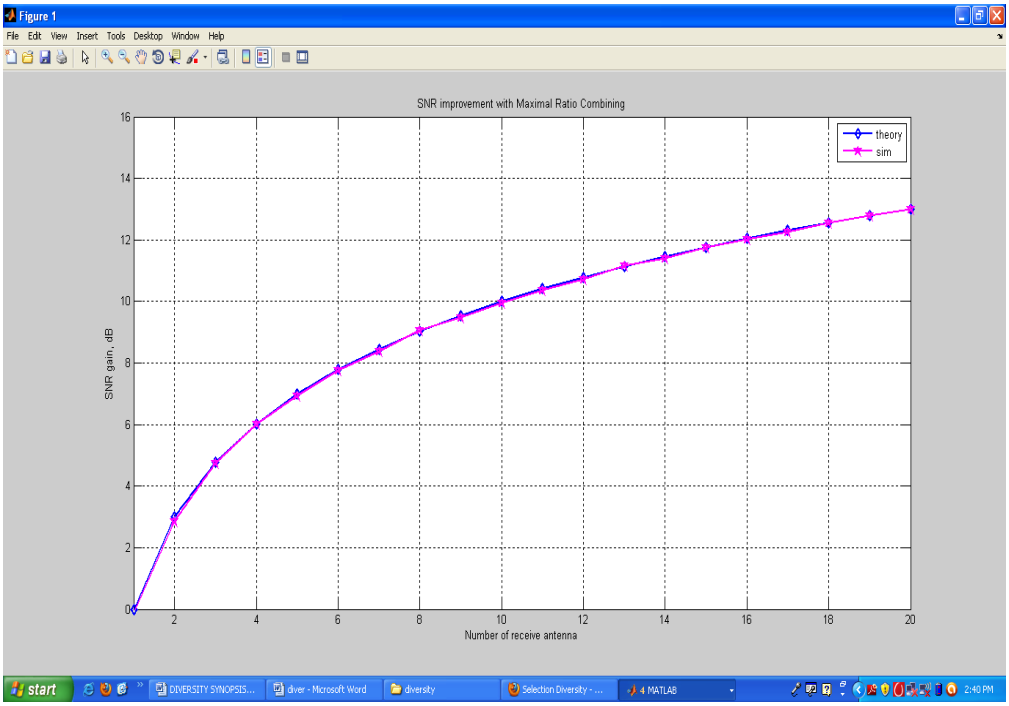

Fig: SNR for Maximal Ratio Combining

V.II.I Result Comparison:

In the figure below, plot of the SNR with the different no. of antenna for all the three techniques have been shown. This clearly shows that SNR in case of MRC is much than that of Equal Gain and selection diversity. It is also observed that as the number of receiver increases SNR increases gradually. If the no. of antenna is 4 then it can be observed from the below figure the value of signal to noise ratio is more for Maximal Ratio Combining diversity technique as compare to Equal Gain Combining and Selection diversity technique and SNR value for Equal Gain Combining is more than the Selection diversity technique.

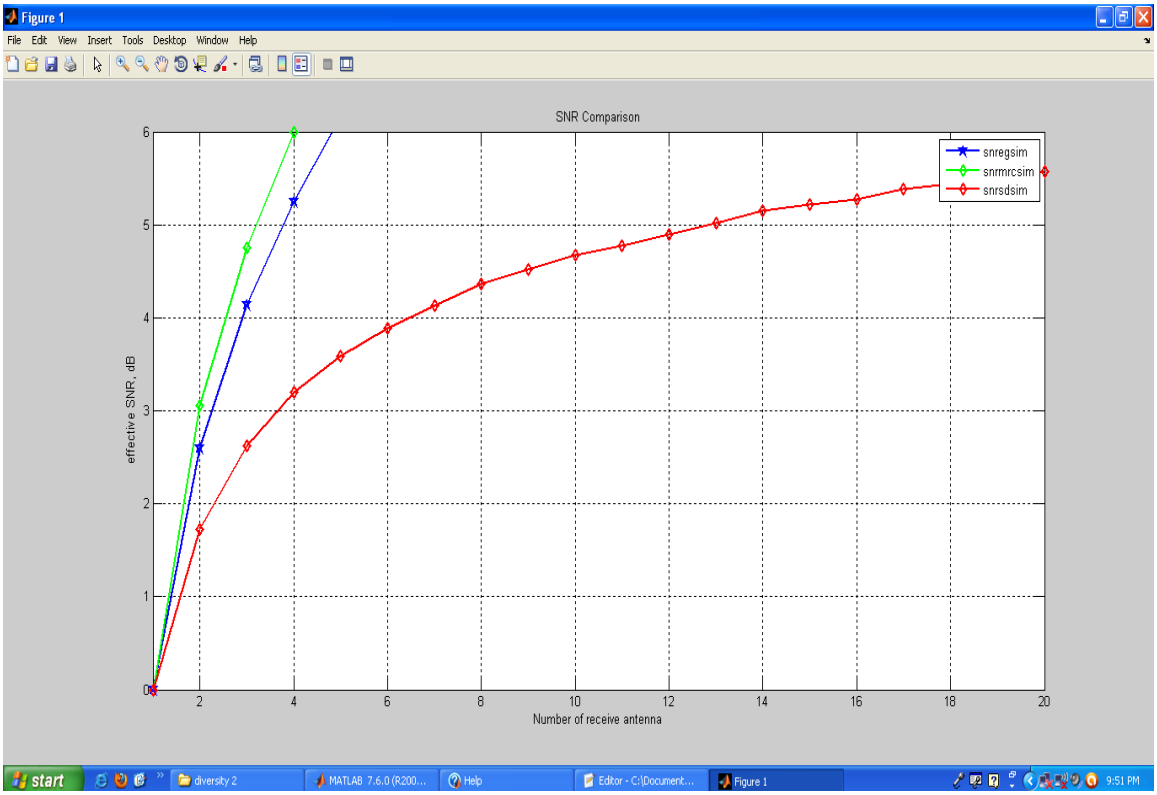

Fig: SNR Comparison

VI. Conclusion

As we know for the receiver diversity we have different diversity technique, out of which we used three technique-selection diversity, maximal ratio combining and equal gain combining for our work. BPSK modulation technique and rayleigh fading is used for checking the performance of these technique. We observed that when we calculated the value of SNR with different no. of antenna for these three techniques, selection diversity. For the calculation the bit error rate with respect to the Eb/No then again maximal ratio combining have lesser value as compare to the equal gain combining and selection diversity. So, we can say that the performance of the maximal ratio combining is better as compare to the equal gain combining and selection diversity.

References

[1] W. C. Jakes, Ed. Microwave Mobile Communications. New York: Wiley, 1974.

[2] IEEE TRANSACTIONS ON COMMUNICATIONS, VOL. 16, NO. 8, OCTOBER 1998" A simple Diversity Technique for Wireless Communications " Siavash M. Alamouti, Senior Technical Leader, Alta Business Unit of Cadence Design Systems, Sunnyvale, CA.

[3] IEEE,Abdulkareem Adinoyi, Yijia Fan, Halim Yanikomeroglu, H. Vincent Poor, and Furaih Al-Shaalan "Performance of Selection Relaying and Cooperative Diversity".

[4] IEEE TRANSACTIONS ON COMMUNICATIONS, VOL. 49, NO. 10, OCTOBER 2001" Optimum Selection Diversity for BPSK Signals in Rayleigh Fading Channels" Young Gil Kim and Sang Wu Kim, Senior Menber, IEEE

[5] International Journal of Advanced in Compter Science and Software Engineering " Diversity – A Fading Reduction Technique" Nikita Sachdeva, Deepak Sharma MMU Mullana.

[6] IEEE TRANSACTIONS ON WIRELESS COMMUNICATIONS, 2004 (TO APPEAR) "Performance Analysis of Combined Transmit Selection Diversity and Receive Generalized Selection Combining in Rayleigh Fading channels" Xiaodong Cai, Member, IEEE, and Georgios B. Giannakis, Fellow, IEEE

[7] Vehicular Technology Conference, 2006. VTC-2006 Fall. 2006 IEEE 64th "BER Analysis of BPSK Modulation Over the Weibull Fading Channel with CCI "25-28 Sept. 2006.

[8] D. B. Smith and T. D. Abhayapala are with Wireless Signal Processing, National ICT Australia (NICTA) Locked Bag 8001, Canberra, ACT, 2601 "Maximal Ratio Combining Performance Analysis in Practical Rayleigh Fading Channels".

[9] IEEE David B. Smith and Thushara D. Abhayapala "Maximal Ratio Combining Performance Analysis in Spatially Correlated Rayleigh Fading Channels".

[10] International Journal of Computer Applications (0975 – 8887) Volume 21– No.6, May 2011, "SER Analysis of OFDM System over Rayleigh Fading Channel"

[11] Communications, IEE Proceedings- "Maximal ratio combining performance analysis in practical Rayleigh fading channels" Oct. 2006 .

[12] Wireless Communications, IEEE Transactions on "Analysis of a two-branch maximal ratio and selection diversity system with unequal SNRs and correlated inputs for a Rayleigh fading channel" Apr 2002

[13] Communications, IEEE Transactions on "A Closed-Form BER Expression for BPSK Using MRC in Correlated CCI and Rayleigh Fading" Dec. 2007

[14] International Journal of Computer Networks & Communications (IJCNC) Vol.2, No.6, November 2010 "BER PERFORMANCE EVALUATION OF TWO TYPES OF ANTENNA ARRAY-BASED RECEIVERS IN A MULTIPATH CHANNEL", Rim Haddad1, Ridha Bouallègue.

[15] IEEE TRANSACTIONS ON COMMUNICATIONS, VOL. 53, NO. 8, AUGUST 2005 "Performance Analysis of Predetection EGC in Exponentially Correlated Nakagami-m Fading Channel" P. R. Sahu, Student Member, IEEE, and A. K. Chaturvedi, Senior Member, IEEE

[16] IEEE TRANSACTIONS ON COMMUNICATIONS on "Performance Evaluation of Binary Modulation Schemes with Dual-Diversity EGC in Rayleigh Fading Environment"

[17] Communications, IEEE Transactions on "Performance of Equal Gain Combining with Quantized Phases in Rayleigh Fading Channels" January 2011

[18] IEEE TRANSACTIONS ON COMMUNICATIONS, Vol. 52 NO. 5, May 2004 on "Performance analysis of Equal Gain Diversity in Nakagami – m Fadin" George K. Karagiannidis, Senior Member, IEEE.

IOSR Journal of Electronics and Communication Engineering (IOSR-JECE)
e-ISSN: 2278-2834,p- ISSN: 2278-8735. Volume 5, Issue 6 (Mar. - Apr. 2013), PP 97-105
www.iosrjournals.org

Designing and Performance Evaluation of 64 QAM OFDM System

Sahasha Namdeo[1], Reena Rani[2]
[1](M.Tech, Electronics and Communication, Maharshi Dayanand University, Rohtak, Haryana India)
[2](M.Tech, Electronics and Communication, Maharshi Dayanand University, Rohtak, Haryana India)

Abstract (11Bold) : *— In this report, the performance analysis of 64 QAM-OFDM wireless communication systems affected by AWGN in terms of Symbol Error Rate and Throughput is addressed. 64 QAM (64 ary Quadrature Amplitude Modulation) is the one of the effective digital modulation technique as it is more power efficient for larger values of M(64). The MATLAB script based model of the 64 QAM-OFDM system with normal AWGN channel and Rayleigh fading channel has been made for study error performance and throughput under different channel conditions. This simulated model maximizes the system throughput in the presence of narrowband interference, while guaranteeing a SER below a predefined threshold. The SER calculation is accomplished by means of modelling the decision variable at the receiver as a particular case of quadratic form D in complex Gaussian random variables. Lastly comparative study of SER performance of 64 QAM-OFDM simulated & 64 QAM-OFDM theoretical under AWGN channel has been given. Also performance of the system is given in terms of throughput (received bits/ofm symbol) is given in a plot for different SNR.*

Keywords (11Bold) *–64 QAM, BPSK, OFDM, PDF, SNR.*

I. INTRODUCTION

1.1 Orthogonal Frequency Division Multiplexing

In OFDM systems, the available bandwidth is broken into many narrower subcarriers and the data is divided into parallel streams, one for each subcarrier each of which is then modulated using varying levels of QAM modulation e.g. QPSK, 16QAM, 64QAM or higher orders as required by the desired signal quality. The linear combination of the instantaneous signals on each of the subcarriers constitutes the OFDM symbols. The spectrum of OFDM is depicted in fig.1.1. Each of the OFDM symbol is preceded by a cyclic prefix (CP) which is effectively used to eliminate Intersymbol Interference (ISI) and the subcarriers are also very tightly spaced for efficient utilization of the available bandwidth [1].

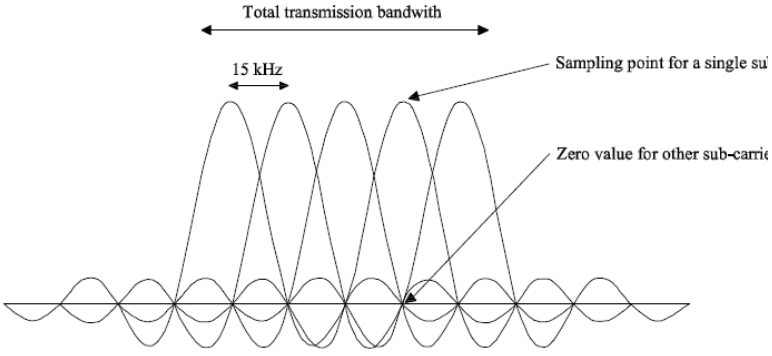

Figure 1.1 OFDM Spectrum

OFDM provides an effective method to mitigate intersymbol interference (ISI) in wideband signalling over multipath radio channels. The main idea is to send the data in parallel over a number of narrowband flat subchannels (see Fig. 1.2). This is efficiently achieved by using a set of overlapped orthogonal signals to partition the channel. A transceiver can be realized using a number of coherent QAM modems which are equally spaced in the frequency domain and which can be implemented using the IDFT on the transmitter end and the DFT on the receiving end [6,7]. Due to the fact that the intercarrier spacing in OFDM is relatively small, OFDM transceivers are somewhat more sensitive to phase noise by comparison to single carrier transceivers. It is the purpose of this paper to examine the impact of L.O. phase noise on the BER performance of OFDM signals over both AWGN and frequency selective channels. The paper first discusses the relationship between the continuous time, continuous frequency L.O. phase noise model and the discrete time, discrete frequency process that is seen by the OFDM system. An analysis of the OFDM receiver is presented to assess

the impact of the phase noise on the decision variables at the receiver (which are the received signal samples corrupted by noise, just before making hard decisions regarding the received data). It is then shown that the effect of phase noise on the decision variables is composed of two components: a common component which affects all data symbols equally and as such causes a sometimes visible rotation of the signal constellation, and a second component which is more like Gaussian noise and thus affects the received data points in a somewhat random manner. This representation in terms of common and foreign components has been pointed out in the literature [8]–[10]. What we introduce here that is different, is that the temporal variations of the rotational component and its dependence on the frequency spacing between the system carriers play an important role in determining the symbol-error rate performance of the OFDM system, particularly at higher operating SNR conditions. Taking the temporal variations of the rotational component of the phase noises into account, we then proceeded to derive analytical expressions for the average probability of error for 64-QAM OFDM. The resulting formulas are in a closed form which includes several integrals over the Gaussian probability curve. The analytical results are then used to quantify the impact of certain phase noise masks on the average BER performance under different SNR conditions and also subject to variations of the OFDM frame length. Computer simulation is used to treat the problem over channels with arbitrary multipath profiles and also, to investigate the impact of phase noise on channel estimation and channel equalization. The simulation model requires a user specified phase noise mask as an input. It also requires the user to identify system parameters such as sampling frequency, OFDM frame length and the size of the signal constellation.

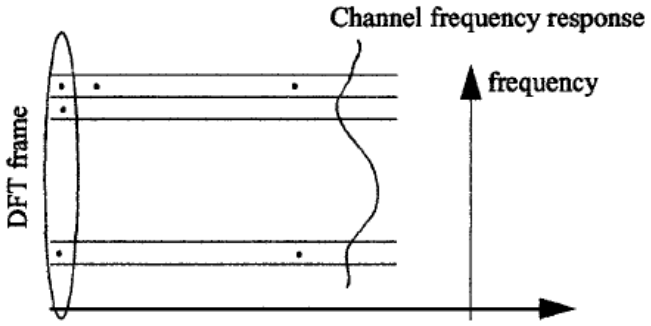

Figure 1.2 Using OFDM to mitigate ISI

1.2. System Description and Model

A functional block diagram of an OFDM system is shown in Fig. 1.3. The incoming data is fist applied to a baseband M-ary QAM modulator which maps each L= log2M binary bits into one of the M constellation points. The M-QAM points coming out of the baseband modulator are then grouped into frames, each containing N complex constellation points. Each frame is applied to an inverse DFT processor which outputs N-complex transform coefficients. A circular prefix of length Np is then appended to the N complex transform coefficients to form a transmitted frame which is N + Np points long. The transmitted frame is then applied to a serial-to-parallel converter and then applied to an IQ modulator to translate the spectral content of the signal to some UHF or microwave frequency band. The IQ modulation is accomplished by multiplying the complex envelope of the signal with the output of a local oscillator. This step is often accomplished at a convenient IF frequency and the modulated signal is then upconverted using a higher frequency local oscillator. For our purpose, it is sufficient to consider one local oscillator as indicated in, Fig. 1.3. The local oscillator is not perfect. Its output is usually degraded due to many factors, including short term frequency drift that may in part be caused by temperature variations. The short term frequency drifts manifest themselves as phase noise which has traditionally been characterized in terms of its power spectral density.

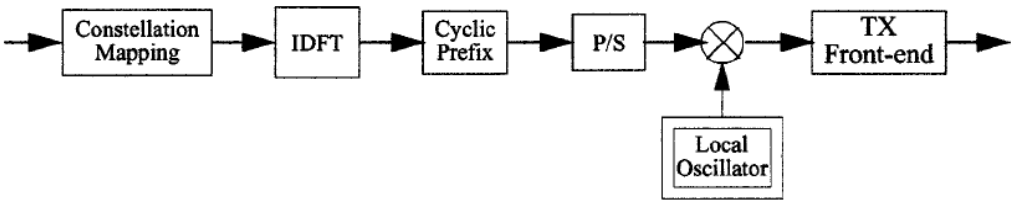

Figure 1.3 Block diagram of an OFDM transmitter.

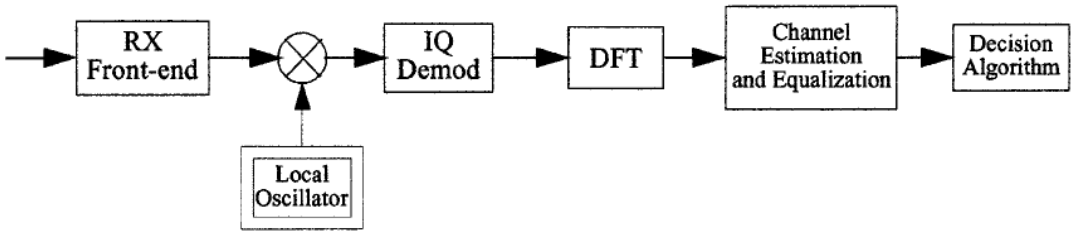

Figure 1.4 Block diagram of an OFDM receiver.

A functional block diagram of a simplified OFDM receiver is depicted in Fig. 1.4. The received signal, usually corrupted by additive noise and channel distortion, is first applied to a low noise microwave front-end where it is amplified and perhaps filtered to suppress unwanted interference. The received signal is then downconverted to an IF frequency and applied to an I&Q demodulator which brings the signal down to baseband in the form in-phase and quadrature components. These in turn are applied to a A/D converter which outputs complex baseband samples at a rate of one sample per received symbol. The complex samples are then grouped into received frames which contain N + Np points each. Assuming that the frame synchronization is working, the received frames are first reduced to N points each by removing the circular prefix, and then are applied to an N -point DFT processor. The received frame is also used to estimate the frequency response of the channel. The DFT output is then equalized to generate -decision variables which may be used to recover the data either based on threshold comparison or applied to a sequential estimation procedure such as the Viterbi algorithm.The important block in Fig. 1.4 is the local oscillator, which like the transmitter local oscillator may have its own phase noise which will degrade the quality of the received signal and the overall BER performance. For analog TV (ATV) applications the Tx local oscillator is of much better spectral purity since this exists only in the base station and as such it does not have to be very economical. The Rx local oscillator signal on the other hand is provided with a cheap commercial TV tuner which exhibits high levels of phase noise. It is for this reason that we will concentrate on the Rx LO phase noise without explicit mention of the Tx LO phase noise. It should however be mentioned that the analysis we will develop can still be applied to cases where the phase noise is introduced by a combination of both local oscillators.

1.3. M-QAM constellation

The number of points in the constellation is defined as, $M = 2^b$ where b is the number of bits in each constellation symbol. In this analysis, it is desirable to restrict b to be an even number for the following reasons :

1. Half the bits are represented on the real axis and half the bits are represented on imaginary axis. The in-phase and quadrature signals are independent $b/2$ level Pulse Amplitude Modulation (PAM) signals. This simplifies the design of mapper.
2. For decoding, symbol decisions may be applied independently on the real and imaginary axis, simplifying the receiver implementation.

Note that the above square constellation is not the most optimal scheme for a given signal to noise ratio.

1.3.1. Average energy of an M-QAM constellation

In a general M-QAM constellation where $M = 2^b$ and b the number of bits in each constellation is even, the alphabets used are:

$$\alpha_{MQAM} = \{\pm(2m-1) \pm (2m-1)j\}, \text{ where } m \in \left\{1, \cdots, \frac{\sqrt{M}}{2}\right\}. \quad (1)$$

For example, considering a 64-QAM ($M = 64$) constellation, $m \in \{1, 2, 3, 4\}$ and the alphabets are:

$$\alpha_{64\ QAM} = \begin{matrix} \pm 7 \pm 7j & \pm 7 \pm 5j & \pm 7 \pm 3j & \pm 7 \pm 1j \\ \pm 5 \pm 7j & \pm 5 \pm 5j & \pm 5 \pm 3j & \pm 5 \pm 1j \\ \pm 3 \pm 7j & \pm 3 \pm 5j & \pm 3 \pm 3j & \pm 3 \pm 1j \\ \pm 1 \pm 7j & \pm 1 \pm 5j & \pm 1 \pm 3j & \pm 1 \pm 1j \end{matrix}$$

For computing the average energy of the M-QAM constellation, let us proceed as follows:

(a) Find the sum of energy of the individual alphabets:

$$E_\alpha = \sum_{m=1}^{\frac{\sqrt{M}}{2}} \left|(2m-1)+j(2m-1)\right|^2 = \frac{\sqrt{M}}{3}(M-1) \quad (2)$$

(b) Each alphabet is used $2\sqrt{M}$ times in the M-QAM constellation.

(c) So, to find the average energy from M constellation symbols, divide the product of (a) and (b) by M.

Plugging in the number for 64-QAM:

$$E_{64QAM} = \frac{2}{3}(64-1) = 42.$$

Plugging in the number for 16-QAM:

$$E_{16QAM} = \frac{2}{3}(16-1) = 10.$$

From the above explanations, it is reasonably intuitive to guess that the scaling factor of $\frac{1}{\sqrt{10}}, \frac{1}{\sqrt{42}}$ which is seen along with 16-QAM, 64-QAM constellations respectively is for normalizing the average transmit power to unity.

1.3.2. Types of constellation points in M-QAM

There are three types of constellation points in a general M-QAM constellation:

(a) Constellation points in the corner (red-square)

The number of constellation points in the corner in any M-QAM constellation is always 4, i.e

$$N_{corner} = 4$$

(b) Constellation points in the inside (magneta-diamond)

The number of constellation points inside is,

$$N_{inside} = (\sqrt{M}-2)(\sqrt{M}-2). \quad (3)$$

For example with M=64, there are 36 constellation points in the inside.

(c) Constellation points neither at the corner, nor at the center (blue-star) The number of constellation points of this category is:

$$N_{\text{neither inside nor corner}} = 4(\sqrt{M}-2). \quad (4)$$

For example with M=64, there are 24 constellation points in the inside.

1.4. Additive White Gaussian Noise (AWGN) channel

Let the received symbol is,

$y = k\sqrt{E_s}s+n$, where

E_s is the energy,

$k = \sqrt{\frac{1}{\frac{2}{3}(M-1)}}$ is the normalizing factor,

s is the transmit symbol and

n is the noise.

Assume that the additive noise n follows the Gaussian probability distribution function,

$$p(x) = \frac{1}{\sqrt{2\pi\sigma^2}} e^{\frac{-(x-\mu)^2}{2\sigma^2}} \quad (5)$$

With mean $\mu = 0$ and variance $\sigma^2 = \frac{N_0}{2}$.

Symbol in the inside $I = +1, Q = +1$ (magenta-diamond)

The conditional probability distribution function (PDF) of y given that the transmitted symbol is $\left\{+k\sqrt{E_s}, +k\sqrt{E_s}\right\}$:

$$p(y|inside) = \frac{1}{\sqrt{\pi N_0}} e^{\frac{-(y-k\sqrt{Es})^2}{N_0}}. \quad (6)$$

As can be seen from the above figure, the symbol in the inside is decoded correctly only if real part of y $(\Re y)$ lies in between 0 to 2 and the imaginary part of y $(\Im y)$ lies in between 0 to 2. The probability of

correct demodulation is,

$$p(c|inside) = p\left(\Re y>0, \Re y \le 2k\sqrt{E_s}|+1\right)p\left(\Im y>0, \Im y \le 2k\sqrt{E_s}|+1\right) \quad (7)$$

The probability of the real component falling within 0 to 2 can be found by integrating the probability distribution function of two parts:

(a) Find the probability that the real component lies from 2 to $+\infty$.

(b) Find the probability that the real component lies from $-\infty$ to 0.

(c) Given that the total probability is always 1, for finding the probability of the real component lies between 0 to 2, subtract the sum of (a) and (b) from 1.

$$erfc(x) = \frac{2}{\sqrt{\pi}}\int_{x}^{\infty} e^{-x^2}dx$$

Note: The complementary error function, . (8)

Similarly,

$$p\left(\Im y>0, \Im y \le 2k\sqrt{E_s}|+1\right) = 1-erfc\left(k\sqrt{\frac{E_s}{N_0}}\right). \quad (9)$$

From the above equations,

$$p(c|inside) = \left[1-erfc\left(\sqrt{\frac{E_s}{10N_o}}\right)\right]\left[1-erfc\left(\sqrt{\frac{E_s}{10N_o}}\right)\right]. \quad (10)$$

The probability of the symbol decoded being in error is as follow.

.

Symbol in the corner $I=+7, Q=+7$ **(red-square)**

The conditional probability distribution function (PDF) of y given that the transmitted symbol is $\left\{+7k\sqrt{E_s}, +7k\sqrt{E_s}\right\}$:

$$p(y|inside) = \frac{1}{\sqrt{\pi N_0}}e^{\frac{-(y-7k\sqrt{Es})^2}{N_0}} \quad . \quad (11)$$

As can be seen from the above figure, the symbol in the inside is decoded correctly only if real part of y $(\Re y)$ lies from 6 to ∞ and the imaginary part of y $(\Im y)$ lies from 6 to ∞.

$$p(c|corner) = p\left(\Re y>6, \Re y \le \infty|+7\right)p\left(\Im y>0, \Im y \le \infty|+7\right) \quad (12)$$

For finding the probability that the real component lies from 6 to ∞, one can integrate the probability distribution function of the received symbol.

$$p\left(\Re y>6, \Re y \le \infty|+7\right) = \frac{1}{\sqrt{\pi N_0}}\int_{6k\sqrt{E_s}}^{+\infty} e^{\frac{-(y-7k\sqrt{Es})^2}{N_0}}dy$$

$$= 1-\frac{1}{2}erfc\left(k\sqrt{\frac{E_s}{N_0}}\right) \quad (13)$$

Similarly,

$$p\left(\Im y>6, \Im y \le \infty|+7\right) = \frac{1}{\sqrt{\pi N_0}}\int_{6k\sqrt{E_s}}^{+\infty} e^{\frac{-(y-7k\sqrt{Es})^2}{N_0}}dy$$

$$= 1-\frac{1}{2}erfc\left(k\sqrt{\frac{E_s}{N_0}}\right) \quad (14)$$

.

So, probability that the decoded symbol is correct given $I=+7, Q=+7$ is transmitted is,

$$p(c|corner) = \left[1-\tfrac{1}{2}erfc\left(k\sqrt{\frac{E_s}{N_0}}\right)\right]\left[1-\tfrac{1}{2}erfc\left(k\sqrt{\frac{E_s}{N_0}}\right)\right]$$
$$= 1-erfc\left(k\sqrt{\frac{E_s}{N_0}}\right)+\tfrac{1}{4}erfc^2\left(k\sqrt{\frac{E_s}{N_0}}\right)$$

. (15)

Now, the probability of the symbol decoded being in error is,

$$p(e|corner) = 1-p(c|corner)$$
$$= erfc\left(k\sqrt{\frac{E_s}{N_0}}\right)-\tfrac{1}{4}erfc^2\left(k\sqrt{\frac{E_s}{N_0}}\right)$$

. (16)

Symbol neither at the corner nor inside $I=+7,Q=+1$ **(blue-star)**

As can be seen from the above figure, the symbol in the inside is decoded correctly only if real part of y $(\Re y)$ lies from 6 to ∞ and the imaginary part of y $(\Im y)$ lies from 0 to 2.

$$p(c|corner) = p\left(\Re y>6,\Re y\le\infty|+7\right)p\left(\Im y>0,\Im y\le\infty|+7\right) \quad (17)$$

For finding the probability that the real component lies from 6 to ∞, one can integrate the probability distribution function of the received symbol.

$$p\left(\Re y>6,\Re y\le\infty|+7\right) = \frac{1}{\sqrt{\pi N_0}}\int_{6k\sqrt{E_s}}^{+\infty} e^{\frac{-(y-7k\sqrt{E_s})^2}{N_0}}dy$$
$$= 1-\tfrac{1}{2}erfc\left(k\sqrt{\frac{E_s}{N_0}}\right)$$

. (18)

As described for the symbol in the inside scenario, the probability of the imaginary component falling with in 0 to 2 can be found by integrating the probability distribution function of two parts:

(a) Find the probability that the imaginary component lies from 2 to $+\infty$.

(b) Find the probability that the imaginary component lies from $-\infty$ to 0.

(c) As the total probability is 1, for finding the probability of the imaginary component lies within 0 to 2, subtract the sum of (a) and (b) from 1.

$$p\left(\Im y>0,\Im y\le 2k\sqrt{E_s}|+1\right) = 1-\left[\frac{1}{\sqrt{\pi N_0}}\int_{-\infty}^{0} e^{\frac{-(y-k\sqrt{E_s})^2}{N_0}}dy+\frac{1}{\sqrt{\pi N_0}}\int_{2k\sqrt{E_s}}^{+\infty} e^{\frac{-(y-k\sqrt{E_s})^2}{N_0}}dy\right]$$
$$= 1-erfc\left(k\sqrt{\frac{E_s}{N_0}}\right)$$

(19)

So the probability that the symbol is decoded correctly technologies. The analytical performance of most of wireless communication systems under different fading conditions has already been accomplished when perfect channel state information (CSI) is assumed to be known at the receiver side (or even at the transmitter side, if required) [5, 6]. These results hence are useful to determine the maximum achievable performance of these systems under ideal conditions. However, in practice there exist many factors which may limit their performance: the appearance of interfering signals, the consideration of imperfect CSI, or non-idealities due to physical implementation such as carrier frequency offset (CFO), in-phase/quadrature (I/Q) imbalance and direct-current (DC) offsets are valid examples. is,

$$p(c|\text{neither inside nor corner}) = \left[1-erfc\left(k\sqrt{\frac{E_s}{N_0}}\right)\right]\left[1-\frac{1}{2}erfc\left(k\sqrt{\frac{E_s}{N_0}}\right)\right]$$
$$= 1-\frac{3}{2}erfc\left(k\sqrt{\frac{E_s}{N_0}}\right)+\frac{1}{2}erfc^2\left(k\sqrt{\frac{E_s}{N_0}}\right)$$

(20)

The probability of error is,

$$p(e|\text{neither inside nor corner}) = 1-p(c|\text{neither inside nor corner})$$
$$= \frac{3}{2}erfc\left(k\sqrt{\frac{E_s}{N_0}}\right)-\frac{1}{2}erfc^2\left(k\sqrt{\frac{E_s}{N_0}}\right)$$

(21)

1.5. Total symbol error probability

Given that we have computed the individual symbol error probability for each of the three types of constellation points, to find the joint symbol error rate we compute the average error i.e.

$$P(e|MQAM) = \frac{\begin{array}{l}N_{inside}p(e|inside)+\\ N_{corner}p(e|corner)+\\ N_{\text{neither inside nor corner}}p(e|\text{neither inside nor corner})\end{array}}{M}$$

(22)

Pluging in the equations,

$$P(e|MQAM) = 2\left(1-\frac{1}{\sqrt{M}}\right)erfc\left(k\sqrt{\frac{E_s}{N_0}}\right)-\left(1-\frac{2}{\sqrt{M}}+\frac{1}{M}\right)erfc^2\left(k\sqrt{\frac{E_s}{N_0}}\right)$$

(23)

The measurement of the performance in communication systems has always been a matter of extreme interest since their very origin [1–3]. Besides the channel capacity, which basically provides information about the limiting error-free information rate that can be achieved, this performance is usually quantified in terms of the Symbol Error Rate (SER) or the Bit Error Rate (BER). Depending on the characteristics of the channel fading and the modulation scheme, the performance analysis can be conducted following different approaches. One of the milestone reference works in this area was published by Simon and Alouini [4], where the performance of a number of digital communication systems under different fading conditions was analyzed following a common strategy. Most of the results provided in this paper allows obtaining the SER in exact closed-form, whereas in other cases a numerical integration was necessary. The appearance of new digital communication systems that employ new modulation or transmission schemes leads to the necessity of evaluating their performance in order to enable a fair comparison with the existing techniques. Some examples are the use of multiple antennas, usually referred to as multiple-input multiple-output (MIMO) systems, or the orthogonal frequency division multiplexing (OFDM) technique. Both MIMO and OFDM have been incorporated in many commercial and under-development wireless communication

II. METHODOLOGY

2.1. *64 QAM*

1. Use OFDM Specifications like FFT Size, Number of Data Subcarriers,Number of Bits Per OFDM Symbol (Same as the Number of Subcarriers for BPSK), Number of OFDM Symbols
2. Find Out Modulation & Average Energy of 64-QAM
3. Find out SNR according to the accounting for the used subcarriers and cyclic prefix.
4. Find out Transmitter Input
5. Now Calculate Gaussian Noise of Unit Variance, 0 Mean
6. Add Noise to the Transmitter Input

7. Formatting the Received Vector into Symbols and Converting to Frequency Domain
8. Apply Demodulation and Converting to Vector
9. Counting the Errors by Subtracting output Demodulated Vector on receiving side from the Transmitter input.

III. RESULTS AND DISCUSSIONS

3.1. COMPARATIVE BER PERFORMANCE OF M-ARY QAM-OFDM.

The Bit Error Rate (BER) performance against signal to noise ratio (Eb/No) of 64QAM-OFDM & 128QAM-OFDM in both AWGN channel & multipath fading channel has been shown in figure 4 & figure 5 respectively. The BER decreases sharply with the increase in the signal to noise ratio in both AWGN channel & multipath fading channel but the bit error rate in multipath fading channel is higher than normal AWGN channel.

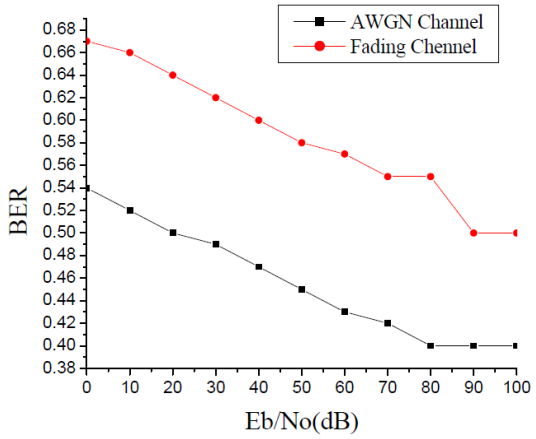

Figure 3.1: E_b/N_0 vs. BER for 64QAM-OFDM system in AWGN channel & Multipath fading channel [12]

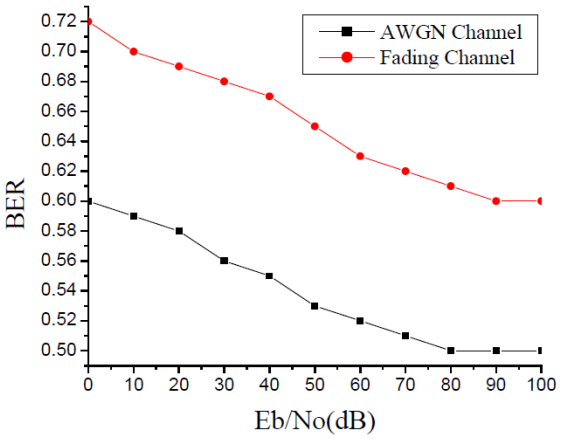

Figure3.2: E_b/N_0 vs. BER for 128QAM-OFDM system in AWGN channel & Multipath fading channel [12]

IV. CONCLUSION

In this document, an algorithm is designed to maximize the OFDM system throughput in the presence of AWGN imperfect channel estimation. The average throughput of the OFDM system is maximized under the constraint of a BER below a target value. As expected, the average throughput increases as the SIR increase, respectively. Moreover, increasing the channel estimation error variance reduces the average throughput. In future work, we will extend the proposed algorithm to include power loading, and impose a constraint on the maximum transmit power to reduce the OFDM cognitive user spectrum leakage, in addition to considering spectrum sculpting techniques.

REFERENCES

Journal Papers:

[1] Pussadee Kiratipongvooth, "Bit Error Probability of Cooperative Diversity for M-ary QAM OFDM-based system with Best Relay Selection" , *International Conference on Information and Electronics Engineering 2011IPCSIT vol.6 (2011) © (2011) IACSIT Press, Singapore*

[2] Abhijyoti Ghosh, "Comparative BER Performance of M-ary QAM-OFDM System in AWGN & Multipath Fading Channel", International Journal on Computer Science and Engineering (IJCSE), Vol. 4 No. 06 June 2012

[3] Ebrahim Bedeer, "Adaptive Bit Allocation for OFDM Cognitive Radio Systems with Imperfect Channel Estimation", 2012 IEEE

[4] Mitalee Agrawal , "BER Analysis of MIMO OFDM System for AWGN & Rayleigh Fading Channel" , *International Journal of Computer Applications (0975 – 8887) Volume 34– No.9, November 2011*

[5] M. Di Renzo, F. Graziosi, and F. Santucci, "On the cumulative distribution function of quadratic-form receivers over generalized fading channels with tone interference," *Communications, IEEE Transactions on*, vol. 57, pp. 2122 –2137, jul. 2009.

[6] F. J. Lopez-Martinez, E. Martos-Naya, J. F. Paris, and A. J. Goldsmith, "BER Analysis for MIMO-OFDM Beamforming with MRC under Channel Prediction and Interpolation Errors," in *Proc. IEEE Global Telecommunications Conf. GLOBECOM 2009*, pp. 1–7, 2009.

[7] F. J. Lopez-Martinez, E. Martos-Naya, J. F. Paris, and U. Fernandez-Plazaola, "Generalized BER Analysis of QAM and its Application to MRC under Imperfect CSI and Interference in Ricean Fading Channels," *IEEE Transactions on Vehicular Technology*, vol. 59, pp. 2598–2604, June 2010.

[8] F. J. Lopez-Martinez, E. Martos-Naya, J. F. Paris, and J. T. Entrambasaguas, "BER analysis of direct conversion OFDM systems with MRC under channel estimation errors," *IEEE Communications Letters*, vol. 14, pp. 423–425, May 2010.

[9] F. J. Lopez-Martinez, E. Martos-Naya, K. K. Wong, and J. Entrambasaguas, "Closed- Form BER Analysis of Alamouti-MRC Systems with ICSI in Ricean Fading Channels," *IEEE Communications Letters*, vol. 1, no. Accepted for publication, pp. 1–3, 2011.

[10] F. J. Lopez-Martinez, E. Martos-Naya, J. F. Paris, and J. Entrambasaguas, "Exact Closed-Form BER Analysis of OFDM Systems in the presence of IQ imbalances and ICSI," *IEEE Transactions on Wireless Communications*, vol. 1, no. 2nd round of reviews, pp. 1–7, 2011.

[11] M. Inamori, A. Bostamam, Y. Sanada, and H. Minami, "IQ imbalance compensation scheme in the presence of frequency offset and dynamic DC offset for a direct conversion receiver," *IEEE Transactions on Wireless Communications*, vol. 8, pp. 2214 –2220, may 2009.

[12] Y. Yoshida, K. Hayashi, H. Sakai, and W. Bocquet, "Analysis and Compensation of Transmitter IQ Imbalances in OFDMA and SC-FDMA Systems," IEEE Transactions on Signal Processing, vol. 57, pp. 3119 –3129, aug. 2009.

[13] Q. Zou, A. Tarighat, and A. Sayed, "Joint compensation of IQ imbalance and phase noise in OFDM wireless systems," *IEEE Transactions on Communications*, vol. 57, pp. 404 –414, february 2009.

[14] H. Minn and D. Munoz, "Pilot Designs for Channel Estimation of OFDM Systems with Frequency-Dependent I/Q Imbalances," in *IEEE Wireless Communications and Networking Conference, 2009. WCNC 2009.*, pp. 1 –6, april 2009.